

Spring 2019

ATRC PROCESSES AND ARCHITECTURES AS TOOLS FOR ADVANCING THE COMPLEXITY OF SINGLE-CHAIN POLYMERIC NANOPARTICLES

Elizabeth Bright

University of New Hampshire, Durham

Follow this and additional works at: <https://scholars.unh.edu/dissertation>

Recommended Citation

Bright, Elizabeth, "ATRC PROCESSES AND ARCHITECTURES AS TOOLS FOR ADVANCING THE COMPLEXITY OF SINGLE-CHAIN POLYMERIC NANOPARTICLES" (2019). *Doctoral Dissertations*. 2438.
<https://scholars.unh.edu/dissertation/2438>

This Dissertation is brought to you for free and open access by the Student Scholarship at University of New Hampshire Scholars' Repository. It has been accepted for inclusion in Doctoral Dissertations by an authorized administrator of University of New Hampshire Scholars' Repository. For more information, please contact nicole.hentz@unh.edu.

ATRC PROCESSES AND ARCHITECTURES AS TOOLS FOR ADVANCING THE
COMPLEXITY OF SINGLE-CHAIN POLYMERIC NANOPARTICLES

BY

ELIZABETH R. BRIGHT

B.S., University of New Mexico, 2014

DISSERTATION

Submitted to the University of New Hampshire

in Partial Fulfillment of

the Requirements for the Degree of

Doctor of Philosophy

in

Chemistry

May 2019

This dissertation has been examined and approved in partial fulfillment of the requirements for the degree of Doctor of Philosophy in Chemistry by:

Dissertation Director, Erik Berda, Professor of Chemistry

Christine Caputo, Associate Professor of Chemistry

Margaret Greenslade, Professor of Chemistry

John Tsavalas, Professor of Chemistry

Corinne Lipscomb, 3M Company

On April 11, 2019

Original approval signatures are on file with the University of New Hampshire Graduate School.

DEDICATION

To my Dad, who encouraged curiosity and independence above all else.

ACKNOWLEDGEMENTS

Berda – You gave me every opportunity I asked for and let me wrestle with the consequences in a supportive environment. I grew tremendously because of this and I am emphatically grateful.

Committee – Each of you regularly and meaningfully invested in my education. You challenged me when I was afraid to challenge myself. Thank you.

Berda Group Family and Cohort – You know about disappearing small stir bars, the noisy v.s. not noisy downstairs coffeemaker, and double cookie day at lunch talk. You know about something called an air handler being down. Some of you have trophy dinosaurs. You're a remarkably vivid, caring, and generous group; thanks for sharing this experience with me.

Students – Teaching and mentoring are the most gratifying things I have ever done. Thank you.

Cindi, Laura, Pat – I am not sure how you are possibly so helpful, but I hope to learn from the example.

Family and friends – I'm not sappy. You're sappy!

Lastly, I would like to thank the Army Research Laboratories for the funding to make this research possible though grant number W911NF-14-1-0177.

TABLE OF CONTENTS

DEDICATION.....	iii
ACKNOWLEDGEMENTS.....	iv
LIST OF SCHEMES	ix
LIST OF FIGURES	x
LIST OF TABLES	xv
ABSTRACT.....	xvi
Chapter I: Introduction	xviii
Motivation to Develop Complex Synthetic Macromolecules.....	xviii
The Role of Controlled Radical Polymerizations	xviii
Sequence Control.....	xx
Intramolecular Cross-linking	xxi
Evaluating SCNP Morphology	xxii
Orthogonal Folding Approach.....	xxvi
Intrachain Polymerization Approach.....	xxvii
Early Examples of Complex SCNP Designs	xxvii
Chapter II. Understanding and Promoting Intramolecular ATRC.....	29
Introduction	29
ATRC as a Versatile Handle for Post-Polymerization Modifications	29
Intramolecular ATRC: Role of Reducing Agent	31
Intramolecular ATRC: Interaction of Substrate, Ligand, and Process Conditions	32

Research Objective.....	33
Results and Discussion.....	33
Experimental Design	33
NMR Methods for Monitoring Extent of Incorporation and Disproportionation	34
ATRC of PA.....	42
ATRC of PB, p(MMA-co-PhBrema).....	49
ATRC of terpolymer PAB.....	55
Conclusions.....	58
Chapter III. Sequencing ATRP and ATRC to form advanced SCNP architectures	60
Introduction	60
Research Objective.....	62
Results and Discussion.....	63
Comparing ATRC in the presence of MMA or MeBrema	63
Kinetics of and Livingness of ATRP/C.....	66
Comonomer Graft System.....	67
Coupled Brush System.....	68
Kinetics of ATRP/C.....	69
Conclusions	72
Chapter IV. Experimental.....	73
General Experimental Section	73
Solvents.....	73

Reagents	73
Reactions.....	74
Flash Chromatography	75
Instrumentation	75
Detailed Experimental Section	80
Syntheses in Chapter II.....	80
Monomer Synthesis.....	80
<i>Monomer 1 (MeBrema)</i> ⁷¹	80
General Procedure for RAFT.....	82
General Procedure for Intramolecular ATRC	82
Cu(0)-free Control for Intramolecular ATRC.....	83
ATRC of a Terpolymer to Examine the Persistent Radical Effect	84
Syntheses in Chapter III.....	1
Preparation of Brushes and Hypergrafts	1
LIST OF REFERENCES.....	2
Appendices	20
Appendix A: Characterization.....	20
Polymer Samples	20
ATRC Products.....	29
Reaction Progress of NPA-2	35
Series A: Variations in L	38

Series B: Variations in L, Continuous Addition	45
Hyperbranched and Brush Architectures.....	53
Appendix B: Additional Reactions Not Described in this Dissertation.....	68
Dimerization by ATRC	68
SCNP <i>via</i> Thermal Diels-Alder Chemistry	69

LIST OF SCHEMES

Scheme 1. Systematic investigation of intramolecular ATRC.....	34
Scheme 2. Parent Polymer Synthesis	37
Scheme 3. Formation of SCNP with and without Cu ⁰ reductant.....	38
Scheme 4. ATRC of PB.....	49
Scheme 5. Synthesis of terpolymer PAB using RAFT. $f_{\text{MeBrema}} = 33.1 \text{ mol\%}$ $f_{\text{PhBrema}} = 38.1 \text{ mol\%}$, Mw = 15 kDa.....	55
Scheme 6 Reimagining p(MMA-co-MeBrema) as both an ATRP macroinitiator and SCNP precursor.....	60
Scheme 7. Formation of p(MMA-co-MeBrema-g-MeBrema) hypergrafted SCNP.....	63
Scheme 8. Reaction of PA under combined ATRP/C conditions in the presence of MMA and MeBrema to form NPA-MMA-MeBrema.	68
Scheme 9. The preparation of furan-incorporated Diels-Alder active <i>via</i> RAFT.....	71
Scheme 11. An intrachain thermal Diels-Alder reaction between furan functionalized parent polymers and bi- or tri- functional external cross-linkers was used to form SCNP.	71

LIST OF FIGURES

- Figure 1. Strategy for building star block copolymers using a core-first approach and ATRP. Reprinted with permission from Ref. 13. Copyright 2016 American Chemical Society. .xix
- Figure 2. Bottle brush polymers have a wide variety of uses. Amphiphilicity or other self-assembly mechanisms may be incorporated. Reproduced from Ref. 14 with permission from The Royal Society of Chemistry.....xix
- Figure 3. Photoswitchable foldamer design by Wooley and coworkers. Adapted from reference 19; Copyright 2000 National Academy of Sciences.....xx
- Figure 4. ATRAC method for preparing periodic vinyl copolymers. Reproduced from Ref. 24 with permission from The Royal Society of Chemistry.....xxi
- Figure 5. Generic representation of the collapse of a parent polymer to a single-chain nanoparticle.xxi
- Figure 6. GPC evidence of a decrease in hydrodynamic radius after intramolecular cross-linking. xxiii
- Figure 7. GPC-MALS trace of externally cross-linked Diels-Alder system. A maximum degree of collapse was observed when the maleimides were in a 9:1 ratio with furan groups on the polymer. Reproduced from Ref. 34 with permission from The Royal Society of Chemistry. xxiv
- Figure 8. SCNP tend to have elongated structures with local cross-links (left) rather than the compact and globular morphology which would be expected if coupling between pendants was entirely random (right).xxv
- Figure 9. GPC MALS trace of a copolymer capable of multiple orthogonal folding mechanisms. It becomes denser after each transformation. Reproduced from Ref. ⁴⁰ with permission from The Royal Society of Chemistry..... xxvii

Figure 10. Combination of sequence-controlled polymerizations and intramolecular “click” chemistry was used to sequentially control folding. Adapted with permission from Ref. ⁴⁸ . Copyright 2014 American Chemical Society.....	xxviii
Figure 11. Single-chain nanoparticle design with a chiral internal structure and hydrophilic grafts. Reproduced from Ref. ⁵³ with permission from The Royal Society of Chemistry.....	xxviii
Figure 12. Products of intramolecular cross-linking.....	30
Figure 13. Mechanistic relationship between ATRP and ATRC.....	31
Figure 14. Symmetrical block copolymer synthesis by ATRC.....	31
Figure 15. Modular monomer design.....	34
Figure 16. ¹ H NMR can be conveniently used to track the desired ATRC product as well as alkyl and vinyl byproducts caused by competition of disproportionation. To do so, the integration of the signals representing H _A , H _{A'} , and H _V can be compared with that of the inert ethylene spacer, H _B	36
Figure 17. ⁷⁴ k _{ATRP} values measured by Matyjaszewski et al. under the following reaction conditions: EtBrI/B/Cu(I)Br/MeCN/22 °C.....	37
Figure 18. NMR spectra comparing ATRC with (left) and without (right) a Cu(0) reductant. The integration of resonances H _V , H _A , and H _B is used to calculate the extent of coupling and disproportionation.	39
Figure 19. The formation of an organometallic species may promote disproportionation.	40
Figure 20. Multi-detection GPC comparing parent polymers PA-1 and PA with their respective SCNP. NPA-1: Cu(I)Br/PMDETA, x _{c'} = 2%; NPA-2: Cu(I)Br/PMDETA/Cu(0), x _{c'} = 10%.	41
Figure 21. Tracking coupling and disproportionation of ATRC by ¹ H NMR.	42
Figure 22. ¹ H NMR array comparing SCNP created in ATRC of PA (bottom, black); L = PMDETA, TPEN, and TPMA for NPA-2 (blue), NPA-3 (green), and NPA-4 (top, red).	44

Figure 23. Vinyl region of the ^1H NMR spectra of series A. Top to bottom: NPA-4 (L = TPMA), PA, NPA-3 (L = TPEN), NPA-2 (L = PMDETA).	45
Figure 24. Series A GPC traces and M-H-S plots comparing the morphologies of SCNP products using PMDETA, TPEN, and TPMA catalyst systems. The activity of the ligand, approximated by k_{ATRP} , was positively correlated with increased coupling efficiency, leading to more compact structures.	47
Figure 25. Bayesian projection of DOSY plots for Series A. The x-axis is normalized such that the diffusion coefficient of THF is 0.0. Molecular volume decreases from left to right. Top to bottom: NPA-3, NPA-2, NPA-1, PA.	48
Figure 26. The GPC-MALS traces of PB (solid line), and NPB-3 before (small dashed line) and after (long dashed line) rigorous purification to remove low molecular weight species. .	50
Figure 27 GPC-MALS Traces of Series B (standard procedure at 0.25 mg/mL).....	50
Figure 28. ^1H NMR array comparing SCNP created in ATRC of PB prepared using a continuous addition procedure. $\text{Cu(I)Br/L/Cu(0)}/1 \text{ mg mL}^{-1}/1:1 \text{ MeCN:THF}/55 \text{ }^\circ\text{C}$; L = PMDETA, TPEN, and TPMA for NPB-2, NPB-3, and NPB-4, respectively.	51
Figure 29. GPC-MALS trace of CA-NPB-2, 3 and 4 (continuous addition procedure).	52
Figure 30. M-H-S plot of Series B (standard procedure).	53
Figure 31. ^1H NMR of terpolymer PAB_{15} . The broad signal in this case is due to a highly concentrated sample.....	56
Figure 32. ^1H NMR of SCNP made from terpolymer PAB.	57
Figure 33. GPC-MALS traces of PAB and NPAB.	58
Figure 34. Preparation of a diverse set of architectures from a common substrate under a unified set of reaction conditions by sequencing ATRC with ATRP.	61
Figure 35. SCNP with low DP “hyperbranched” cross-links.	62
Figure 36. Preparation of brush polymers or “knit” SCNP using MMA or inimer.	64
Figure 37. ^1H NMR of Hypergrafted SCNP NPA-MeBrema4 (4 eq. inimer).	65

Figure 38. ^1H NMR of Hypergrafted SCNP NPA-MeBrema10 (10 eq. inimer).	65
Figure 39. The fit of the intrinsic viscosity to the MALS trace for PA (blue) and NPA-MeBrema10 (red).	66
Figure 40. Extending the arms of hyperbranched chains was used to test for the presence of “live” halogenated chain ends.....	66
Figure 41. Kinetic plot of ATRP/C showing reasonable fidelity to the pseudo first order kinetics usually observed in ATRP.....	67
Figure 42. Coupled brush SCNP.	68
Figure 43. GPC-MALS of coupled brush SCNP.	69
Figure 44. DOSY Calibration Curve prepared for narrowly disperse PS standards in THF-d6. .	76
Figure 45. DOSY Calibration Curve prepared for narrowly disperse PS standards in DMF-d7. .	77
Figure 46. Determination of dn/dc of a PMMA research sample using the multiple injection volumes method.....	79
Figure 47. An illustration of the substantial physical difference between freely diffusing functional groups (left) and those tethered to a polymer backbone (right). When external cross-linkers are used for systems like that on the right, they should be used in a 2 to 3 fold excess to adjust their stoichiometry to account for the local concentration.	69
Figure 48. Key variables in the design of SCNP via thermal Diels-Alder reactions.....	70
Figure 49. FMA incorporation of the parent chains was calculated by comparing the integrations of the ^1H NMR signals for peak E representing methyl protons in the MMA moieties and A representing a furfuryl proton in the FMA moieties.	73
Figure 50. A focused comparison of the effects of varying cross-linker for polymer B.	74
Figure 51. Array of GPC-MALS traces showing the collapse to form SCNP using rigid or flexible di- or tri- functional cross-linkers with 10–40 mol% furfuryl methacrylic parents.	75
Figure 52. ^1H NMR of furan-functionalized methacrylate parent polymers. Clockwise from top left: P-A, P-B, P-C, and P-D.....	76

Figure 53. A syringe pump is used to slowly add concentrated polymer solution. 77

Figure 54. Polymer concentrations can be increased ten-fold using the continuous addition procedure, with higher degree of collapse being observed at higher concentrations without the appearance of multi-chain aggregates..... 78

LIST OF TABLES

Table 1. The efficiency and selectivity of the intramolecular ATRC of PA to form SCNP.....	39
Table 2. Progression of coupling and disproportionation in a typical ATRC of PA.	43
Table 3. Series A Polymer Properties.....	46
Table 4. Series B-CA DOSY	54
Table 5. Series B Polymer Properties.....	54
Table 6. Characterization of PAB and NPAB.....	58
Table 7. Comparison of GPC characterization data for higher molecular weight brushes.	69
Table 8. Summary of Properties of Polymers and Brushes or SCNP products of ATRP/C.....	71
Table 9. Diffusion coefficients used to DOSY calibration curve, above.....	76
Table 10. Diffusion coefficients used to DOSY calibration curve, above.....	77

ABSTRACT

ATRC PROCESSES AND ARCHITECTURES AS TOOLS FOR ADVANCING THE COMPLEXITY OF SINGLE-CHAIN POLYMERIC NANOPARTICLES

by

Elizabeth R. Bright

Atom transfer radical coupling (ATRC) is gaining recognition for its utility in building complex polymeric architectures because it features efficiency, a wide range of compatible substrates, and a lack of byproducts. These qualities are especially desirable in applications requiring intramolecular cross-linking as in the synthesis single-chain nanoparticles (SCNP).

This dissertation aims to (I) provide motivation and context for developing ATRC technology for intramolecular cross-linking, (II) provide guidance into the impact of catalyst selection and substrate on reaction efficiency and morphology, and (III) demonstrate the possibility to sequence intrachain ATRC with ATRP to create advanced SCNP architectures.

Chapter II describes the preparation of SCNP from parent polymers containing alkyl or benzyl bromide ester pendants using ATRC catalyzed by copper halides complexes. Tri- or tetradentate alkyl or pyridyl amines (PMDETA, TPEN, and TPMA), which tune the redox potential of the Cu(I)/Cu(II) system, were directly compared. Coupling efficiency was positively correlated with the k_{ATRP} of the respective catalyst systems. However, PMDETA complexes afforded greater control as evidenced by lower polydispersity. In the case of alkyl halide pendants, selectivity for coupling over disproportionation systematically decreased under conditions designed to increase the concentration of Cu^I/L. Polymers with benzyl bromide pendants, which cannot disproportionate, tended to produce high molecular weight products, even in ultradilute solutions (0.25 –1.0 mg/mL).

Chapter III describes the preparation of SCNP from parent polymers capable of initiating intra-chain polymerization by ATRP under conditions favoring termination by coupling. Because of the wide variety of compatible monomers that have been well-established for ATRP systems, the ATRP/C framework both simplifies reaction procedures (one pot polymerization and coupling strategies are feasible) and imparts handles with which to control both architecture and functionality. To demonstrate this potential, model simple brushes and hyperbranched examples were prepared. SCNP with the hyperbranched motif were remarkably dense, a result which demonstrates the potential to facilitate more globular SCNP structures using modifications of intrachain polymerizations. Methacrylic brush arms, which are not non-ATRC active, could be induced to couple by adding 5 equivalents of styrene under the shared ATRP/C conditions. In addition, it was determined that hyperbranched SCNP retain “living” ω -ends which may be initiated to perform post-collapse polymerizations. A model styrene example is presented; despite occurring in an ultradilute solution, the polymerization maintains fidelity to pseudo-first order kinetics.

In sum, there is currently a great impetus for pushing the boundaries of structural and functional complexity that can be designed using the single-chain nanoparticle motif. Atom transfer radical chemistry is a particularly versatile example and it is my hope that this work facilitates the creation of new creative and functional designs.

Chapter I: Introduction

Motivation to Develop Complex Synthetic Macromolecules

In nature, the ability of a polymer to perform a task depends on a combination of its chemical composition and morphology. Together, these tightly controlled structural features create remarkably specific chemical associations. This specificity is key because, unlike the isolated models of chemistry built in laboratory reactors, biological macromolecules operate in complex systems. Further, conditions such as solvent, temperature, and pH are controlled at a systems level rather than optimized for individual reactions. Despite this, biomacromolecules regularly and often dramatically outperform synthetic analogues in providing structural integrity, energy storage, or catalytic activity.¹⁻⁴

Given the breadth of these capabilities, it is unsurprising that so much research is dedicated to understanding structure-function relationships in biopolymer chemistry. For their part, chemists and materials scientists have been developing increasingly sophisticated synthetic polymer architectures with the goals of understanding the fundamental principles governing biopolymer processes (e.g. protein folding) and advancing these understandings to an application stage (e.g. as catalysts, drug delivery systems, or nanoreactors).

The Role of Controlled Radical Polymerizations

The development of versatile controlled radical polymerization techniques, especially atom transfer radical polymerization (ATRP) and reversible addition/fragmentation chain transfer polymerization (RAFT), has been one of the most impactful achievements to this end.^{56,78} The combination of control over molecular weight and polydispersity, functional compatibility, and control over composition has made sophisticated block and graft copolymer chemistry possible. Multi-functional initiators or grafting approaches can be used to create controlled topological architectures such as star polymers or bottle brushes. Polymers with these or similarly distinct

structures tend to have special and unexpected properties, some of which are technologically useful.^{9–12} For example, bottle brush drug delivery systems tend to outperform their linear counterparts. The “living” nature of controlled radical polymerizations makes combinations of structural control and block copolymer technology possible, as in the star block¹³ or brush block¹⁴ architectures shown in Figure 1 and Figure 2.

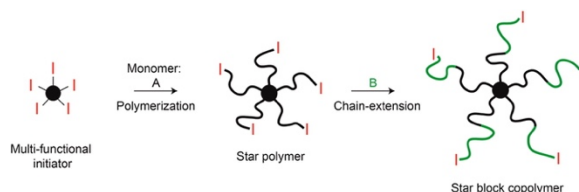


Figure 1. Strategy for building star block copolymers using a core-first approach and ATRP. Reprinted with permission from Ref. 13. Copyright 2016 American Chemical Society.

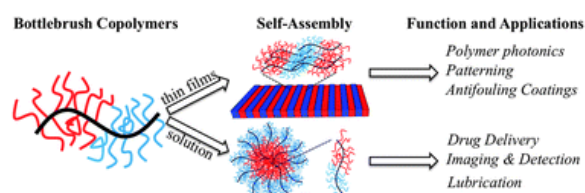


Figure 2. Bottle brush polymers have a wide variety of uses. Amphiphilicity or other self-assembly mechanisms may be incorporated. Reproduced from Ref. 14 with permission from The Royal Society of Chemistry.

Because these polymerizations are compatible with a wide range of monomers and functional groups, it is possible to use chemically distinct monomers for the blocks. This property is most often exploited to make frustrated systems or amphiphiles with self-assembly behavior, as seen in block copolymer micelles.^{15,16} However, the possibilities do not end at hydrophobic/hydrophilic functionalities. For example, monomers can be designed to form predictable motifs on the basis of bulk, hydrogen bonding, or chirality.¹⁷ These so-called foldamer designs are analogous to the secondary structure of proteins.¹⁸ Dynamic chemistries can be used to create switchable morphologies. A particularly illuminating example of this is the peptide-based photoswitchable loop designed by Wooley and coworkers (Figure 3).¹⁹ When triggered by visible light, the bis(para-acetamido)azobenzene derivative linker reversibly isomerizes, causing a helix–

coil transition (Figure 3). Facile access to amphiphilic or otherwise asymmetric and self-assembling or dynamic motifs represents an important step to mimicking natural processes.

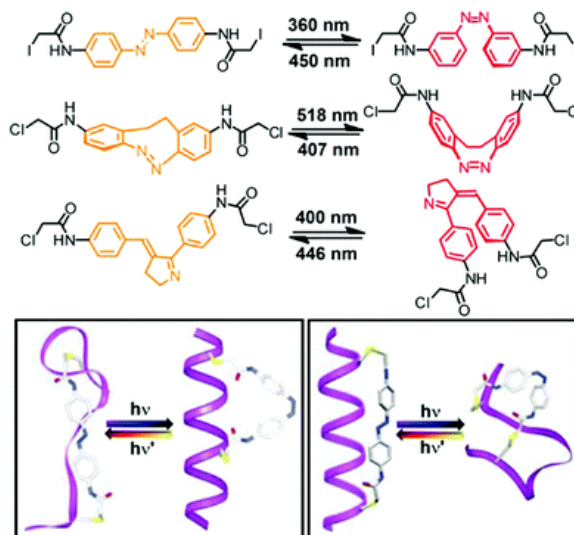


Figure 3. Photoswitchable foldamer design by Wooley and coworkers. Adapted from reference 19; Copyright 2000 National Academy of Sciences.

Sequence Control

While self-assembly processes are important, other methods of controlling solution architecture are necessary to form robust structures. True architectural control relies on the development of efficient sequence-controlled polymerization strategies, which is a significant challenge. The majority of attempts at sequence control come from traditional step-growth polymerizations such as polycondensations, however, the development of more functionally tolerant approaches is necessary. This work often takes the form of ring-opening,²⁰ acyclic diene metathesis,²¹ or “click” reactions²² to create periodic copolymers. Radical step growth mechanisms are gaining relevance in this landscape. For example, Li and coworkers recently reported the synthesis of periodic vinyl copolymers using atom transfer radical addition and coupling (ATRA and ATRC, respectively).²³ In their system, two alkyl halides first combined using

ATRA, creating a biradical AB block which combines through ATRC to form repeating ABBA repeats (Figure 4).

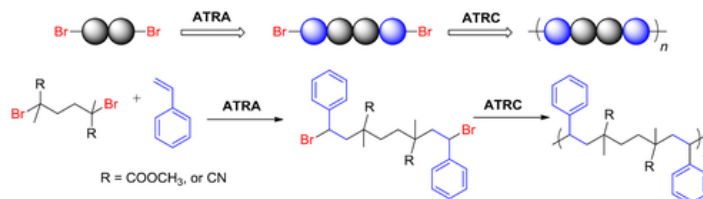


Figure 4. ATRA/C method for preparing periodic vinyl copolymers. Reproduced from Ref. 24 with permission from The Royal Society of Chemistry.

Intramolecular Cross-linking

The capability to efficiently and precisely select multiple functional group placements on a chain promises to be revolutionary for both architectural and functional control. Architectural control will come from a system of intramolecular cross-linking between functional monomer units. Regardless of cross-linking chemistry, these reactions come with a unique set of challenges. These may be studied in isolation using the single-chain nanoparticle motif, which generally consists of a copolymer chain with cross-links between pendants (Figure 5). Although the concept was first reported in the 1960's by Kuhn and Balmer, SCNP chemistry did not garner significant research interest until controlled radical polymerizations dramatically opened the design space.²⁵

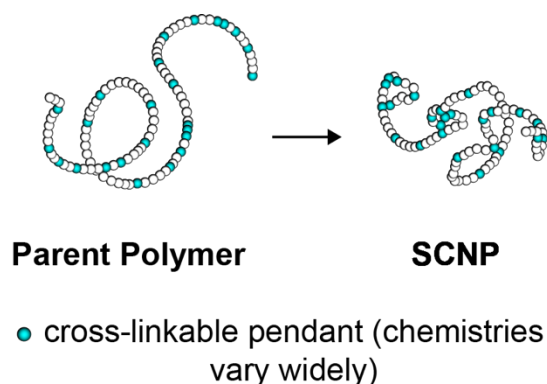


Figure 5. Generic representation of the collapse of a parent polymer to a single-chain nanoparticle.

As these intramolecular cross-links form, the hydrodynamic radius of the macromolecule decreases. This collapse is analogous in form and, ideally, function to the coil-to-globular transition seen in protein folding that results in molecules capable of advanced processes like molecular recognition or catalysis. The parent polymers are often prepared using controlled radical polymerizations because their control over chain length and compatibility with a wide range of functional monomers offer significant advantages. First, control over the radius and size distribution of the final nanostructures is primarily controlled by manipulating the length of the parent chain. Second, broad chemical compatibility maximizes the range of possible post-polymerization modifications, creating a large design space for architectural modifications such as grafting or cross-linking and installations of functional pendants such as catalytic centers or fluorophores.

While, in theory, any cross-linkable comonomer system may be used, practical considerations govern the choice of folding mechanism. Regardless of the backbone chemistry, the synthesis of SCNP is typically conducted in ultra-dilute solutions to prevent interchain cross-linking. Therefore, the cross-linking chemistry must be efficient. Also, purification can be challenging and typically depends on either precipitation or dialysis. In this regard, byproduct-free reactions have a significant advantage. Within these parameters, SCNP have been prepared using a wide variety of covalent,²⁶ non-covalent,²⁷ and coordination motifs.²⁸ These have been recently summarized by our group and others.^{29,30}

Evaluating SCNP Morphology

GPC

As in other polymer work, gel permeation chromatography (GPC) is heavily used in SCNP characterization to study the size distribution of a sample. Retention time is calibrated against molecular weight for a given column set using well-defined polymer standards. Because

intramolecular cross-linking decreases the hydrodynamic volume of the chain, SCNP products elute from GPC columns at longer retention times than do their parents (Figure 6). Therefore, SCNP products have lower relative molecular weights than those of their respective parent polymers. The ability to sort based on size is especially powerful when coupled with other instrumentation to perform techniques like multi-angle light scattering (MALS), UV detectors, and viscometers, which would otherwise result in an average value rather than a distribution.

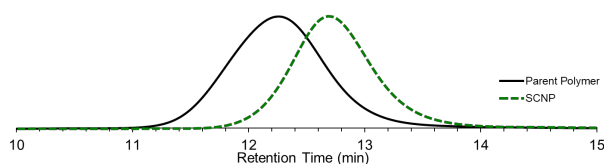


Figure 6. GPC evidence of a decrease in hydrodynamic radius after intramolecular cross-linking.

Light Scattering

Light scattering is very useful in SCNP characterization because it gives insight into molecular weight, form factor, and polydispersity in solution. Molecular weight data from light scattering depends on the intensity of scattered light and the refractive index increment dn/dc of a given polymer solution.³¹³² Therefore, it contributes an absolute molecular weight which may be meaningfully compared to the apparent molecular weight generated using GPC.³³ The effect of cross-linking chemistry, functional incorporation, chain length, and other parameters on size have been systematically studied using GPC with inline multi-angle light scattering. Some of these results are generalizable. For instance, regardless of cross-linking approach, functional incorporations in the range of 10–40 mol% tend to be the most efficient. Multi-chain aggregation, which results in poor solubility and high molecular weight species, and coupling between near neighbors, which does not substantially affect volume, is especially dominant in parents with functional monomer incorporations. Due to the dilute solution requirement, designs which rely on external cross-linkers tend to require them in a 3 to 8 molar excess of functional pendant to maximize collapse efficiency (Figure 7).³⁴

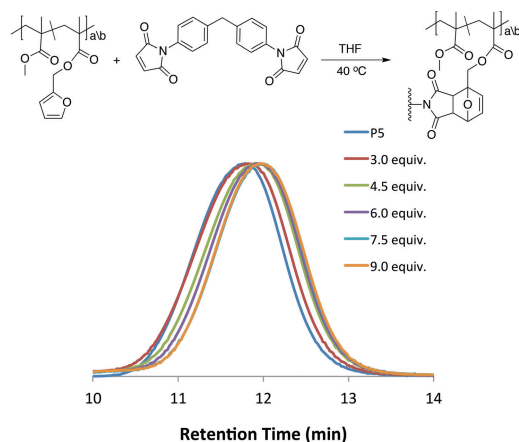


Figure 7. GPC-MALS trace of externally cross-linked Diels-Alder system. A maximum degree of collapse was observed when the maleimides were in a 9:1 ratio with furan groups on the polymer. Reproduced from Ref. 34 with permission from The Royal Society of Chemistry.

Knowledge of these properties for a given system is important beyond evaluating the degree of collapse. Deeper morphological insight, such as density and form factor, can be studied by examining how molecular weight scales with size for a given sample or exploiting angular dependence in multi-angle light scattering (MALS) to determine the radius of gyration (R_g). However, most single-chain nanoparticles are in the sub 10-nm size regime. For this reason, accurate determination of R_g requires the small angles only available in x-ray or neutron scattering (SAXS or SANS) techniques. Although SANS and SAXS are powerful methods for studying particles with radii below 10 nm, the required instrumentation is not widely available.

Viscometry

Fortunately, evidence of this scaling behavior can also be observed using GPC with an online viscometer and multi-angle light scattering (MALS) detector. Intrinsic viscosity, the contribution of the solute to the solvent's viscosity (Equation 2), can be used directly to calculate hydrodynamic radius, R_h . The intrinsic viscosity and molecular weight are related by the Mark-Houwink Equation (Equation 3).

$$\eta_i = (\eta - \eta_s) / \eta_s$$

Equation 1. Incremental viscosity, where η is the measured viscosity and η_s is that of the solvent alone.

$$[\eta] = \lim_{c \rightarrow 0} \left(\frac{\eta_i}{c} \right)$$

Equation 2. Intrinsic viscosity, where η is the sample viscosity and c is concentration.

$$[\eta] = K_{\eta} M^a$$

Equation 3. Mark-Houwink Equation. The Mark-Houwink parameters, K and a , vary based on solvent quality and the polymer architecture; $[\eta]$ is intrinsic viscosity and M is molecular weight.

$$R\eta = \sqrt[3]{\frac{3M[\eta]}{10\pi N_A}}$$

Equation 4. Einstein–Simha Relation, where N_A is Avogadro's number and $R\eta$ is the hydrodynamic radius.

The scaling exponent, a , varies with the quality of the solvent and the polymer architecture. Its value is 0.5 for linear chains in a theta solvent. More extended chains have larger a -values, up to 2 in the case of a rigid rod conformation, while more globular morphologies lead to a -values in the range of 0.3. This is true for other dense morphologies, for example, a can be 0.3–0.5 for hyperbranched polymers with long spacers. Though it varies by chemistry, generally speaking, parent polymers used in SCNP work have values in the range of 0.8 to 1.^{12,35}

Trends in intrinsic viscosity can be used to assess the collapse efficiency and final morphology in SCNP. Upon intramolecular cross-linking, the intrinsic viscosity tends to decrease with the corresponding increase in density as it becomes more like a uniform sphere. In this limiting case, it reaches a value of $5/2$ divided by density.

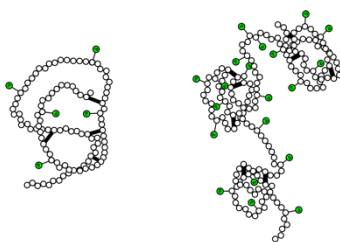


Figure 8. SCNP tend to have elongated structures with local cross-links (left) rather than the compact and globular morphology which would be expected if coupling between pendants was entirely random (right).

The relationship between molecular weight, cross-link density, and hydrodynamic size of various SCNP chemistries have been investigated extensively by Pomposo and coworkers. Scaling behavior has been studied by compiling SANS and SAXS data.³⁵ They have also systematically compared trends in the intrinsic viscosities of synthetic SCNP with those uncovered by molecular dynamics simulations. Both approaches have generated evidence that typical single-chain nanoparticles (those prepared by the intramolecular cross-linking of statistical copolymers) do not take a compact, globular shape. Rather, the trends in their morphology and density are more closely comparable to those seen in intrinsically disordered proteins: local globules distributed within a generally open chain (Figure 8).³⁶⁻³⁸ This relative lack of density is one of the key architectural challenges in SCNP. Using highly efficient cross-linking chemistries at finely tuned incorporations is insufficient to create dense structures. The most impactful approaches must modify chain mobility or segmental length between cross-linkable units, the primary drivers behind the statistics of cross-linking.

Orthogonal Folding Approach

Systems designed with multiple orthogonal covalent cross-linking chemistries have been more compact than those designed using only one comparable cross-linker type, even at identical overall functional incorporations.^{39,40} For example, Chao and coworkers designed a system with three distinct cross-linking capabilities: supramolecular, anhydride-amine, and thiol-ene click chemistry. These were triggered sequentially, and hydrodynamic volume decreased at each step (Figure 9).⁴⁰ Each step in a sequential folding method effectively brings the next cross-linkable pendants in closer proximity, and the ultimate product's volume was 70% smaller than that of the parent polymer. However, the requirement for performing multiple transformations in ultradilute solutions can result in challenging purification and very low yields.

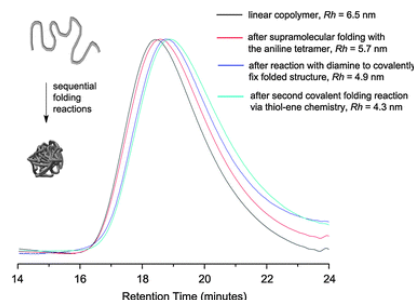


Figure 9. GPC MALS trace of a copolymer capable of multiple orthogonal folding mechanisms. It becomes denser after each transformation. Reproduced from Ref. ⁴⁰ with permission from The Royal Society of Chemistry.

Intrachain Polymerization Approach

By nature, intrachain polymerizations also modify segmental mobility and chain length and can therefore become a route to globular structures. A diverse set of SCNP prepared through intrachain polymerization is available in the literature.^{41–47} This strategy is particularly useful in overcoming restricted motion when using parent polymers with relatively rigid primary backbones. In theory, with the proper monomer choice, intrachain polymerization could also become a versatile way to functionalize cross-links.

Early Examples of Complex SCNP Designs

The confluence of these developments has created the opportunity and demand to attempt more complex designs. For example, Lutz and Roy used a combination of sequence-controlled polymerization and orthogonal “click” chemistries to prepare asymmetric SCNP (Figure 10).⁴⁸ Their parent polymer system consisted of an inert styrene backbone with a pentafluorophenyl-functionalized maleimide on one side, which reacts with an external amine cross-linker, and protected propargyl maleimide on the other which couples with a second propargyl group upon deprotection.

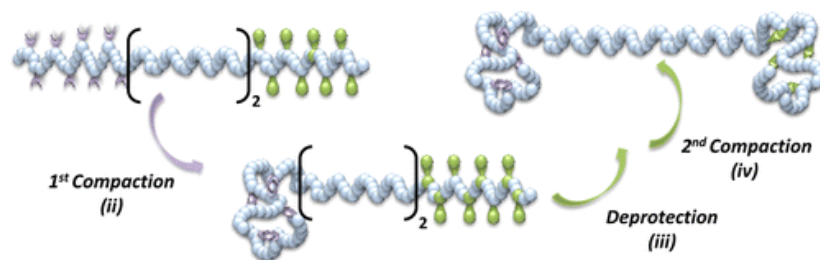


Figure 10. Combination of sequence-controlled polymerizations and intramolecular “click” chemistry was used to sequentially control folding. Adapted with permission from Ref. ⁴⁸. Copyright 2014 American Chemical Society.

Foldamer chemistry has also been instructive to the creation of single-chain nanoparticles with secondary structural characteristics.^{29,49,50} This potential is well-illustrated by a system designed by the Meijer group (Figure 11) which uses a chiral motif (3,3'-bis(acylamino)-2,2'-bipyridine-substituted benzene-1,3,5-tricarboxamide) in conjunction with hydrophilic polymer grafts.^{51,52} Examples of grafted SCNP are relatively rare. In this case, the hydrophilic grafts shown here are used to introduce finer morphological features – in poor solvent, the structure of these SCNP are reminiscent of globular proteins with a hydrophobic pocket.⁵³ The chiral motif makes it possible to study these changes using circular dichroism.

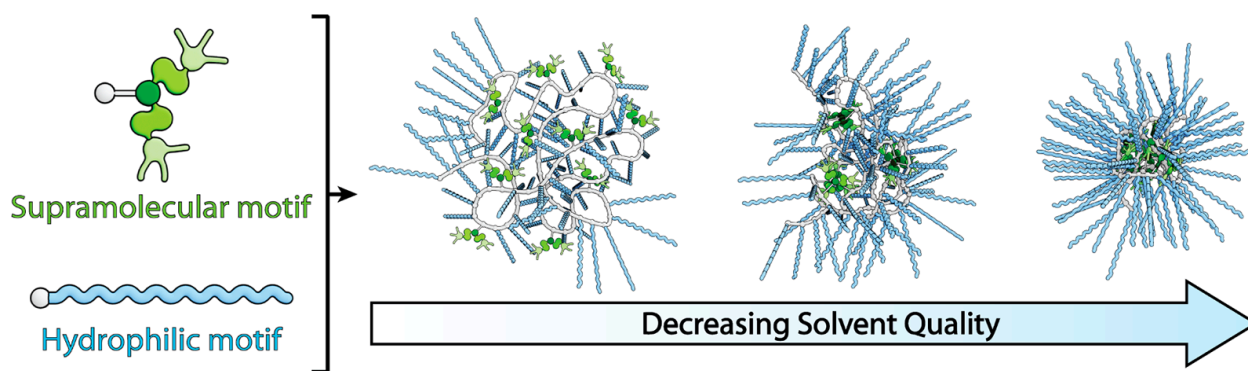
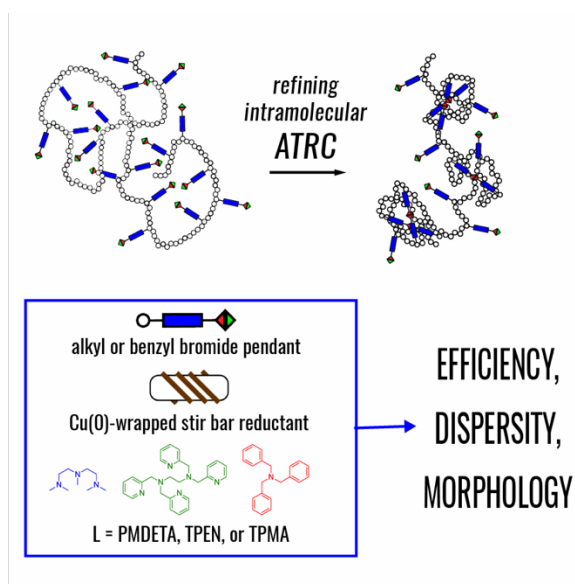


Figure 11. Single-chain nanoparticle design with a chiral internal structure and hydrophilic grafts. Reproduced from Ref. ⁵³ with permission from The Royal Society of Chemistry.

Chapter II. Understanding and Promoting Intramolecular ATRC



Introduction

ATRC as a Versatile Handle for Post-Polymerization Modifications

Progress toward truly structurally defined soft nanomaterials is fueled by rapid advancement in controlled polymerizations and an increasingly sophisticated toolbox of compatible organic transformations. Many current examples are designed for applications in medicine and biotechnology such as targeted drug delivery or sensing. Post-polymerization modifications, especially “click” reactions and similarly efficient chemistries, are at the heart of the advancement of these technologies because they are used heavily to both install functional groups and control architecture. They can also be used to prepare diverse species from a common precursor and minimize functional incompatibility.

Architectural control remains a high-priority challenge. The power of the connection between form and function in proteins is undeniable. The stable globular designs characteristic of tertiary protein structures are reliant on robust intramolecular cross-linking strategies. This is especially challenging because of the entropy penalty of forming a conserved structure in solution,

however, the scope of these reactions has rapidly expanded in the past decade with the development of macrocycles and SCNP, which are prepared using end-to-end and pendant-to- pendant coupling, respectively (Figure 12).^{54,55} A range of covalent, dynamic-covalent, and non-covalent cross-linking strategies is well-documented in the recent literature.

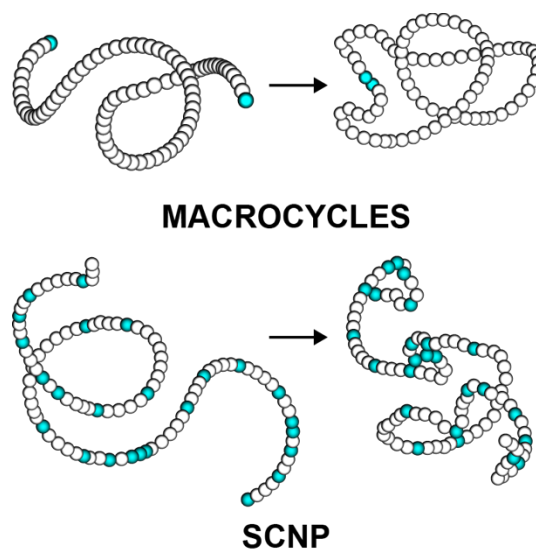


Figure 12. Products of intramolecular cross-linking.

Among these, atom-transfer radical coupling (ATRC) has the unique potential to become a unifying methodology for post-polymerization modifications, especially grafting and cross-linking. However, it is best known as the undesirable product of termination by coupling during atom-transfer radical polymerizations (ATRP). Their mechanistic relationship is shown in Figure 13. The reductant is an adjunct which can be used to lower the necessary catalyst concentration or introduce a degree of oxygen tolerance in ATRP or promote coupling in ATRC. As a synthetic tool, it shares many of the advantages of ATRP: it can be performed on a wide range of alkyl halide substrates, is tolerant to many functional groups, and can be adapted to suit various conditions (low temperatures, aqueous solutions, and minor oxygen exposure).

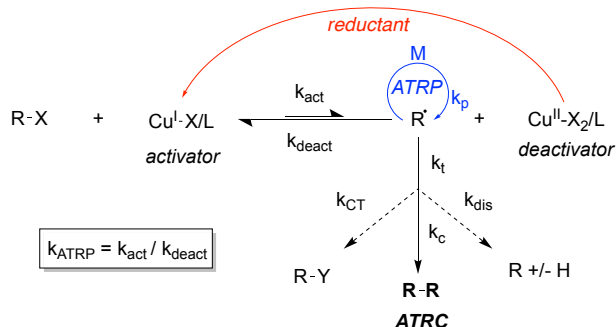


Figure 13. Mechanistic relationship between ATRP and ATRC.

Because it can be used to directly couple the halogenated ω -ends of ATRP products, ATRC is particularly adaptable for the preparation of telechelic, functionally diverse,^{56–58} and/or symmetrical block copolymers (Figure 14).^{59–61} The first report of its synthetic utility and surprising efficiency came from Fukuda and coworkers in 2002.⁶² Using ATRC, 90% of bromo-terminated polystyrene chains could be coupled, thereby doubling their molecular weight in a controlled fashion, in a ten minute reaction. Soon thereafter, Yagci demonstrated its utility in forming aldehyde, alcohol, carboxylic acid, or amine-functionalized telechelic chains.⁶³ More recently, its broad compatibility with copper-mediated polymerizations (CMP) and atom transfer radical addition (ATRA) conditions have been exploited in higher-order sequential polymerization-coupling strategies.^{23,64} Because it is also efficient and byproduct-free, it is a good candidate for intramolecular cross-linking in applications like the synthesis of well-defined macrocycles and single-chain nanoparticles.^{54,65–67}

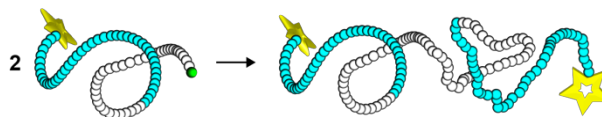


Figure 14. Symmetrical block copolymer synthesis by ATRC.

Intramolecular ATRC: Role of Reducing Agent

In ATRP, the lower valent metal species ($\text{Cu}^{\text{I}}/\text{L}$) serves an important role in limiting the number of radicals produced at a given time, thereby controlling the polymerization. As a

consequence, high concentrations of this deactivating species (in relation to the corresponding activator, $\text{Cu}^{\text{I}}/\text{L}$) suppress termination by ATRC. Although “classical” ATRP conditions have been used to couple low molecular weight (~ 1 kDa) polystyrenes in the absence of monomer, these procedures are not popular. More typically, a secondary reducing agent is added to regenerate the activating Cu^{I} complex and thereby increase the concentration of radicals. Due to the persistent radical effect, most applications practically require a reducing agent to undergo efficient ATRC.^{5,68}

In analogy to activators regenerated by electron transfer, or ARGET, ATRP,^{69,70} the reducing agent may be organic or inorganic, most often ascorbic acid or zero-valent metals, respectively. Cu^0 is a popular choice because it is remarkably user-friendly: copper nanoparticles and wires are readily available, effective, and easy to separate from the reaction mixture. Relative to organic reducing agents, copper is less likely to participate in side reactions with monomers, initiators, or other adjuncts. It comproportionates with the deactivator to generate two Cu^{I} complexes (as in ATRP, the ligand is added in substantial excess, usually 5 times the molar concentration of the metal salt). It may also provide a convenient handle for controlling ATRC because copper wire can be wrapped around a magnet (such as a stir bar) which may be removed from solution without exposing the flask reaction to oxygen. Switchable procedures of this type could be used to streamline sequential polymerization and coupling strategies.

Intramolecular ATRC: Interaction of Substrate, Ligand, and Process Conditions

As in ATRP, ATRC is highly sensitive to the properties of the substrate (radical stability and propensity to chain transfer or disproportionation) as well as the catalyst system (k_{ATRP} varies over 8 orders of magnitude depending on the structure of the ligand). In addition, intramolecular cross-linking reactions are often performed under unusual reaction conditions (involving ultradilute solutions and/or semi-batch procedures) to avoid the formation of aggregates. These conditions reduce the coupling efficiency and affect the reaction stoichiometry, effectively

increasing the necessary equivalents of the metal salt and ligand. Both effects are consistent with other findings in SCNP literature, as described in Chapter I. In analogy to externally cross-linked systems, the increased catalyst requirement can be attributed to the considerable difference in halide concentration within the pervaded volume of the polymer chain and that of the overall solution. The results of the present study provide guidance in the selection of catalyst and reaction parameters for performing ATRC under such conditions.

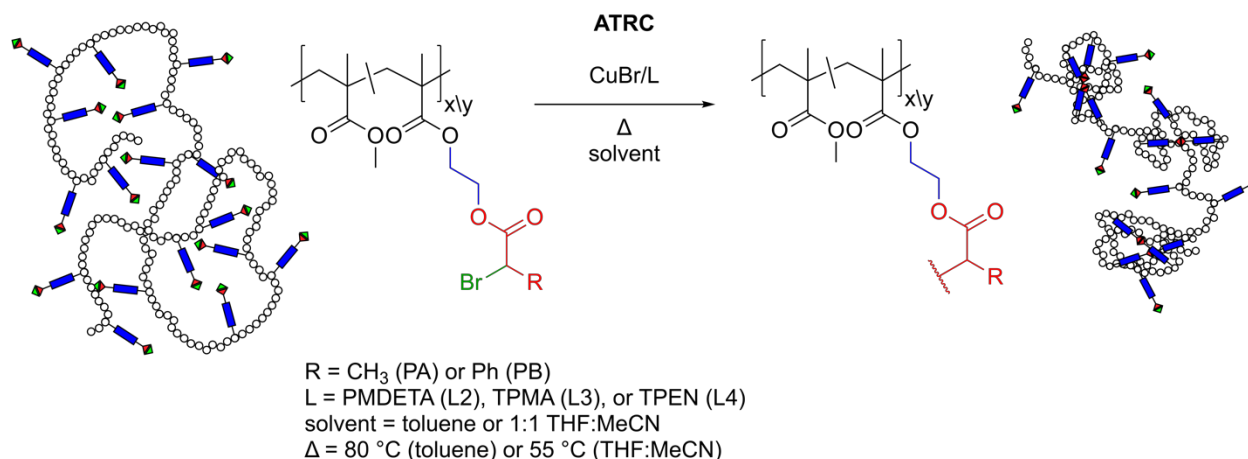
Research Objective

Although ATRC is most often an undesirable side reaction, it can be used advantageously as a post-polymerization modification to create more complex architectures (e.g. telechelic blocks, macrocycles, SCNP). Further, its innate compatibility with ATRP systems could greatly promote the development of facile sequential polymerization and coupling strategies. While the interaction between Cu-mediated ATRP components (including ligands, imitators, monomers, and substrates) is well-studied, relatively little is known about the ATRC process. This is especially true under conditions favoring SCNP formation, including ultra-dilute solutions or semi-batch procedures. The goal of this study is to understand the effect of catalyst and substrate on ATRC chemistry under these conditions and relate these to morphologies. We also aim to examine the possibility of the formation of an organometallic species as alternative mechanism for disproportionation under high concentrations of Cu(I)/L complex.

Results and Discussion

Experimental Design

The model system employed for this study, Scheme 1, is designed to complement and expand upon our recent demonstration of the feasibility of performing ATRC to form SCNP using methacrylic statistical copolymers with ATRC-active pendants.



Scheme 1. Systematic investigation of intramolecular ATRC.

NMR Methods for Monitoring Extent of Incorporation and Disproportionation

The ATRC-active comonomer, shown in Figure 15, is modular by design. It consists of a methacrylic backbone coupled to a pendant ethylene spacer and terminated by a methyl or phenyl bromopropionate. The ester, which activates the carbon toward heterolytic cleavage, is readily synthesized using nucleophilic substitution or Steglich esterification; appropriate syntheses, including those used here, are well-documented in the literature.⁷¹ In analogy to comparable ATRP initiating systems, the ability of the R-substituent to stabilize the radical is important to its reactivity.

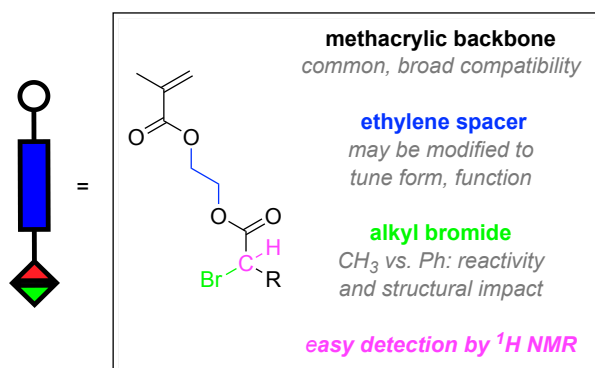


Figure 15. Modular monomer design.

While a more highly substituted carbon would be expected to be more active, secondary alkanes (where R = Me or Ph in MeBrema or PhBrema, respectively) were selected for this study to facilitate tracking by ^1H NMR (Figure 15). In both cases, the chemical shift of the proton neighboring the halide shifts markedly upfield upon coupling (Figure 16). The coupled fraction, x_c , was calculated by taking a proportion of the integration of the unreacted alpha proton signals (H_A) normalized against that of a resonance from the inert ethylene spacer, H_B (Equation 5). In the case of p(MMA-co-MeBrema), where ATRC faces competition from disproportionation, the degree of side product formation (x_{dis}) was calculated using the relative integrations of vinyl resonances (Equation 6).

$$x_c = 1 - \left[\frac{2 \int H_A}{\int H_A + \left(\int H_B / 2 \right)} \right]$$

Equation 5. Extent of coupling, x_c .

$$x_{dis} = 1 - \left[\frac{\int H_v}{\int H_v + \int H_B} \right]$$

Equation 6. Extent of disproportionation, x_{dis} .

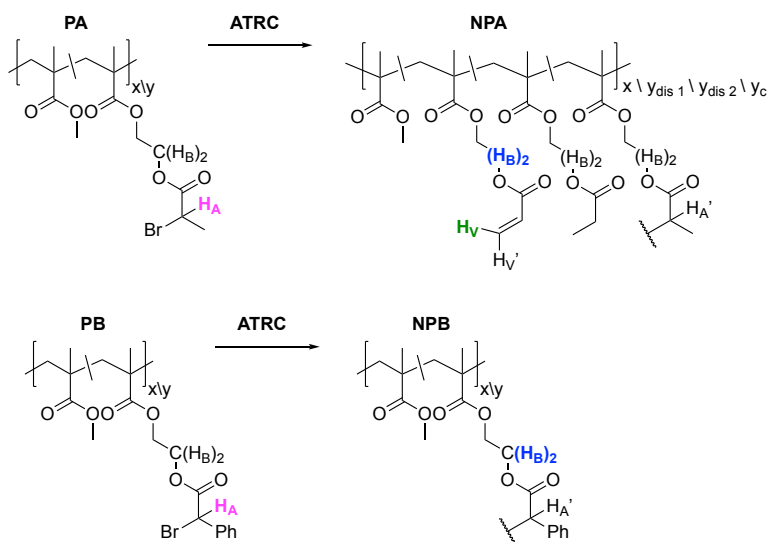


Figure 16. ^1H NMR can be conveniently used to track the desired ATRC product as well as alkyl and vinyl byproducts caused by competition of disproportionation. To do so, the integration of the signals representing H_A , $H_{A'}$, and H_V can be compared with that of the inert ethylene spacer, H_B .

This methodology allowed us to correlate coupling efficiency to morphological insights from multi-detection GPC to glean insight into the impact of substrate and catalyst combinations. The rich body of knowledge regarding ATRP is highly instructive for ATRC given their shared mechanism. Although metal and metal-free catalysts are available, $\text{Cu}^I\text{Br}/\text{L}$ systems, where L is a polyamine or pyridine chelator, are versatile, popular, and well-studied by Matyjaszewski and others.^{70,72–77} In these systems, the effect of ligand structure on ATRP kinetics is pronounced. Three of the most common ATRP ligands, PMDETA, TPEN, and TPMA were selected to sample this structural diversity and corresponding range of activity, which spans 3 orders of magnitude (Figure 17).

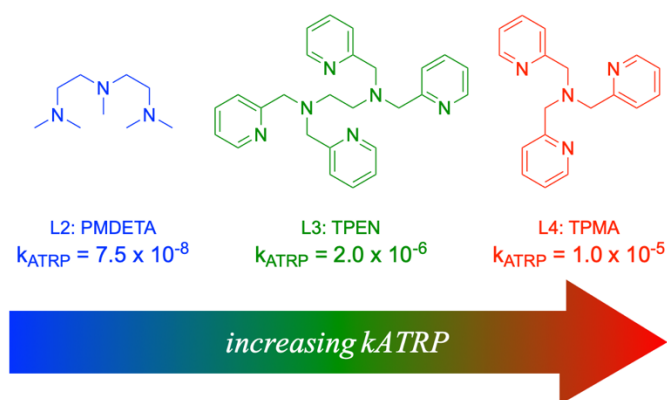
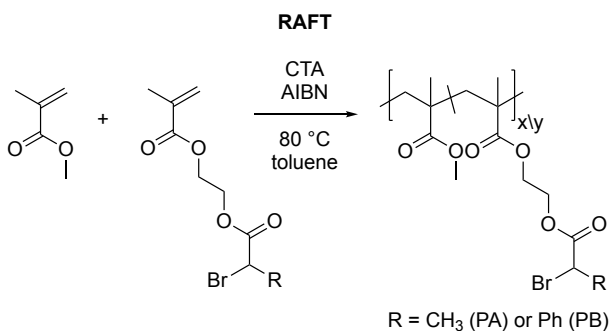


Figure 17.⁷⁴ k_{ATRP} values measured by Matyjaszewski et al. under the following reaction conditions: EtBrI/Cu(I)Br/MeCN/22 °C.

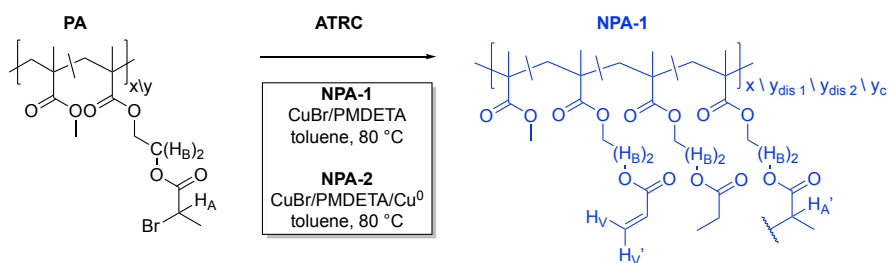
Examples of each backbone chemistry were tested with each ligand in a 50:50 MeCN:THF solvent mixture. These results were directly compared to those obtained using the most prevalent ATRC conditions, Cu^{II}Br/PMDETA/Cu⁰ in toluene.



Scheme 2. Parent Polymer Synthesis

Statistical copolymers with molecular weights in the range of 30-50 kDa were prepared using reversible addition–fragmentation chain-transfer (RAFT) polymerization (Scheme 2) to target the 5–10 nm size regime. RAFT provides a controlled polymerization orthogonal to ATRP. The proportion of the functional comonomer (f) was limited 35 mol% to maximize the controlled collapse in radius from parent polymer to SCNP according to literature precedent.

Effect of Cu⁰ Reductant on ATRC and Byproduct Formation



Scheme 3. Formation of SCNP with and without Cu⁰ reductant.

With this utility in mind, ATRC of PA was performed under both standard and reducing conditions (Scheme 3). The ¹H NMR spectra of the nanoparticle products, which are shown in Figure 18, were used to determine x_c and x_{dis} using the procedure described above. Because the usual calculation of x_c assumes no side reactions at the radical site, it is more accurately considered an apparent coupling efficiency. Given the observed tendency of P_A to disproportionate, an effective coupling constant, x_c' , was calculated by subtracting x_{dis} from x_c . As expected, the extents of coupling and disproportionation were both higher when Cu⁰ wire was included as a reductant (NPA-2) than when standard ATRC conditions were used (NPA-1). Indeed, negligible evidence of coupling was observed in the spectrum of NPA-1 ($x_c' = 2.8\%$). The extent of coupling of NPA-2 was higher but incomplete ($x_c' = 10.0\%$). Disproportionation was the minor product in both cases: $x_{dis} = 0.1\%$ and 8.9% for NPA-1 and NPA-2, respectively. These results are summarized in Table 1.

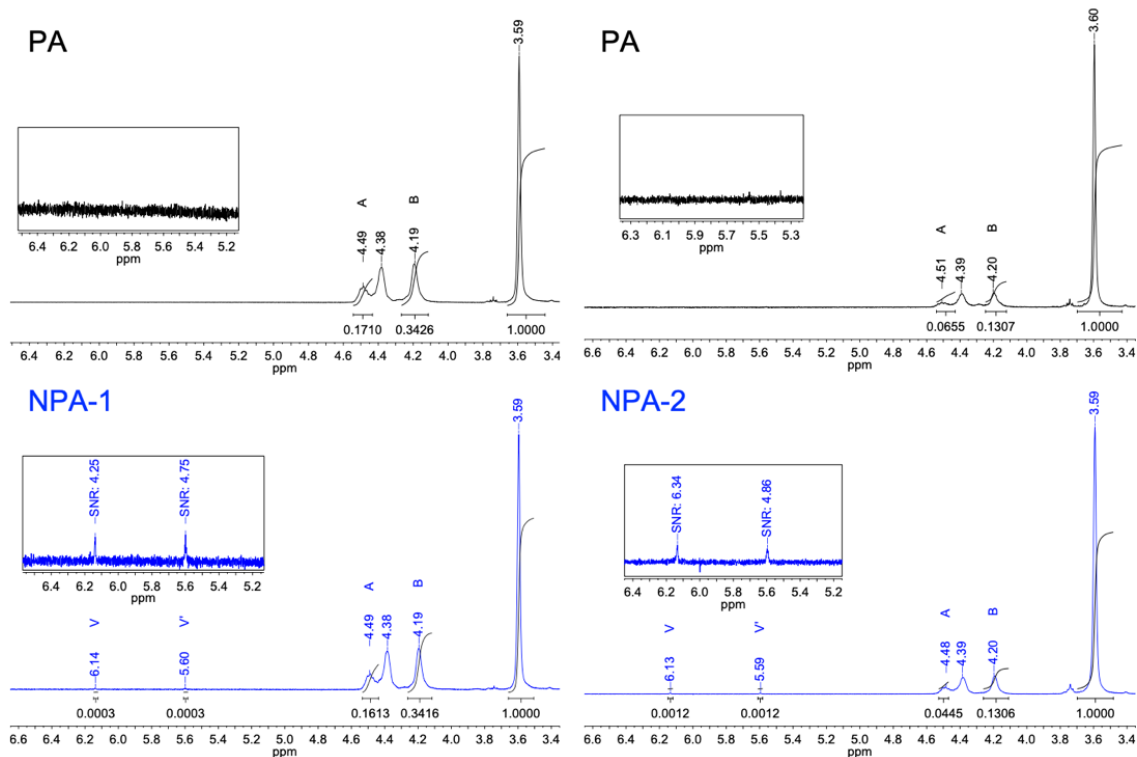


Figure 18. NMR spectra comparing ATRC with (left) and without (right) a Cu(0) reductant. The integration of resonances HV, HA, and HB is used to calculate the extent of coupling and disproportionation.

Table 1. The efficiency and selectivity of the intramolecular ATRC of PA to form SCNP.

	PA-1	NPA-1	PA	NPA-2
f	0.339	0.339	0.164	0.164
X_{dis}	-	0.001	-	0.089
X_{C}	-	0.028	-	0.100
$X_{\text{C}}' / X_{\text{dis}}$	-	28.0	-	1.12

Despite their shared starting material, the ratio of disproportionation to coupling products did not scale proportionally; $x_{\text{C}}'/x_{\text{dis}}$ decreased from 28.0 to 1.12 when Cu⁰ was present. The implication of this result is that the abstraction of an alkyl proton is favored over radical recombination when the concentration of the activating Cu^I complex is relatively high. Given the shared substrate, ligand, solvent, and temperature of these systems, this result raises the

question of whether a reasonable alternative pathway to disproportionation products could be proposed. One possible explanation is that the high activator concentration generated from comproportionation of the copper and deactivator species leads to a formation of an organometallic Cu^I species which could undergo β-elimination, thereby producing a catalytic disproportionation pathway which may proceed alongside radical abstraction (Figure 19). This existence of similar organometallic species is not without precedent; they have been isolated using radical traps for certain ARGET ATRP systems.^{78,79} However, direct comparisons must be made cautiously given the large number of variables at play, including the substrate, catalyst system, reaction conditions, and/or adjuncts.

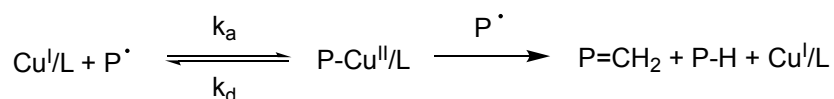


Figure 19. The formation of an organometallic species may promote disproportionation.

Morphological Implications of Inefficient Coupling

Because the primary motivation to develop intramolecular ATRC chemistry is architectural control, multi-detection GPC and diffusion NMR (DOSY) were used to relate the coupling efficiency and disproportionation with their morphological implications.⁸⁰ The outcomes of these competing reaction pathways are conveniently detected and distinguished using GPC with inline light scattering and viscometry capabilities. (1) Disproportionation does not noticeably impact the hydrodynamic radius or molecular weight; (2) cross-linking between pendants reduces the hydrodynamic radius without substantially increasing molecular weight; and (3) intermolecular cross-linking dramatically increases both. Therefore, the SCNP products of an efficient intramolecular “collapse” are distinguished because they elute before their respective parents, effectively decreasing their apparent molecular weights. However, their absolute molecular weights are impacted only by the coupling chemistry (e.g. loss of bromide in the case of ATRC).

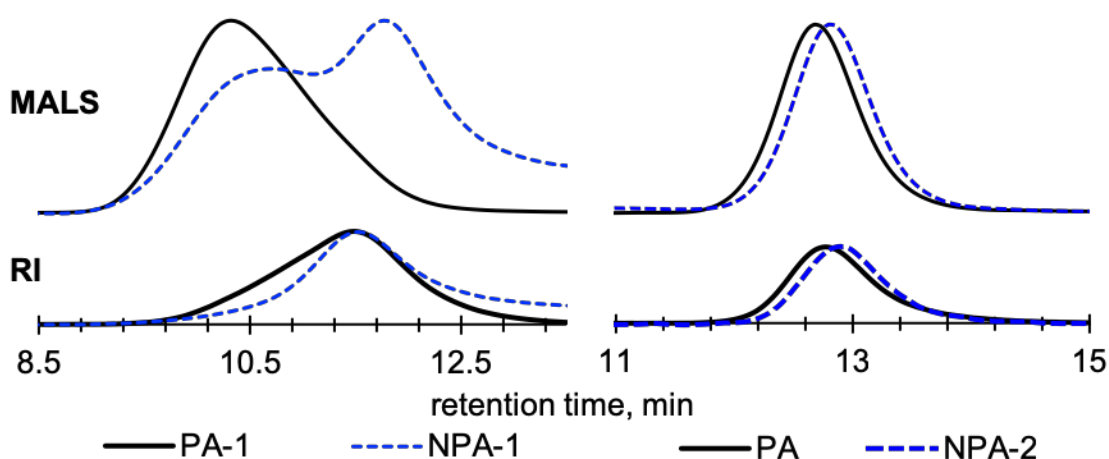


Figure 20. Multi-detection GPC comparing parent polymers PA-1 and PA with their respective SCNP. NPA-1: Cu(I)Br/PMDETA, $x_c' = 2\%$; NPA-2: Cu(I)Br/PMDETA/Cu(0), $x_c' = 10\%$.

The traces of NPA-1 and NPA-2, along with those of their respective parent polymers, are shown in Figure 20. A very low degree of coupling (e.g. 2.0%, as in NPA-1) is likely to broaden the size distribution of the sample due to a large population of chains without cross-links. This effect is pronounced in the broad and bimodal multi-angle light scattering (MALS) trace of NPA-1. As the extent of coupling increases, its polydispersity should decrease to its lower limit, which is that of the parent polymer sample. Practically, that degree of size control is possible for all but the least efficient cross-linking systems. For example, both the MALS and RI traces of NPA-2 ($x_c' = 10.0\%$) share the distribution profile of the parent while eluting at slightly longer retention times. Because dRI responses are a function of concentration, comparison between the dRI traces of P and NP can be meaningfully related to the coupling efficiency data from NMR. As expected, the peak retention times of the RI traces of PA and NPA-1 are practically identical and the distribution of NPA-1 is slightly shifted and broadened.

ATRC of PA

Reaction Progress and Byproduct Formation

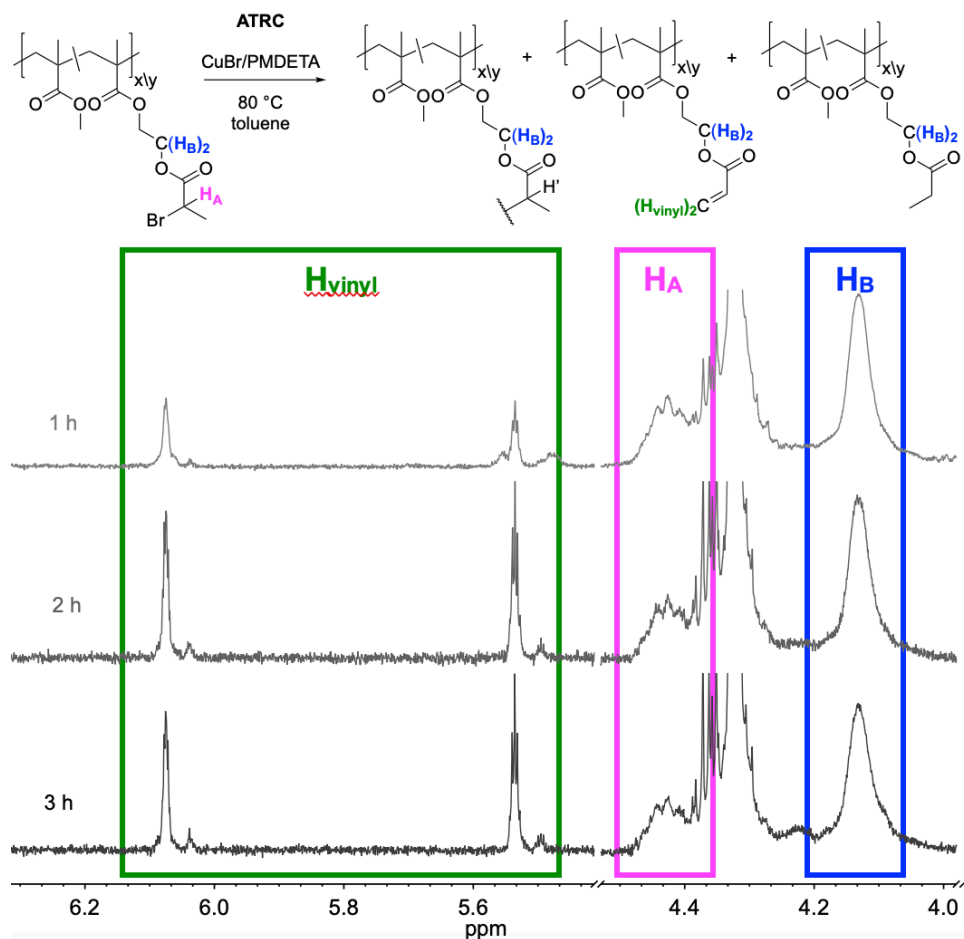
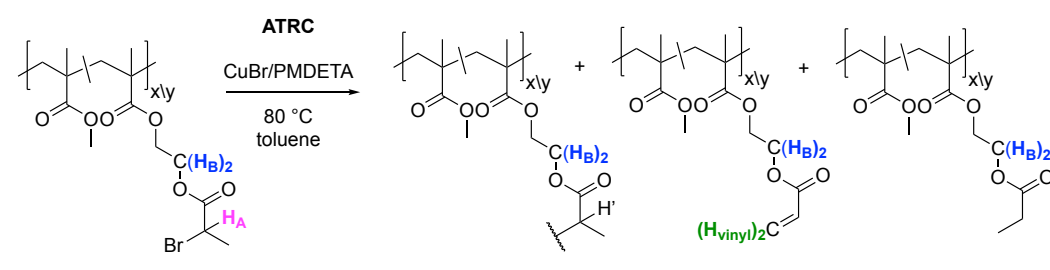


Figure 21. Tracking coupling and disproportionation of ATRC by ^1H NMR.

The progression of the competing coupling and disproportionation processes was tracked during the ATRC of PA to form NPA-2 (Figure 21). Samples were removed at $t = 0, 1, 2, 3,$ and 24 h by ^1H NMR using an air-tight syringe. The results of this study are summarized in Table 2. The extent of coupling, x_c' , reached a maximum of 10.0% after 24 h. This system displayed unique competitive behavior. Early in the reaction (< 1 h), the desired coupled product was favored ($x_c'/x_{\text{dis}} = 2$). While both x_c' and x_{dis} increased with reaction time as expected, x_c'/x_{dis} decreased to approximately unity for subsequent samples. This change in selectivity may correspond to the

time required to build the concentration of the activator species. Each halide transfer early in the reaction generates a deactivator species, and in the absence of a reducing agent, this species would remain deactivated. However, if Cu^0 is available, the comproportionation product with Cu^{II} produces two equivalents of $\text{Cu}^{\text{I}}/\text{L}$, eventually surpassing the original population. In other words, this behavior is consistent with the theory that high $\text{Cu}^{\text{I}}/\text{L}$ concentrations promote disproportionation through some mechanism, possibly formation of an organometallic species followed by β elimination as described above.

Table 2. Progression of coupling and disproportionation in a typical ATRC of PA.



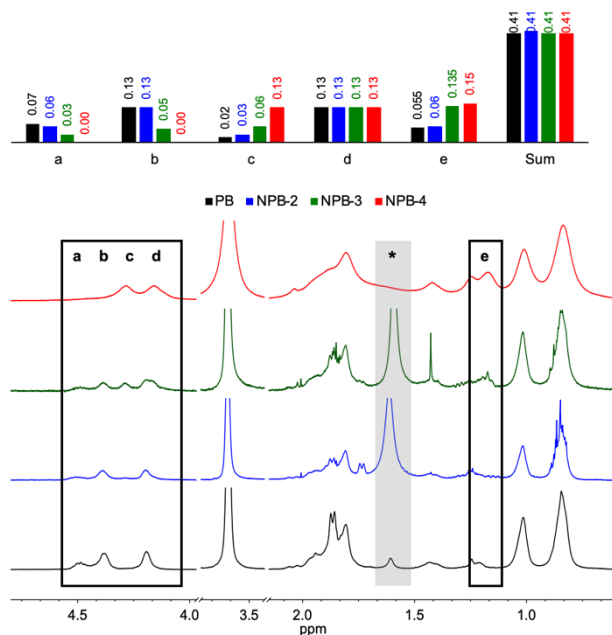
	PA	1 h	2 h	3 h	24 h
f	0.165	0.166	0.163	0.164	0.164
X_{dis}	-	0.001	0.018	0.068	0.089
$x_{\text{c}}^{\text{'}}$	-	0.002	0.017	0.060	0.100
$X_{\text{c}}^{\text{'}}/X_{\text{dis}}$	-	2	0.94	0.99	1.12

Effect of Ligand System

Because the nature of the ligand so heavily modifies the reducing potential of the copper complex, it is expected to impact the progression of ATRC. There are many reasons for tuning the efficiency of halogen extraction, including the possibility to facilitate more efficient coupling or adapt the system for sequential ATRA/C or ATRP/C procedures. Further, variations in reduction

potential or steric effects from ligand bulk could be expected to impact the formation of an organometallic species, thereby providing indirect evidence of such a pathway.

Extent of Coupling



*H₂O in CDCl₃; Cu(I)Br/L/Cu(0)/1 mg mL⁻¹/toluene/80 °C

Figure 22. ¹H NMR array comparing SCNPs created in ATRC of PA (bottom, black); L = PMDETA, TPEN, and TPMA for NPA-2 (blue), NPA-3 (green), and NPA-4 (top, red).

Differences between the samples prepared using each catalyst were evident in their respective ¹H NMR spectra (Figure 22). Full spectra are available in Appendix A. The extent of coupling, x_c , positively correlated with the k_{ATRP} of the catalyst complexes, following the order NPA-4 > NPA-3 > NPA-2. At first glance, this is unintuitive because higher k_{ATRP} ligands should promote a rapid buildup of the Cu(II)/L species, thereby suppressing ATRC through the persistent radical effect. However, these results indicate that the Cu⁰ reduction pathway is sufficiently favored to avoid this consequence. Signal broadening, which can be caused by intramolecular cross-linking and is therefore common in SCNPs chemistry, is also more pronounced in the

samples prepared using TPEN and TPMA. No evidence of the alpha proton is visible above the noise in the spectrum of NPA-4, the sample produced using TPMA as a ligand. While this is largely attributed to differences in reactivity, it could also be due to the significant broadening of neighboring signals. Because f , the incorporation of functional monomer, remains unchanged through this process, its value was used to determine x_c for this system.

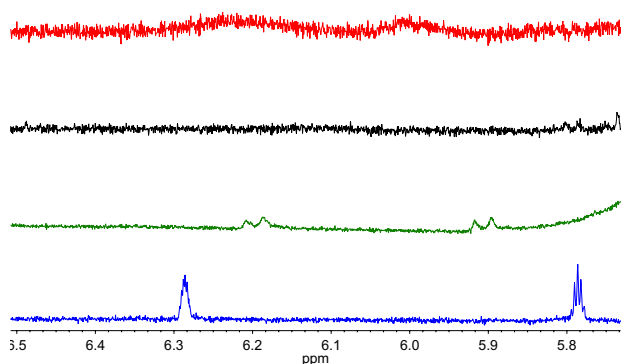


Figure 23. Vinyl region of the ^1H NMR spectra of series A. Top to bottom: NPA-4 (L = TPMA), PA, NPA-3 (L = TPEN), NPA-2 (L = PMDETA).

Unfortunately, signal broadening also precluded the calculation of x_{dis} for this system. Signals for the disproportionation product are visible, but the signal to noise ratio was not sufficient for integration in the case of NPA-4 (Figure 23). Qualitatively, however, higher k_{ATRP} ligands seemed to result in a decrease in the proportion of disproportionation products formed. Because higher k_{ATRP} ligands promote the generation of the $\text{Cu(II)}/\text{L}$ species, they would be expected to suppress the formation of an organometallic species and thereby limit the ratio of disproportionation to coupling to that of the direct interaction between pendants.

Size and Conformation

DOSY NMR and GPC-MALS were used to determine the radius of each species in THF. Additionally, morphological considerations were evaluated by determining the Mark-Houwink a-

parameter of each sample. The trends in these data corroborate the trends in x_c noted above, and the relevant data are tabulated in Table 3.

Table 3. Series A Polymer Properties

Sample	L	Mn (kDa)	Mw (kDa, MALS)	Mw (kDa, DOSY)	\bar{D}	R_η (nm)	R_h (nm)	η_n (mL/g)	M-H-S a f	x_c'	
PA-1	-	48.84	76.86	-	1.57	4.54	-	20.06	0.34	-	
NPA-1	PMDETA*	39.84	62.95	-	1.58	4.56	-	15.86	0.634	0.34	0.028
PA	-	34.25	38.17	38.0	1.11	4.40	2.50	17.83	0.925	0.17	-
NPA-2	PMDETA	39.84	43.04	13.8	1.08	4.06	1.87	15.86	0.803	0.17	0.201
NPA-3	TPEN	38.15	43.22	9.62	1.09	4.15	1.67	16.08	0.734	0.17	0.351
NPA-4	TPMA	40.87	44.87	10.7	1.10	4.00	1.74	11.41	0.727	0.16	0.463

**no Cu⁰ reductant*

GPC

GPC traces for Series A from the MALS and RI detector are shown in Figure 24. The height of the traces are normalized to the intensity of the highest signal to facilitate the comparison of retention time and dispersity. The maximum intensities of the MALS and RI traces were scaled to 1 and 0.5, respectively, to facilitate comparison while avoiding overlapping signals. As expected, each of the SCNP products (NPA2–NPA4) elutes at a longer retention time than that of the parent polymer, providing evidence for intramolecular cross-linking and corresponding decrease in hydrodynamic radius. The polydispersity remained low in each case. The trend in shifts to longer retention times roughly follows the order of x_c , however, NPA-3 and NPA-4 had very similar retention times. The viscometric data tells a similar story: all SCNP have lower intrinsic viscosities than PA. Interestingly, the molecular weights calculated from both light scattering and calibration were moderately elevated compared to that of the parent. Mark-Houwink parameters

and diffusion NMR were used to further probe this result and create a more complete picture of the resultant morphologies.

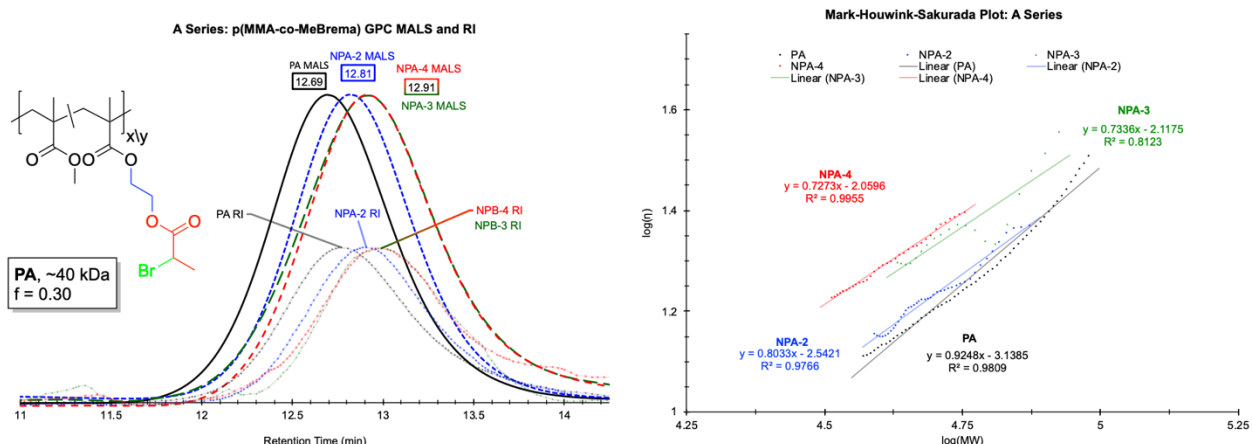


Figure 24. Series A GPC traces and M-H-S plots comparing the morphologies of SCNP products using PMDETA, TPEN, and TPMA catalyst systems. The activity of the ligand, approximated by k_{ATRP} , was positively correlated with increased coupling efficiency, leading to more compact structures.

Mark-Houwink-Sakurada a-parameter

Trends in the Mark-Houwink a-parameter were examined to compare the change in solution morphology induced by ATRC using each ligand. The Mark-Houwink-Sakurada plots in Figure 24 were created using differential pressure trace of the gel permeation chromatogram (a detailed procedure is available in the Supplementary Material). As described above, a value of approximately $a = 0.8$ is considered typical for a methacrylic copolymer in a good solvent such as THF. The a-value of the p(MMA-co-MeBrema) parent is 0.92, which is in line with those expectations. In accordance with expectations from other SCNP systems, the observed a-values for the SCNP after ATRC were smaller (Table 3). The observed trend modestly correlates with ligand activity, obeying the order $NPA-2 > NPA-3 > NPA-4$.

DOSY NMR

Diffusion NMR was used to determine the Stokes radius and apparent molecular weight (MW) of each sample. MW was determined using a calibration curve of PS standards as described

below in accordance with well-established methods.⁸⁰⁻⁸² For a series of SCNPs prepared from a common parent polymer, the apparent molecular weight should be inversely correlated with x_c . The M_w calculated for the parent polymer was in good agreement with the molecular weight data gathered from GPC (M_w , MALS = 38.17 kDa; M_w , DOSY = 38.0 kDa). As predicted, the apparent molecular weights were lower for NPA-2-4 than for PA.

The Stokes radius, like the viscometric radius, is a hydrodynamic radius which can be determined absolutely. Further, the sample was dissolved in THF for both GPC and DOSY experiments. Therefore, the two are expected to be in good agreement for non-interacting materials. Interestingly, the calculated Stokes radius of each sample was smaller than the corresponding viscometric radius. The mechanism behind this behavior is unclear. In order to further investigate, the Bayesian projections of the DOSY spectra were compared (Figure 25).

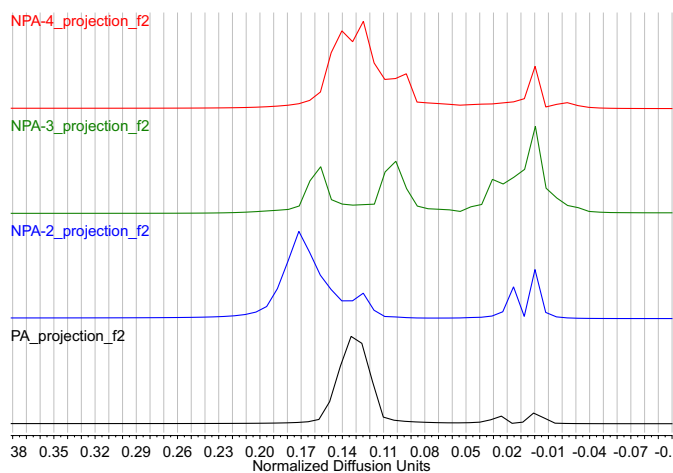
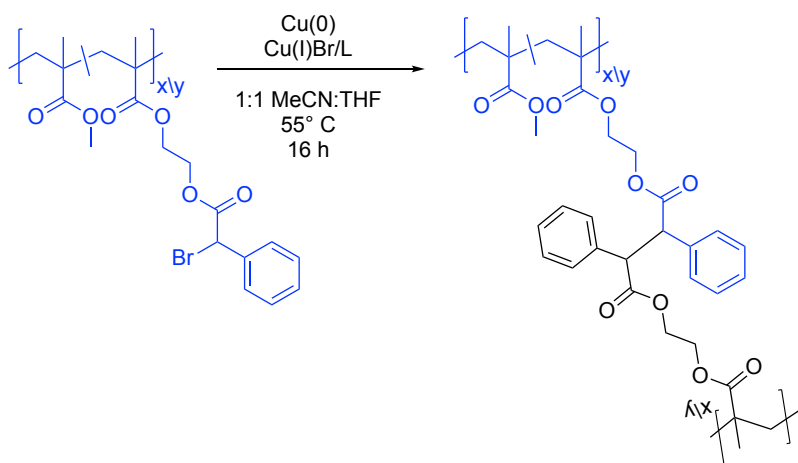


Figure 25. Bayesian projection of DOSY plots for Series A. The x-axis is normalized such that the diffusion coefficient of THF is 0.0. Molecular volume decreases from left to right. Top to bottom: NPA-3, NPA-2, NPA-1, PA.

Although quantitative integration of the Bayesian projections requires low sample concentrations (and correspondingly high magnet strengths and long instrument times), the distribution of signals in the SCNPs spectra was instructive. The shift to smaller volumes was apparent, however, the signals display an abnormal peak shape. Given that the GPC trace did

not show this behavior, this observation is most probably an effect of low resolution. Repetition using an extended number of scans time may be instructive to this end, however, very long acquisitions demand that the instrument maintain stable gradients for an extended period, which proved prohibitively challenging.

ATRC of PB, p(MMA-co-PhBrema)



Scheme 4. ATRC of PB.

As in the previous section, ATRC was performed using three ligands (PMDETA, TPEN, and TPMA) with a common parent polymer. To facilitate comparison between the results, the same molecular weight and incorporation were targeted. However, the SCNP prepared from PB proved notoriously difficult to isolate due to solubility issues. Operating on the assumption that this was due to the highly stable radical generated in halide abstraction, which may react to form multi-chain aggregates upon concentration of the crude product, the reaction was attempted at lower concentrations, first at 0.5 and then at 0.25 mg/mL. While samples prepared at 0.25 mg/mL showed some improvement in solubility, these attempts did not satisfactorily resolve the issue. The polymer seemed to interact with the GPC column and contain some low molecular weight species. This was attributed to excess catalyst trapped within the pervaded volume of the chain, and rigorous purification methods were applied (filtration through neutral alumina followed by dialysis over 72 h and reprecipitation). Acids could not be used for fear of degrading the

methacrylic backbone. The results of this procedure are shown in Figure 26, the GPC-MALS trace of NPB-3. This purification procedure was adapted to examine the remainder of the series.

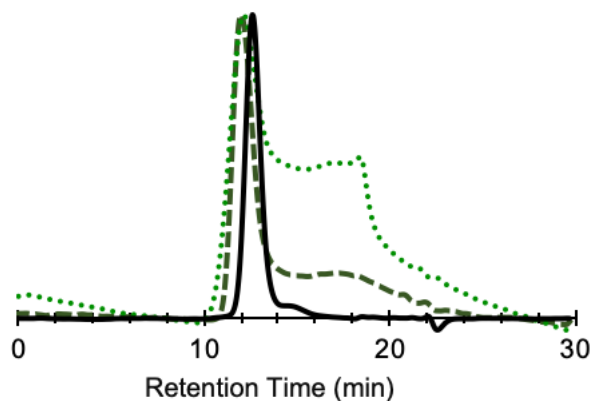


Figure 26. The GPC-MALS traces of PB (solid line), and NPB-3 before (small dashed line) and after (long dashed line) rigorous purification to remove low molecular weight species.

Effect of Ligand System and Unexpected Molecular Weight Profiles

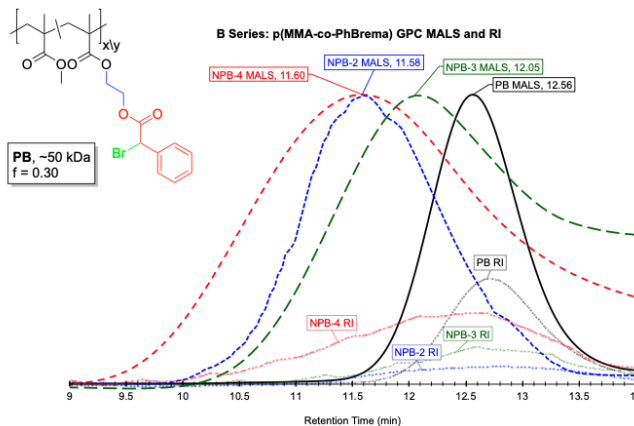


Figure 27 GPC-MALS Traces of Series B (standard procedure at 0.25 mg/mL).

The GPC-MALS trace of samples prepared in this manner are shown in Figure 27. The broadened traces and shortened retention times are typically associated with the formation of multi-chain aggregates rather than single-chain nanoparticles. While the MALS traces have been normalized to facilitate direct comparison, the RI traces are presented as-obtained to highlight

low sample concentrations in NPB-2 and NPB-3. Given the shared structure of these samples with PB and the evidence of aggregation, this is attributed to sample lost during pre-injection filtration with a 0.45 micron syringe filter.

Modified “Continuous Addition” Process Conditions

Therefore, an alternative procedure was attempted to circumvent aggregation. In an adaptation of a “continuous addition” procedure first reported by Harth and coworkers, the parent polymer solution (10 mg/mL, 100 mg polymer) was added by syringe pump over 4 h to a Schlenk flask with the other components (15 mL total solvent, final polymer concentration 2.5 mg/mL).⁸³ With the exception of CANP-3, examples prepared in this manner did not show signs of aggregation, instead shifting to longer retention times. Further, they were soluble enough for analysis by solution NMR.

Extent of Coupling

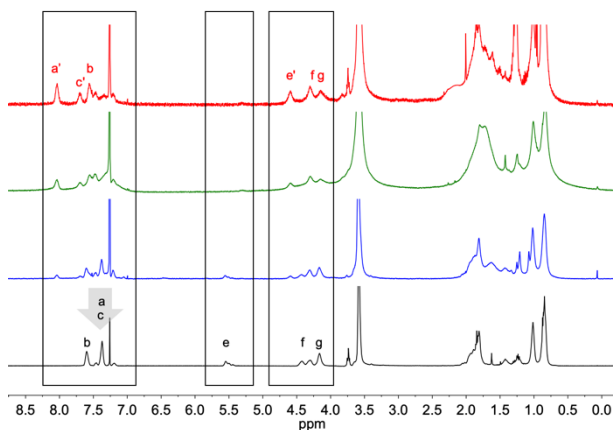


Figure 28. ¹H NMR array comparing SCNP created in ATRC of PB prepared using a continuous addition procedure. Cu(I)Br/L/Cu(0)/1 mg mL⁻¹/1:1 MeCN:THF/55 °C; L = PMDETA, TPEN, and TPMA for NPB-2, NPB-3, and NPB-4, respectively.

The determination of coupling efficiency was made using a similar procedure to that described for Series A. Where possible, the reaction was tracked using the relative integration of

α -proton signals (e) and ethylene spacers (f or g) in the ^1H NMR (Figure 28). As predicted, the α -proton resonances shifted upfield significantly upon abstraction of the halide in ATRC (e'). The resonances from the phenyl ring, a, b, and c, shifted downfield. Signal broadening was observed in CA-PB-3 and CA-PB-4. As noted above, this is not an unusual finding for intramolecularly cross-linked systems.

Size and Conformation

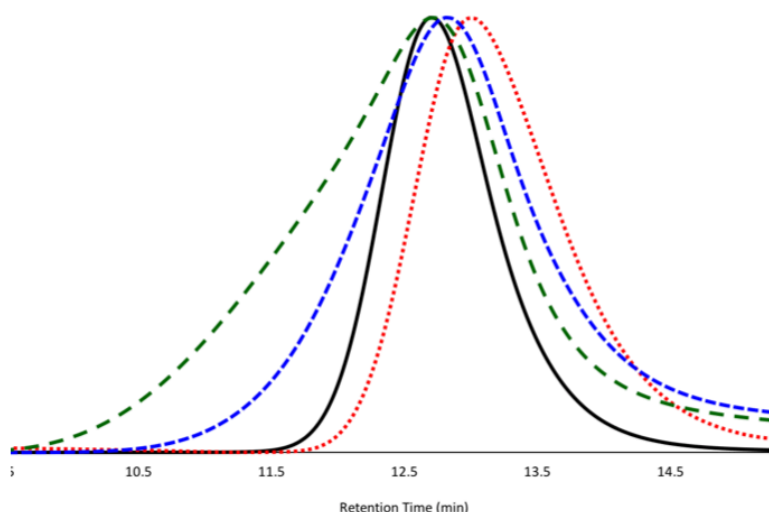


Figure 29. GPC-MALS trace of CA-NPB-2, 3 and 4 (continuous addition procedure).

However, the dispersity increased from that of the parent polymer in each case, as evidenced by broader GPC traces and higher proportions of M_w to M_n (\mathcal{D}) (Figure 29). The inconsistency of results obtained using ATRC of PB regardless of ligand obscure any trends that might otherwise be observed. Although the coupling behavior observed by ^1H NMR is similar to that observed for PA, the GPC data raises the question of whether this result is generalizable. Notably, the products of *intramolecular* and *intermolecular* ATRC cannot be discerned using ^1H NMR. Mark-Houwink parameters and DOSY NMR were examined for this purpose.

Mark-Houwink-Sakurada a-parameter

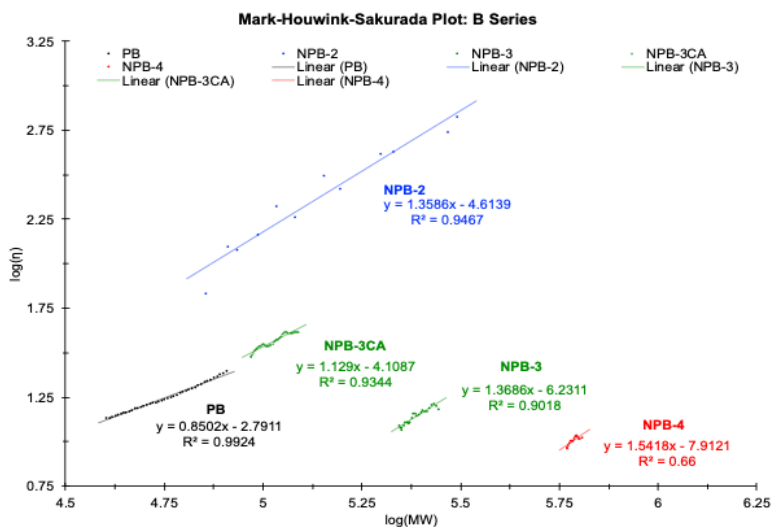


Figure 30. M-H-S plot of Series B (standard procedure).

The observed trend in the Mark-Houwink a-parameter is the reverse of that seen in Series A ($a_{NP-2} < a_{NP-3} < a_{NP-4}$). However, the phenomenon can be similarly attributed to the relatively high coupling efficiency of Cu^{II}/L complexes with TPEN and TPMA. Together, the relatively high M-H-S a-values, increases in polydispersity, and shifts to longer retention times point some combination of two behaviors: a combination of coupling between near neighbors (resulting in a more rigid and cylindrical morphology) and the continued formation of a small concentration of multi-chain aggregates.

DOSY NMR

Although DOSY would ideally be performed in THF to facilitate a direct comparison between the hydrodynamic radii from light scattering and diffusion (viscometric radius and Stokes radius, respectively), some samples exhibited poor solubility in THF. For this reason,

samples from this series were prepared in DMF-d7. The apparent molecular weight of the parent polymer and sample prepared using PMDETA (CA-NPB-2) were of sufficient quality for analysis while the signals for CA-NPB-3 and CA-NPB-4 were weak due to low solubility. The MW and Rh values for PB are in agreement with those obtained using GPC. The apparent molecular weight and Rh of CA-NPB-2 are smaller, providing evidence that the desired intra-chain cross-linking desired to form SCNP occurred.

Table 4. Series B-CA DOSY

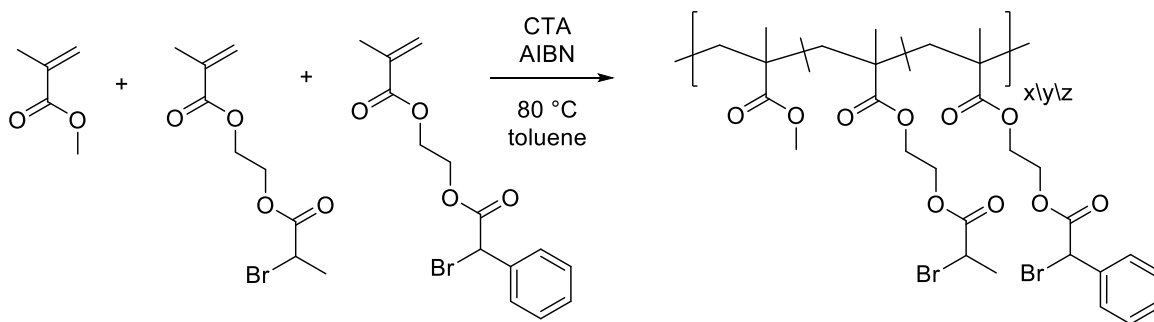
Sample	D (m ² /s)	MW (kDa)	Rh (Stokes)
PB	6.13 x 10 ⁻¹¹	51.5	4.44
CA-NPB-2	6.67 x 10 ⁻¹¹	41.71	4.08
CA-NPB-3 (weak signal)	2.11 x 10 ⁻¹¹	747.98	12.90
CA-NPB-4 (weak signal)	2.39 x 10 ⁻¹¹	1.70	1.14

Table 5. Series B Polymer Properties

Sample	L	Mn (kDa)	Mw (kDa)	Đ	Rh(v) (nm)	η _n (mL/g) a	M-H-S f	x _c	Notes	
PB	-	50.81	55.407	1.09	5.07	17.740	0.850	0.174	-	
NPB-2	PMDETA	-	200.12	-	-	-	-	0.172	0.024	aggregation, low solubility
CA-NPB-2*	PMDETA	50.56	64.10	1.15	8.51	11.91	1.200	0.174	0.031	
NPB-3	TPEN	288.13	330.00	1.15	8.60	14.731	-	-	-	aggregation
CA-NPB-3*	TPEN	55.13	143.30	2.60	6.14	17.710	1.369	-	-	
NPB-4	TPMA	872.24	1085.03	1.24	10.153	8.134	-	-	-	aggregation

ATRC of terpolymer PAB

The unique behavior of PB, especially its tendency to form multi-chain aggregates under unfavorable conditions, is presumably due to the stabilization of the radical from the benzyl and ester moieties. If this is the case, it is effectively forming a persistent radical under ATRC conditions. This raised the question of whether this behavior could be used adventitiously to drive the formation of ATRC over disproportionation (a problem exclusive to MeBrema) and prevent aggregation (a problem exclusive to PhBrema) if the two substrates were concurrently present. To test the feasibility of this application of the persistent radical effect, a model p(MMA-co-MeBrema-co-PhBrema) terpolymer was made (Scheme 5) and reacted under ATRC conditions to form NPAB (Figure 32).



Scheme 5. Synthesis of terpolymer PAB using RAFT. $f_{\text{MeBrema}} = 33.1 \text{ mol\%}$ $f_{\text{PhBrema}} = 38.1 \text{ mol\%}$, $M_w = 15 \text{ kDa}$.

Unlike other samples using PhBrema (PB series), the ATRC of PAB to product NPAB did not require special care. Standard collapse conditions (1 mg/mL) were used without the formation of aggregates. This is particularly impressive because an overall high functional incorporation was used (33.1 mol% MeBrema and 38.1 mol% PhBrema). Evidence of the alpha proton neighboring the bromine from PhBrema (signal at 5.46 ppm in PAB, Figure 31) is completely absent from the

^1H NMR of NPAB, suggesting that most of the PhBrema units formed the desired coupled products (Figure 32). However, unreacted MeBrema groups remain (unfortunately, the signals are too convoluted to accurately determine x_c).

There are also signals in the alkene region that can be assigned to the disproportionation product. This is an especially curious result given that (1) the persistent radical effect would govern that MeBrema should preferentially couple to PhBrema in this case and (2) MeBrema was present in a slight molar excess. This behavior is supporting evidence for the existence of a second pathway to disproportionation. It would be of future interest to explore whether this is the case and, if so, whether it occurs through the formation of an organometallic species.

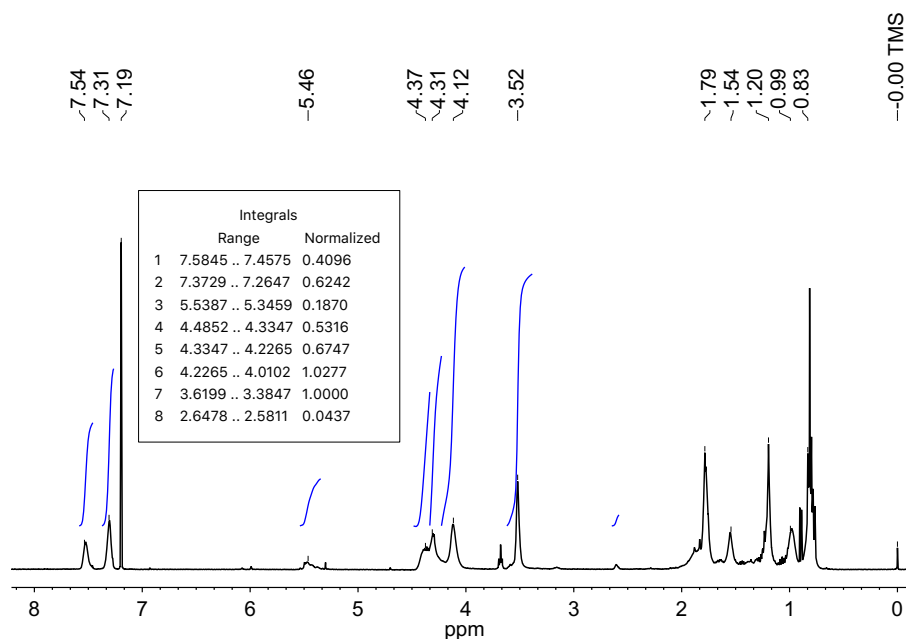


Figure 31. ^1H NMR of terpolymer PAB₁₅. The broad signal in this case is due to a highly concentrated sample.

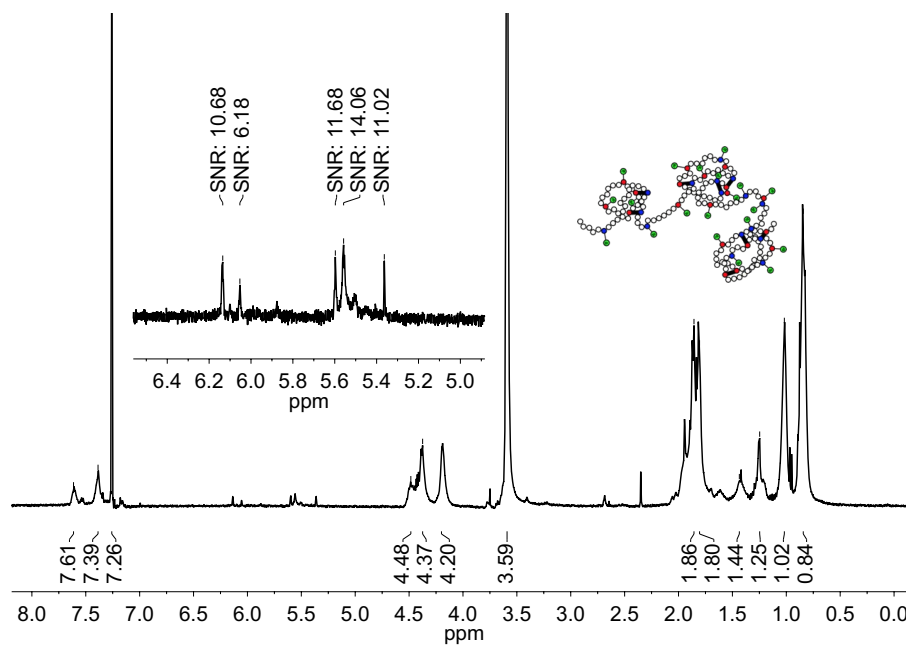
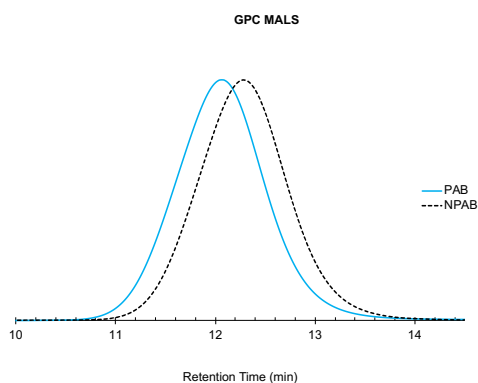


Figure 32. ¹H NMR of SCNP made from terpolymer PAB.

The GPC data showed evidence of an efficient collapse SCNP formation. The change in molecular weight can be attributed to a loss of bromides, particularly given the high overall functional incorporation. The hydrodynamic radius, intrinsic viscosity, and Mark-Houwink a -parameter all decrease from those of the parent. Further, the GPC trace shifts to a longer retention time and maintains narrow size dispersity (Figure 33).



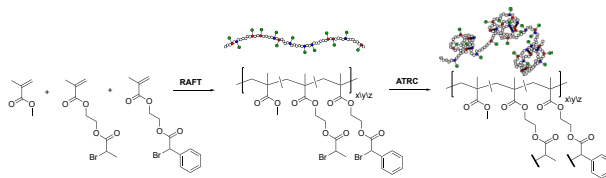


Figure 33. GPC-MALS traces of PAB and NPAB.

Table 6. Characterization of PAB and NPAB.

Sample	L	Mn (kDa)	Mw (kDa, MALS)	\bar{D}	R_{η} (nm)	η_n (mL/g)	M-H-S a	f_{PhBrema}	f_{MeBrema}
PAB	-	10.10	11.61	1.15	3.65	20.13	0.574	0.33	0.38
NPAB	PMDETA	9.30	10.63	1.14	2.79	15.14	0.443	-	-

Conclusions

This work represents significant progress into understanding the impact of catalyst and substrate on ATRC chemistry under conditions favoring intramolecular cross-linking. The copper reducing agent was necessary to efficiently form intrachain cross-links. This property could be exploited to efficiently create sequenced ATRP/ATRC designs.

Coupling efficiency was positively correlated with k_{ATRP} for a given ligand even though these ligands tend to promote the formation of a high concentration of the deactivator species. This speaks to the efficiency of the Cu(0) wire reducing agent at regenerating the active species.

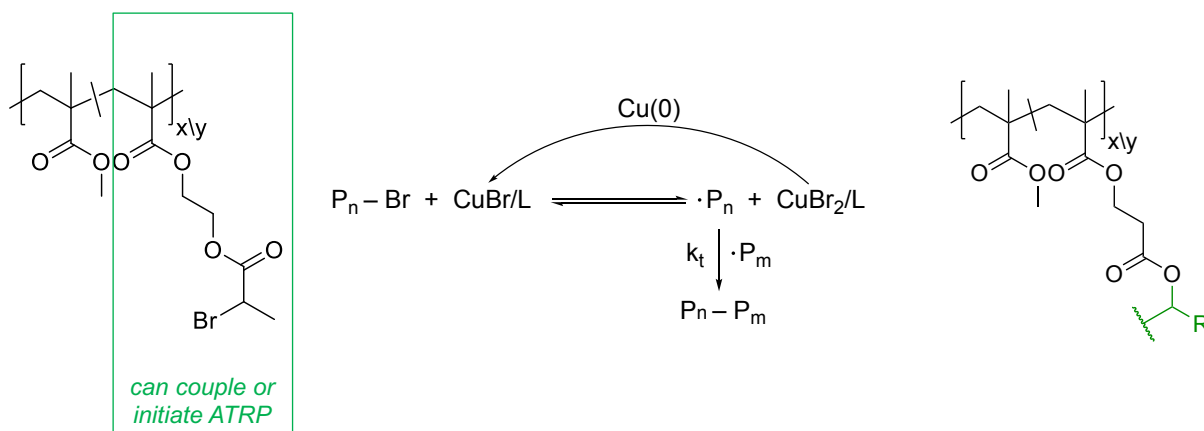
Parents with pendant MeBrema moieties tended to form the desired SCNP product, but the efficiency of coupling was hindered by competition from disproportionation. The degree of disproportionation seemed to vary systematically with the theoretical concentration of the Cu(I) species in solution. This result suggests the existence of an alternative pathway to the disproportionation product which depends on Cu(I). Future work should be done to explore the formation of an organometallic species as alternative mechanism for disproportionation under high concentrations of the Cu(I)/L complex.

Parents with pendant PhBrema moieties were highly prone to aggregation, regardless of ligand system. A continuous addition strategy was used to mitigate this effect with mixed success. A terpolymer system was prepared to explore the possibility of using the persistent radical effect adventitiously. Theoretically, the challenges faced by MeBrema and PhBrema-based ATRC systems (disproportionation and aggregation) could be addressed using their combination. A proof-of-concept showed promising results to this end.

Chapter III. Sequencing ATRP and ATRC to form advanced SCNP architectures

Introduction

As discussed in the Introduction of this dissertation, the most popular approach to promoting dense, globular single-chain nanoparticles is the the installation of orthogonal cross-links. However, the application of these approaches is limited because today's examples require multiple post-polymerization modifications and corresponding challenging and inefficient purifications. Although they are not always selected for this reason, intrachain polymerization strategies, present a viable means for impacting both of the primary drivers behind the statistics of intramolecular cross-linking, chain mobility and segmental length between cross-linkable units.^{41,42,45}



Scheme 6 Reimagining p(MMA-co-MeBrema) as both an ATRP macroinitiator and SCNP precursor.

We imagined that these factors might be addressed by using relatively dense non-linear parent polymer chains. There is limited but promising support for this idea in the literature. For example, ATRC has been used to couple polystyrene brush ends to form SCNP, albeit in several steps.⁸⁴ TEM images showed that the worm-like bottle-brush morphology of the parent formed a

globule after collapse. Interestingly, Lu and coworkers reported physical evidence of intramolecular cross-linking (lower-than expected mechanical strength after cross-linking) when they prepared organogels by performing ATRC on hyperbranched acrylates prepared using ATRP.⁸⁵ This result was particularly remarkable because the reactions were performed in the bulk or concentrated solutions, conditions which heavily favor intermolecular cross-linking in linear analogues.

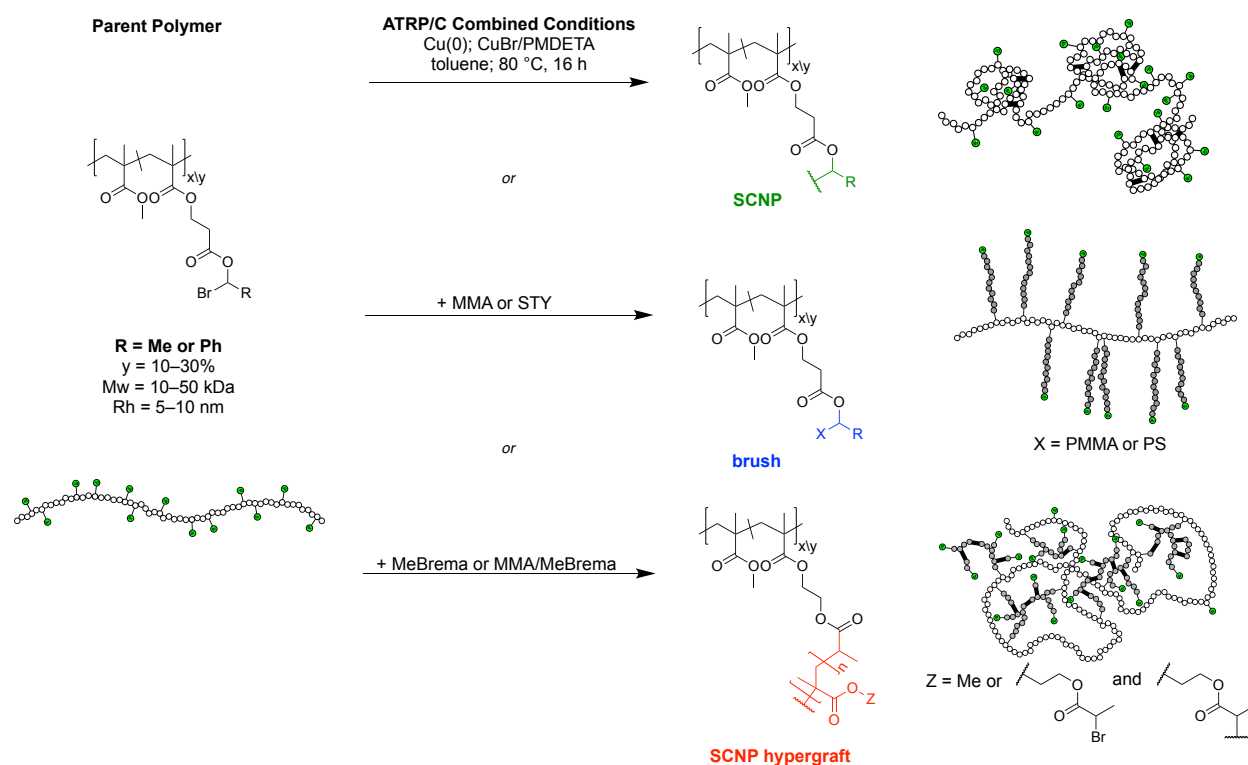


Figure 34. Preparation of a diverse set of architectures from a common substrate under a unified set of reaction conditions by sequencing ATRP with ATRC.

Having developed an understanding of the behavior of the p(MMA-co-MeBrema) system for ATRC, we envisioned it as a platform from which it would be possible to efficiently and flexibly perform sequences of ATRP and ATRC (Figure 34). Although only a handful of similar methodologies exist today, ATRC has been used to efficiently prepare grafted topologies or cross-links in isolation.^{86,87} In theory, the introduction of a controlled intrachain polymerization would allow for the inclusion of functional monomers, whether chiral, reactive, or simply structurally

diverse. The existence of a unified set of reaction conditions between polymerization and coupling is especially convenient because it circumvents the multiple purification steps so commonly required in the formation of complex macromolecules.

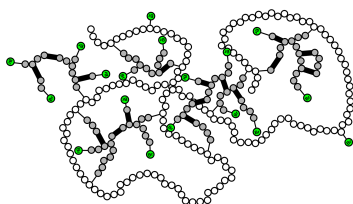


Figure 35. SCNP with low DP “hyperbranched” cross-links.

In addition, it is possible to use bifunctional monomers (capable of both polymerization and coupling) to create hyperbranched cross-links. These systems could dramatically impact the statistics of folding due to their both their unique architectures and introduction of a large number of cross-linkable moieties. To my knowledge, there are no SCNP containing hyperbranched motifs in the literature to date.

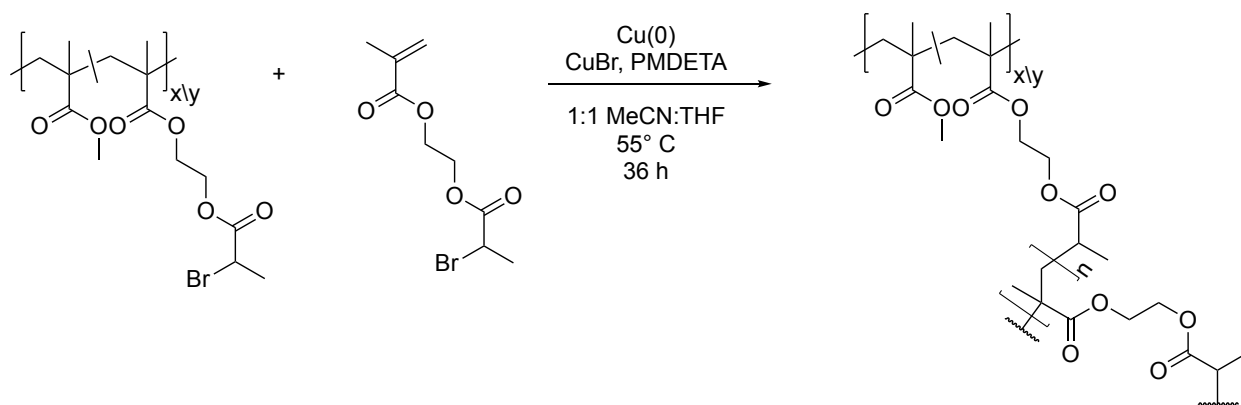
Research Objective

To explore this new design space, we designed a series of experiments comparing SCNP created with brush, and hyperbranched polymers of a comparable chemical composition. One of the major motivations of this work was to determine whether controlled polymerizations were possible in ultra-dilute solutions. If so, it would theoretically be possible to sequence polymerization and coupling to form architecturally or chemically complex species under a unified set of conditions or potentially in one pot. The objectives were therefore (1) demonstrate the presence of intact ω -chain ends after ATRP/C procedures by performing a post-collapse polymerization and (2) monitor monomer conversion to study the polymerization kinetics for a model system.

Results and Discussion

Comparing ATRC in the presence of MMA or MeBrema

Conditions developed for the ATRC of MMA-co-MeBrema, PA, are described at length in Chapter 2 of this dissertation. Although TPMA produced the most efficient ATRC collapse, PMDETA was selected to better control the polymerization component of the sequence. Hereafter, this set of conditions (Cu(I)Br/PMDETA/Cu⁰/80 °C, 1 mg/mL, toluene) is referred to as the ATRP/C combined conditions.



Scheme 7. Formation of p(MMA-co-MeBrema-g-MeBrema) hypergrafted SCNP.

PA was reacted under the ATRP/C combined conditions in the presence of 10 equivalents of MMA or 4 equivalents of MeBrema to produce PA-MMA10 and PA-MeBrema4, respectively (Scheme 7). The monomer equivalents were selected to target the same final molecular weight range and thereby facilitate direct morphological comparison. ATRP is usually performed in much more concentrated solutions (1 g/mL is typical, but concentrations may vary from bulk to 10 g/mL). It was therefore uncertain whether polymerization could efficiently occur to form the brushes. Furthermore, molecular weight control in a typical ATRP can be achieved by monitoring the conversion of monomer (either through GC or NMR) and adjusting the reaction time in real time. This is impractical for dilute-solution systems, especially for those on the 100 mg scale. However, despite these foreseen challenges, early results were extremely promising.

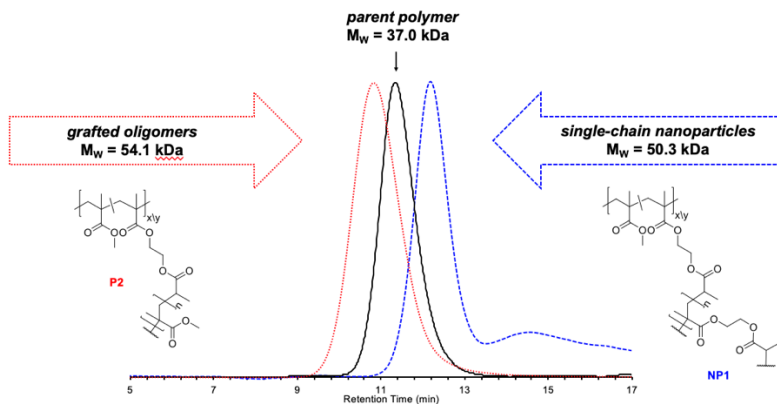


Figure 36. Preparation of brush polymers or “knit” SCNP using MMA or inimer.

Figure 36 compares the SEC-MALS traces for the parent chain PA, brush PA-MMA10, and corresponding SCNP, NPA-MeBrema4. The formation of PA-MeBrema4 was characterized using GPC. The molecular weight as determined by MALS increased after polymerization, and the shift to a longer retention time is consistent with the successful formation of SCNP through ATRC between the pendant alkyl bromide units. As a control, the procedure was repeated using MMA as a monomer, removing the polymer’s ability to participate in ATRC. The expected increase in molecular weight was this time accompanied by a shift to a shorter retention time, which is consistent with the formation of the anticipated brush polymer.

The incorporation of functional monomer was tracked using ^1H NMR experiments (Figure 37). After intra-chain polymerization to produce NPA-MeBrema4, the integration of the pendant ethylene signals increased relative to those of the backbone methacryloyl moieties. An average conversion of 50% was achieved over a 24 h reaction time. We determined that approximately 85% of the bromide units remained unreacted by comparing the integration of signal *a* with those of *b* and *c*. This finding indicates that a relatively small number of cross-links were formed. As such, it may be possible to further react NP1 through these “live” pendants to extend the chains, promote further collapse by intramolecular cross-linking, or introduce application-targeted functionalities.

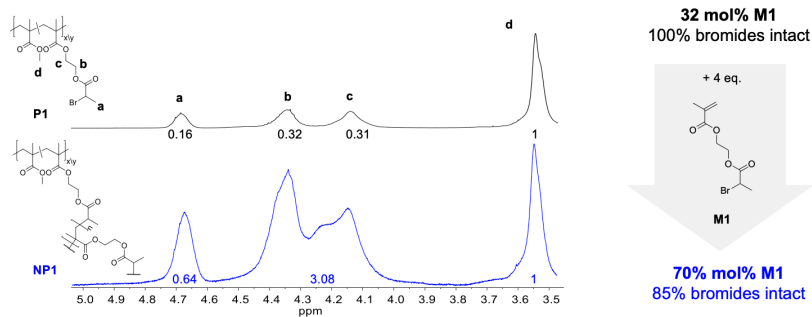


Figure 37. ^1H NMR of Hypergrafted SCNP NPA-MeBrema4 (4 eq. inimer).

The small number of functional equivalents chosen for the first example was selected to keep the molecular weights moderate and thereby circumvent issues with solubility or aggregation. Given the success of the proof-of-concept, the reaction was repeated with a higher number of functional equivalents (10) to explore the true nature and potential limitations of the hyperbranched cross-link motif. As may be expected for a large molecular weight polymer, the ^1H NMR signals are broad (Figure 38). This being the case, it is not possible to reliably determine whether “live” bromo-terminated chain ends are intact by simple NMR. However, the retention time increased and intrinsic viscosity decreased upon hypergraft formation, suggesting the formation of a denser structure (Figure 39).

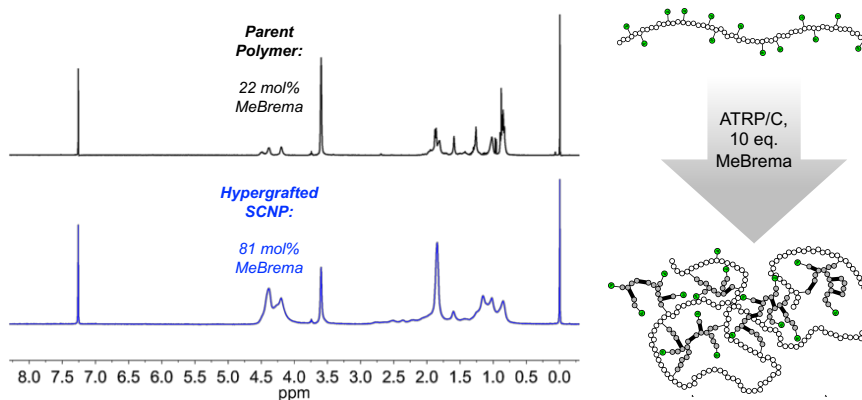


Figure 38. ^1H NMR of Hypergrafted SCNP NPA-MeBrema10 (10 eq. inimer).

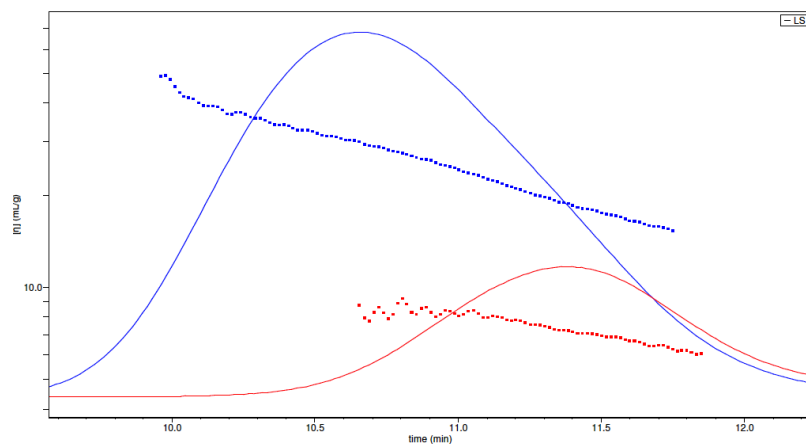


Figure 39. The fit of the intrinsic viscosity to the MALS trace for PA (blue) and NPA-MeBrema10 (red).

Kinetics of and Livingness of ATRP/C

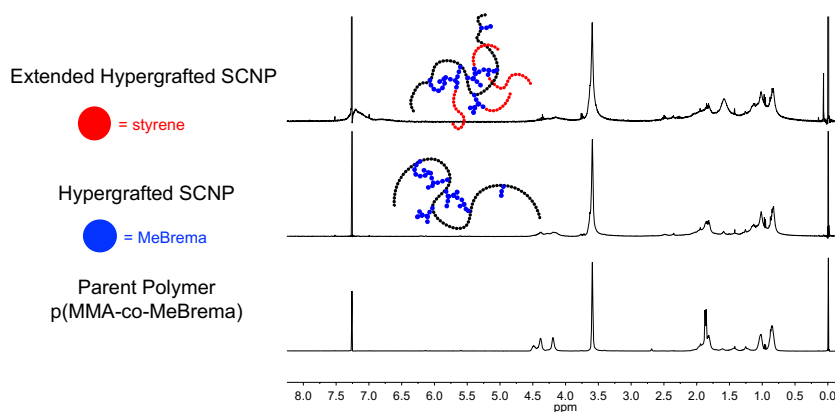


Figure 40. Extending the arms of hyperbranched chains was used to test for the presence of “live” halogenated chain ends.

The “livingness” of the hyperbranched chain, can, however, be assessed by attempting further polymerization. This experiment also presents the opportunity to examine the kinetics of ATRP in ultra-dilute solutions, which may be instructive to future work in intrachain polymerization techniques. NPA-MeBrema10 was reacted under the combined ATRC conditions with 50 functional equivalents of styrene and aliquots were removed over time to assess monomer conversion by tracking the disappearance with of vinyl peaks in the monomer against the those

from the methacryloyl backbone (Figure 41). Somewhat surprisingly, the plot shows reasonable fidelity to the pseudo first order kinetics typically observed in SCNP. However, the ^1H NMR of the final product (Figure 40) displayed extremely broad signals, which is common for both high molecular weight species and SCNP.

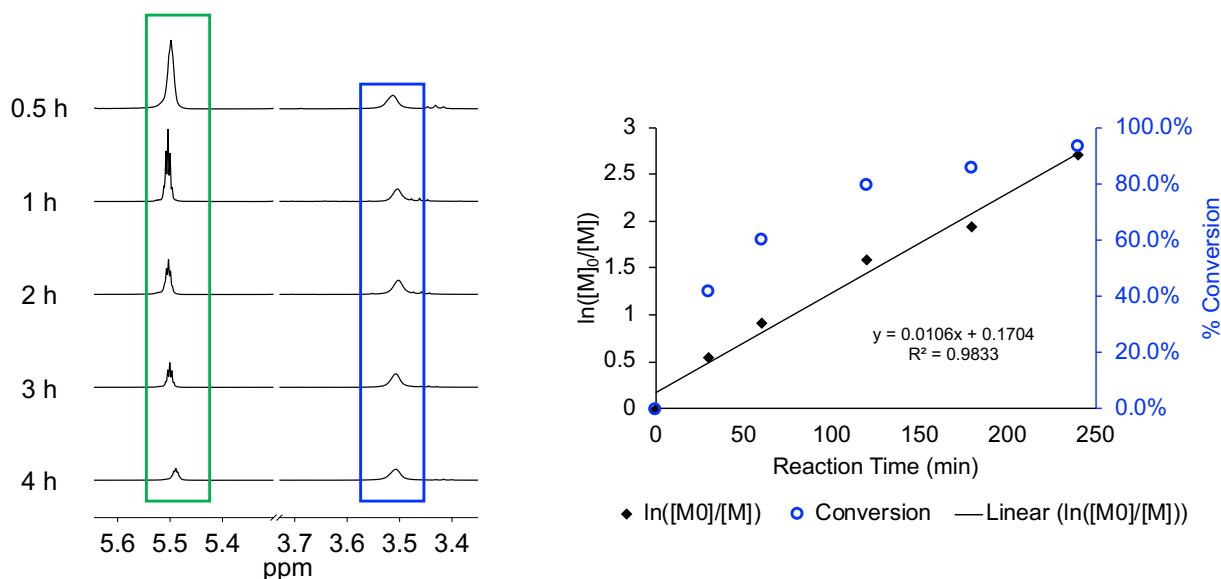
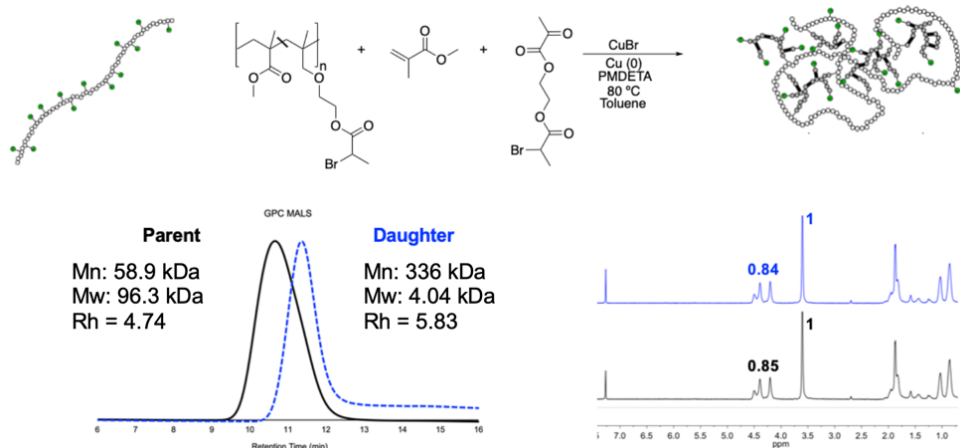


Figure 41. Kinetic plot of ATRP/C showing reasonable fidelity to the pseudo first order kinetics usually observed in ATRP.

Comonomer Graft System

In order to exploit the benefits of hyperbranching while keeping molecular weights low, a co-monomer graft was attempted using 10 functional equivalents of MMA and 4 of MeBrema (Scheme 8). The rationale behind this approach is analogous to that behind segmented hyperbranched polymer work, which employs spacing between hyperbranched units to control the properties.⁸⁸ Using this design, the molecular weight of the polymer could be increased substantially while nominally impacting its radius. The overall incorporation of functional units remained unchanged from the NPA parent to the NPA-MMA-MeBrema product.



Scheme 8. Reaction of PA under combined ATRP/C conditions in the presence of MMA and MeBrema to form NPA-MMA-MeBrema.

Coupled Brush System

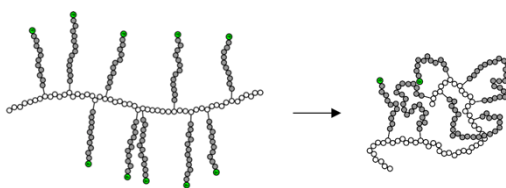


Figure 42. Coupled brush SCNP.

The natural comparison to these systems is the ATRC of to couple brush polymer ends, similar to those prepared by Liu and coworkers.⁸⁴ Any ATRC chemistry used to create telechelic blocks is expected to function similarly to form cross-links, meaning that most brush polymers made in a grafting-from ATRP approach could be convinced to form intramolecular cross-links under the proper conditions. Most examples of ATRC in the literature are block copolymers with styrene.^{24,55,56,59,89-91} As a proof-of-concept, the brush polymer NPA-MMA-20 was reacted under the combined conditions in the presence of 5 functional equivalents of styrene. Although its dispersity was higher than that of the parent, decreases in intrinsic viscosity, the Mark-Houwink a parameter, and the hydrodynamic radius were observed. The MALS trace showed a shift to a longer retention time, indicating a successful collapse (Figure 43).

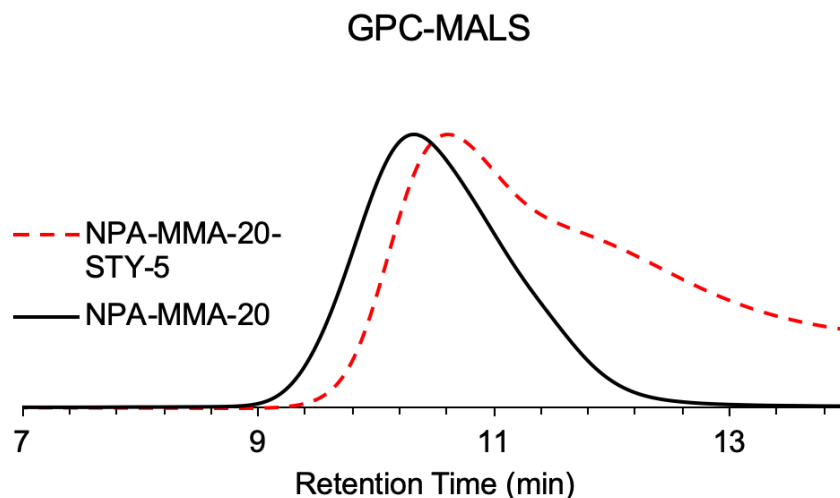


Figure 43. GPC-MALS of coupled brush SCNP.

Kinetics of ATRP/C

Higher molecular weight MeBrema and MMA examples were also prepared (Table 7). Although NMR was not a robust characterization technique for these species, their molecular weights by GPC were close to the target. NPA-MMA-20 maintained a narrow molecular weight population while that of the hyperbranching example broadened. This could be expected for its expected morphology, which includes a complex mixture of coupled and branched products. The Mark-Houwink a -parameters of these species are also instructive – while that of NPA-MMA-20 is greater than one (characteristic of a brush), that of NPA-MeBrema-10 is below 5 (characteristic of a globule).

Table 7. Comparison of GPC characterization data for higher molecular weight brushes.

	NPA-MeBrema-10	NPA-MMA-20
Mw	2.21E+05	2.11 x 10 ⁵
Mn	1.33E+05	1.82E x 10 ⁵
\bar{D}	1.66	1.16

[η]	19.87	6.92
R _H	7.25	5.79
M-H-S a	0.362	1.663

Table 8. Summary of Properties of Polymers and Brushes or SCNP products of ATRP/C.

Sample	f	Mw kDa	Mn kDa	Đ	[η]	R _g (nm)	a	Notes
NPA-MMA-20- STY-5	-	2.21 x 10 ⁵	1.33 x 10 ⁵	1.66	15.87	5.25	0.358	Coupled Brush
NPA-MMA-20	-	2.11 x 10 ⁵	1.82 x 10 ⁵	1.16	16.92	5.79	0.963	MMA Brus (large)
NPA-MMA- MeBrema-10- STY-5	-	4.04 x 10 ⁵	3.54 x 10 ⁵	1.14	13.65	5.83	0.373	1) MeBrem Hypergraft 2) STY
NPA-MMA- MeBrema-10	-	2.30 x 10 ⁵	2.06 x 10 ⁵	1.12	14.20	5.13	0.521	MeBrema Hypergraft
PA	0.220	3.68 x 10 ⁴	3.90 x 10 ⁴	1.06	15.73	4.55	0.323	PA(37k) Low d
NPA-MeBrema-4	0.721	1.16 x 10 ⁵	8.44E x 10 ⁴	1.37	4.73	3.88	0.533	“hyperbranched” SCNP 1) Low dp SCNF
NPA-MeBrema- 4-sty	0.093	3.09 x 10 ⁵	2.47 x 10 ⁵	1.25	6.60	6.25	0.172	hype 2) STY
NPA-MeBrema- 4-sty (repeat)	0.345	1.87 x 10 ⁵	9.59 x 10 ⁴	1.95	14.13	5.58	0.279	Low dp SCNF hype
NPA-MMA-10	0.327	54.1 x 10 ⁴	4.33 x 10 ⁴	1.32	21.82	5.20	0.380	MMA Brush

NPA-MeBrema-4	0.684	50.3×10^4	6.48×10^4	1.12	11.01	4.79	0.381	Low dp SCNP-hype
---------------	-------	--------------------	--------------------	------	-------	------	-------	------------------

Conclusions

We found that poly(methyl methacrylates) decorated with pendant bromopropionate units can be converted to SCNP using a facile intra-chain polymerization process. Our early findings suggest that the coupling of a small proportion of the chains drives SCNP formation while the majority of pendant ends remain active.

A range of topologies was prepared using a common p(MMA-co-MeBrema) precursor prepared using RAFT polymerization, where MeBrema is active both as an ATRP initiator and a coupling substrate. Sequences of ATRP and ATRC were therefore possible using a unified set of reaction conditions. The topologies prepared include MMA brushes, styrene brushes, MeBrema hypergrafts, p(MMA-co-MeBrema) copolymer hypergrafts and hypergrafts. The brush and hyperbranched morphologies had Mark-Houwink alpha parameters characteristic of rod-like and globular-like morphologies, respectively. The globular nature of the hypergrafted SCNP morphology may be exploited by future designs to mimic the hydrophobic pockets found in nature.

It was possible to perform the atom transfer radical polymerization of styrene from SCNP hypergrafts in a controlled fashion; monomer conversion approximately obeyed pseudo first order kinetics. This evidence of chain end fidelity speaks to the possibility of building more complex systems through further functionalization or chain extension. However, thorough characterization of these species by NMR or GPC becomes increasingly difficult with advanced molecular weight and corresponding inflexibility.

Chapter IV. Experimental

General Experimental Section

Solvents

Anhydrous solvents [tetrahydrofuran (THF), acetonitrile (MeCN), toluene (tol.)] passed through drying agent with nitrogen pressure, were obtained from an Innovative Technology, Inc. Solvent Delivery System prior to use and stored over 4 Å molecular sieves.

Reagents

All reagents were received from commercial sources and were used as received unless otherwise noted. Reagents were purchased from the indicated suppliers and used without further purification unless otherwise stated:

1. Methyl methacrylate and 2-hydroxyethyl methacrylate were filtered through a plug of basic alumina before use.
2. 4-Cyano-4-[(dodecylsulfanylthiocarbonyl)sulfanyl]pentanoic acid was recrystallized from methanol and 2,2'-azobisisobutyronitrile from ethanol before use. Freshly purified samples were blanketed with nitrogen, stored in the freezer, and used within a week.
3. Copper (I) bromide (approximately 100 mg in 10 mL) was purified before each use by stirring in glacial acetic acid at room temperature for at least 1 h. The resulting light gray powder was recovered by vacuum filtration, washed with ethanol and diethyl ether (2 x 5 mL each), and dried under vacuum for at least 1 h. This was critical to the success of ATRC using these substrates.

Dichloromethane (DCM, Fisher Scientific), petroleum ether (Sigma-Aldrich), toluene (Fisher Scientific), tetrahydrofuran (THF, inhibited with BHT, Fisher Scientific), 4-cyano-4-[(dodecylsulfanylthiocarbonyl)sulfanyl]pentanoic acid (Sigma-Aldrich), 2,2'-azobisisobutyronitrile (Sigma-Aldrich), methyl methacrylate (Sigma-Aldrich), copper(I) bromide (STREM Chemicals Inc.), 2-hydroxyethyl methacrylate (HEMA, Sigma-Aldrich), triethylamine (TEA, Sigma-Aldrich), toluene (EMD Chemicals), 2-bromopropionyl bromide (Sigma-Aldrich), α -bromoisobutryl bromide (Sigma-Aldrich), α -bromophenylacetic acid (Sigma-Aldrich), sodium sulfate (Fisher Scientific), N,N,N',N'',N''-pentamethyldiethylenetriamine (PMDETA, Sigma-Aldrich), N,N,N',N'-Tetrakis(2-pyridylmethyl)ethylenediamine (TPEN, Fisher Scientific), Tris(2-pyridylmethyl)amine (TPMA, Fisher Scientific), copper(0) (The Hilman Group Inc.), methanol (Fisher Scientific), 4-(dimethylamino)pyridine (DMAP, Sigma-Aldrich), N,N'-dicyclohexylcarbodiimide (DCC, Alfa Aesar), sodium bicarbonate (Fisher Scientific), alumina (activated basic, Alfa Aesar), alumina (neutral, Alfa Aesar), chloroform-d (CDCl_3 , Cambridge Isotope Laboratories), tetrahydrofuran- d_6 (THF- d_6 , Cambridge Isotope Laboratories), and N,N-dimethylformamide- d_7 (DMF- d_7 , Cambridge Isotope Laboratories).

Reactions

Glassware and Teflon coated magnetic stir bars were dried in an oven at 75 °C prior to use. Sigma-Aldrich natural rubber septa were used. Unless otherwise noted, nitrogen gas was introduced to the reaction vessel through a Tygon® tube with a needle or glass inlet adapter. Henke Sass Wolf Norm-ject® plastic syringes were used for volumetric addition of reagents with oven-dried Popper & Sons needles, Precision Glide sterile needles, or Sterican® sterile needles unless otherwise noted.

Flash Chromatography

Flash column chromatography was performed with Silicycle SiliaFlash P60 Flash Silica Gel or with a Teledyne Isco CombiFlash Rf 200 purification system. Purifications using CombiFlash Rf used RediSep® pre-packed silica gel columns (20-70 μm particle size). Preparative chromatography was completed with Analtech Uniplate Silica Gel GF 100 micron UV 254 glass-backed plates. Thin Layer Chromatography (TLC) analysis used Whatman polyester-backed Silica Gel, 60 \AA , 250 μm thickness, on flexible plates with a fluorescent indicator. Mobile phases were prepared per-use as described in the detailed experimental section.

Instrumentation

NMR

Nuclear Magnetic Resonance (NMR) spectra were measured on a Varian Mercury Plus 400 FT-NMR operating at 400 MHz for ^1H and 100 MHz for ^{13}C spectroscopy. All ^1H resonances were reported relative to an internal standard tetramethylsilane (TMS, δ 0 ppm), unless otherwise noted.

Diffusion-ordered spectroscopy (DOSY) experiments were performed on a Varian UnityINOVA 500 spectrometer running VnmrJ 3.2 and equipped with a 5 mm broadband probe. 20–30 mg of polymer was dissolved in 0.75 mL of THF- d_6 or DMF- d_7 . All samples were stabilized at 25 $^\circ\text{C}$ for 10 min before acquisition. The maximum gradient strength was 0.135 T/m. The pulse sequence used was a DOSY bipolar pulse paired stimulated echo with convection compensation (Dbppste_cc). The following acquisition parameters were employed: diffusion gradient length = 2.0 ms, diffusion delay = 200 ms, gradient stabilization delay = 0.5 ms, gradient steps = 15, and transients = 16. The relative molecular weight (Mw) of each polymer was determined by referencing the diffusion coefficient to a calibration curve generated from polystyrene standards analyzed under the same conditions (Figure 44, Table 9). DOSY spectra were processed with

MestReNova 11.0 software. Diffusion coefficients were gathered by performing a Bayesian transform and selecting the maximum intensity of the diffusion projection.

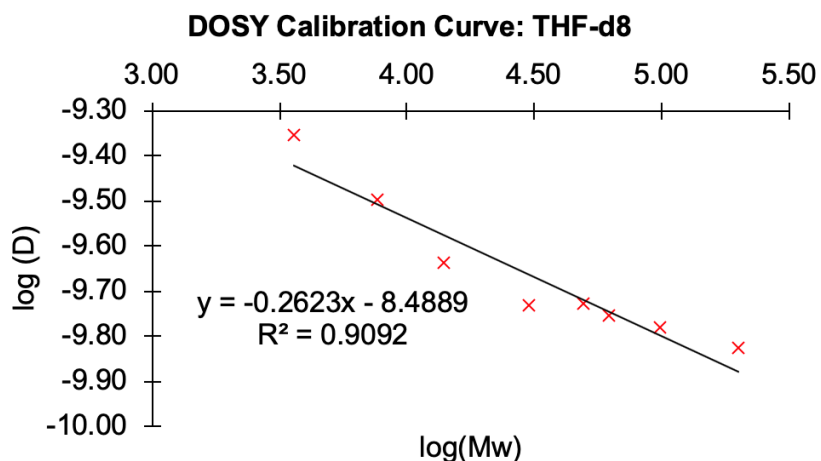


Figure 44. DOSY Calibration Curve prepared for narrowly disperse PS standards in THF-d6.

Table 9. Diffusion coefficients used to DOSY calibration curve, above.

Mw (kg/mol)	D (m/s²)	log (Mw)	log(D)
3.6	4.42251E-10	3.556303	-9.354331
7.6	3.19107E-10	3.880814	-9.496064
14.0	2.30253E-10	4.146128	-9.637795
62.1	1.75426E-10	4.793092	-9.755906
99.0	1.66037E-10	4.995635	-9.779795
200.0	1.49005E-10	5.30103	-9.826799

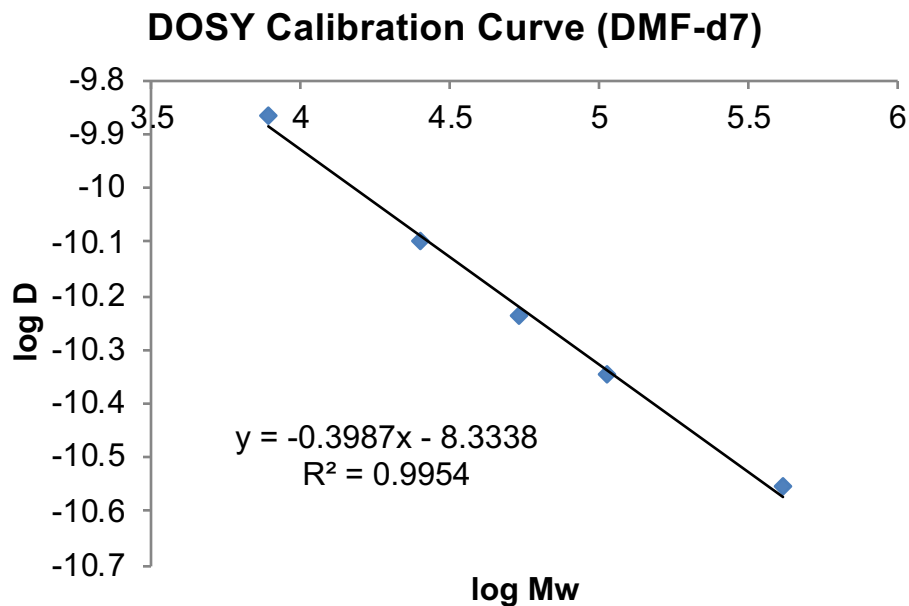


Figure 45. DOSY Calibration Curve prepared for narrowly disperse PS standards in DMF-d7.

Table 10. Diffusion coefficients used to DOSY calibration curve, above.

MW	D (m²/s)	log(MW)	log(D)
7.82	1.36E-10	3.893206753	-9.8664611
25.10	8E-11	4.399673721	-10.09691
53.50	5.8E-11	4.728353782	-10.236572
105.20	4.5E-11	5.02201574	-10.346787
410.00	2.8E-11	5.612783857	-10.552842

SEC

SEC was performed on a Tosoh EcoSEC dual detection (RI and UV) SEC system coupled to an external Wyatt Technologies miniDAWN Treos multiangle light scattering (MALS) detector.

Samples were run in THF at 30 °C at a flow rate of 0.35 mL/min. The column set contained one Tosoh TSKgel SuperH2500 (6 × 150 mm) column, one Tosoh TSKgel SuperHM-M (6 × 150 mm) column, one Tosoh TSKgel SuperH3000 (6 × 150 mm) column, one Tosoh TSKgel SuperH4000 (6 × 150 mm), and two Tosoh TSKgel SuperH-L guard columns (4.6 × 3.5 cm).

Refractive Index Increment (dn/dc)

Unless otherwise noted, refractive index increment values (dn/dc) were calculated online assuming 100% mass recovery (RI as the concentration detector) using the Astra 6 software package (Wyatt Technologies) by selecting the entire trace from analyte peak onset to the onset of the solvent peak or flow marker. The resultant dn/dc values were corroborated by those calculated for each polymer backbone chemistry (MMA, PS, p(MMA-co-MeBrema), and p(MMA-co-PhBrema)) using a multiple injection volume method. An example of this process is shown in Figure 46. The raw dRI was integrated for each of three injection volumes. These integral values were plotted against effective concentration and the slope of the linear fit was then divided by the detector constant (calibrated using narrow PDI polystyrene standards supplied by Wyatt).

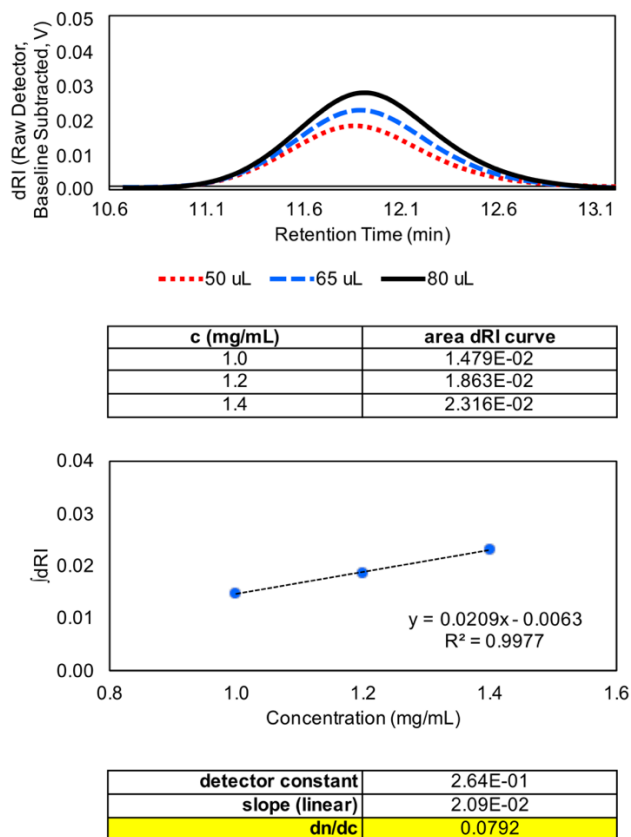


Figure 46. Determination of dn/dc of a PMMA research sample using the multiple injection volumes method.

Both methods gave the expected values for polystyrene ($dn/dc = 0.185$, $M_n = 30K$) when applied to a narrow PDI PS standard supplied by Wyatt. Absolute molecular weights and molecular weight distributions were calculated using the Astra 6 software package. All polymer solutions characterized by SEC were 1.0 mg mL^{-1} and were stirred magnetically for at least 12 h before analysis.

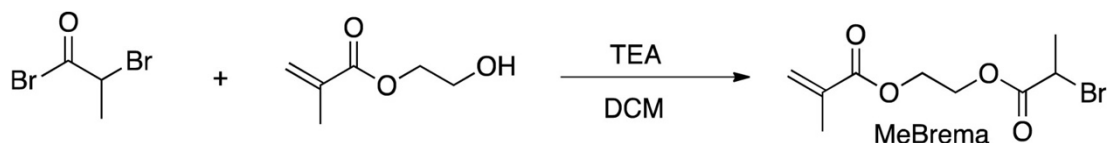
Mark-Houwink parameters

The Mark-Houwink a parameter for each sample was determined by taking the slope of the linear fit of the Mark-Houwink-Sakurada plot ($\log(\eta_n)$ vs. $\log(MW)$) of the differential pressure GPC trace.

Detailed Experimental Section

Syntheses in Chapter II

Monomer Synthesis



Monomer 1 (MeBrema)⁷¹

2-hydroxyethyl methacrylate (4.90 mL, 0.040 mol), triethyl amine (5.63 mL, 0.040 mol), and DCM (30 mL) were added to a dry, 100 mL round bottom flask equipped with a stir bar. The mixture was stirred at 0 °C and a solution of 2-bromopropionyl bromide (4.65 mL, 0.044 mol) in DCM (5 mL) was added dropwise. The reaction mixture was allowed to warm to room temperature after 45 minutes and stirred overnight. The salt byproduct was removed by vacuum filtration and the filtrate was washed with DI water (2 x 25 mL) and a saturated sodium bicarbonate solution (2 x 25 mL). The organic layers were combined and dried over anhydrous sodium sulfate. The solvent was concentrated under reduced pressure to afford a pale yellow oil (9.28 g, 0.035 mol) in an 87% yield. ¹H NMR (400 MHz, CDCl₃, δ, ppm): 1.83 (d, 3H, CH₃), 1.95 (s, 3H, CH₃), 4.37–4.45 (m, 5H, CH₂), 5.60 (s, 1H, C=CH₂), 6.14 (s, 1H, C=CH₂). ¹³C NMR (400 MHz, CDCl₃, δ, ppm): 18.5, 21.8, 39.9, 62.2, 63.6, 126.4, 136.0, 167.2, 170.2.

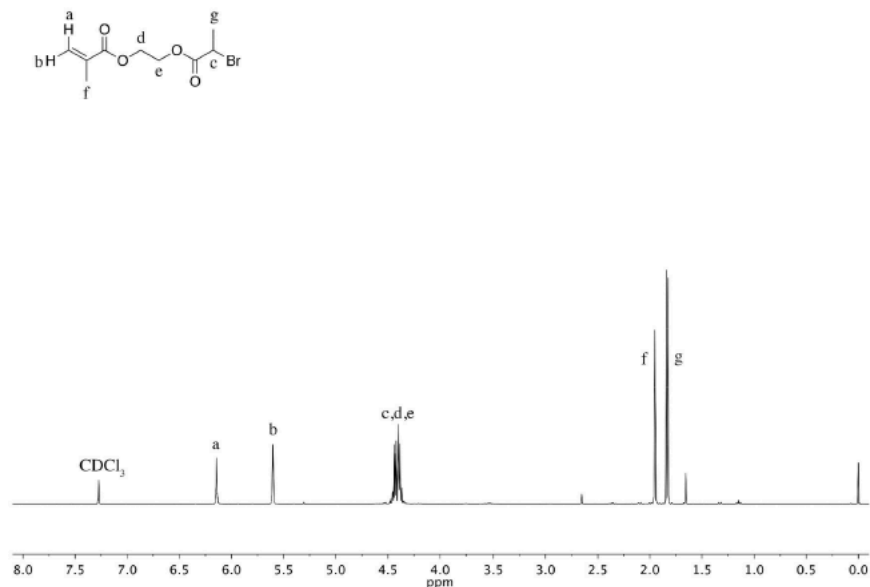
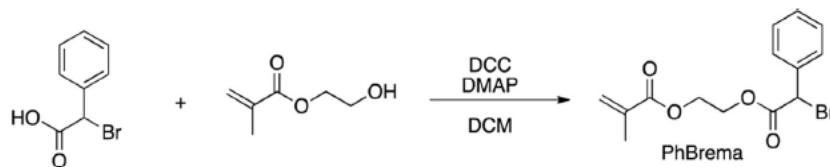


Figure SI 1. ^1H NMR of MeBrema.



Monomer 2 (PhBrema)⁷¹

Synthesis of Monomer 2 (PhBrema). α -bromophenylacetic acid (6.45 g, 0.030 mol) and DCM (75 mL) were added to a 100 mL round bottom flask equipped with a stir bar. The resulting solution was cooled to 0 °C with stirring, HEMA (1.82 mL, 0.015 mol), DCC (6.19 g, 0.030 mol), and DMAP (0.37 g, 3 mmol) were added, and the reaction was allowed to warm to room temperature and stirred overnight. The reaction mixture was filtered through a silica plug. The filtrate was concentrated under reduced pressure and the crude product (a yellow oil) was purified by flash column chromatography using a 4:1 hexanes:ethyl acetate solution as eluent to obtain the pure, pale yellow product (2.79 g, 8.56 mmol) in a 65% yield. ^1H NMR (400 MHz, CDCl_3 , δ , ppm): 1.90 (dd, 3H, CH₃), 4.34–4.39 (m, 2H, CH₂), 5.37 (s, 1H, CH), 5.56 (p, 1H, C=CH₂), 6.06 (p, 1H, C=CH₂), 7.31–7.40 (m, 3H, Ar-H), 7.50–7.60 (m, 2H, Ar-H). ^{13}C NMR (400 MHz, CDCl_3 , δ , ppm): 18.5, 46.6, 62.1, 64.1, 126.5, 128.9, 129.1, 129.6, 135.7, 135.9, 168.3, 167.2.

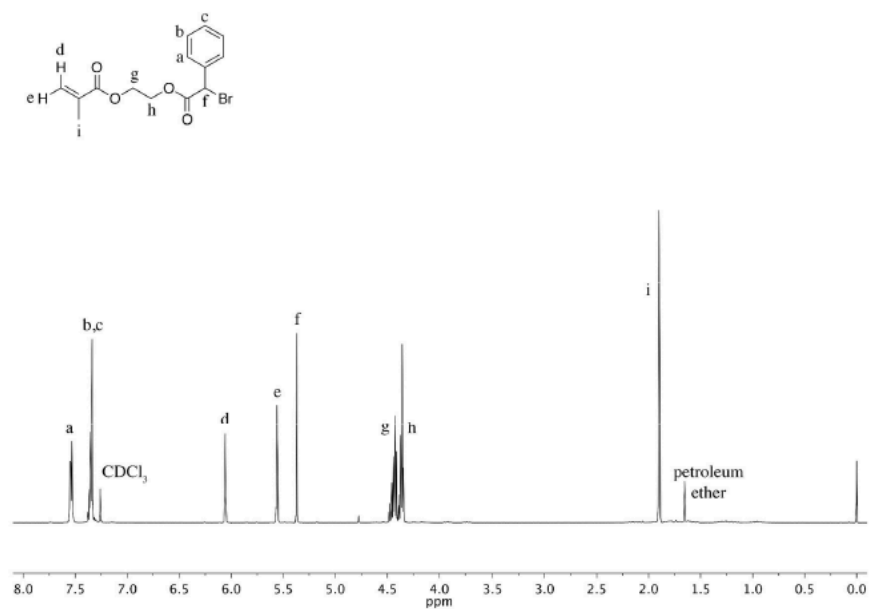


Figure SI 2. ^1H NMR of PhBrema.

General Procedure for RAFT

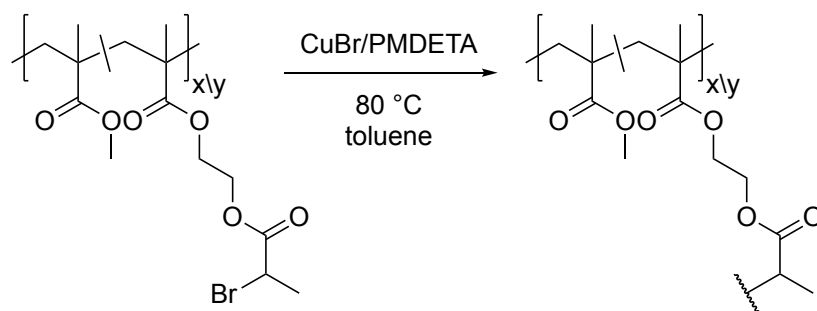
Monomers (methyl methacrylate, MeBrema, and/or PhBrema), CTA (4-cyano-4-[(dodecylsulfanylthiocarbonyl)sulfanyl] pentanoic acid) and initiator (2,2'-azobis(2-methylpropionitrile)) were dissolved in dry toluene (1 g/mL) in a 10 mL Schlenk flask equipped with a magnetic stir bar. The solution was sparged with nitrogen for 30 min, then heated at 80 °C for 12–20 h. Conversion was monitored via ^1H NMR. At 50–80% conversion, the polymerization was halted by removing the solution from heat and exposing it to atmosphere. It was then diluted with 2–5 mL THF, precipitated into cold hexanes, and dried under vacuum to afford a white powder. Spectra, GPC traces, and all other relevant characterization for these materials is available in Appendix A, below.

General Procedure for Intramolecular ATRC

The polymer was dissolved in dry, degassed THF (10 mL) and stirred overnight. The solution was added to a separate 200 mL Schlenk flask containing a mixture of dry and degassed acetonitrile and THF (45 and 35 mL, respectively), and a stir bar wrapped in copper(0). The flask was

subjected to at least 3 cycles of freeze-pump-thaw and backfilled with argon for 40 min then placed in an oil bath at 55 °C and allowed come to temperature. The ligand (PMDETA, TPMA, or TPEN, 10 equivalents to functional monomer unit) was then added and the reaction was allowed to stir overnight. After 14-16 h, the reaction mixture was then opened to air and immediately put through a plug of neutral alumina twice to remove the copper bromide catalyst. The crude nanoparticle was isolated by removing the solvent through rotary evaporation. It was then taken up in 2–5 mL of THF, precipitated into cold hexanes, and filtered to afford a fine white to pale yellow powder in up to a 60% yield. Spectra, GPC traces, and all other relevant characterization is available in Appendix A, below.

Cu(0)-free Control for Intramolecular ATRC

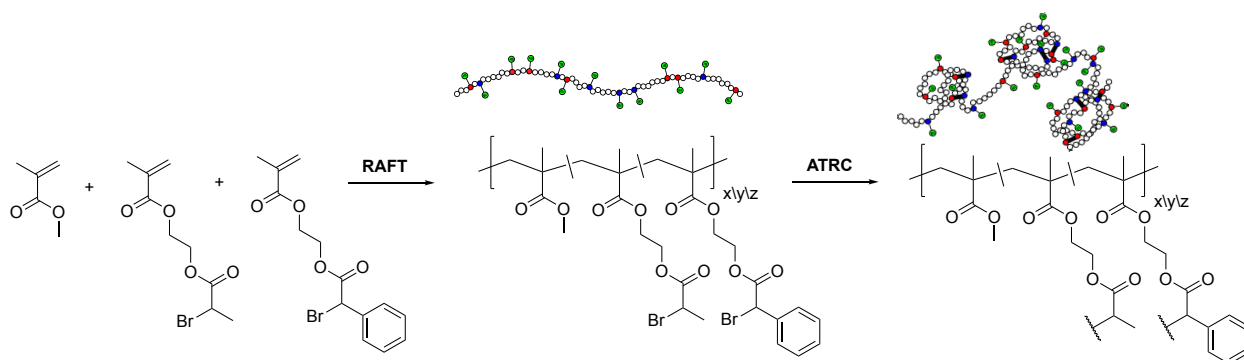


NPA-1.

A 200 mL Schlenk flask containing the parent polymer (PA) (100 mg), Cu(I)Br (2–5 eq.), dry and degassed toluene (95 mL), PMDETA (10 eq.), and a magnetic stir bar was subjected to three cycles of freeze-pump-thaw. The reaction was backfilled with nitrogen and stirred for 16 h at 80 °C. It was then removed from heat, opened to atmosphere and immediately filtered through a plug of neutral alumina to remove the copper catalyst. The nanoparticle solution was concentrated under reduced pressure, taken up in a minimal volume of THF (2–5 mL), and precipitated into cold hexanes. The resulting white to light green powder product was recovered using vacuum

filtration (25-45 mg recovered). Spectra, GPC traces, and all other relevant characterization is available in Appendix A, below.

ATRC of a Terpolymer to Examine the Persistent Radical Effect



NPAB.

A 200 mL Schlenk flask containing the parent polymer (PAB) (100 mg), Cu(I)Br (5 eq.), dry and degassed toluene (100 mL), PMDETA (10 eq.), and a magnetic stir bar was subjected to three cycles of freeze-pump-thaw. The reaction was backfilled with nitrogen and stirred for 18 h at 80 °C. It was then removed from heat, opened to atmosphere and immediately filtered through a plug of neutral alumina to remove the copper catalyst. The nanoparticle solution was concentrated under reduced pressure, taken up in a minimal volume of THF (2–5 mL), and precipitated into cold hexanes. The resulting white to light green powder product was recovered using vacuum filtration (48 mg recovered). Spectra, GPC traces, and all other relevant characterization is available in Appendix A, below.

Syntheses in Chapter III

Preparation of Brushes and Hypergrafts

A 200 mL Schlenk flask containing the appropriate parent polymer (50 mg), monomer (MMA, STY, PhBrema, or MeBrema, 10–100 eq.), Cu(I)Br (2 eq.), Cu(0) wire, dry and degassed toluene (100 mL), and a magnetic stir bar was sparged while stirring at 80 °C for 30 min. The ligand (PMDETA, 5 eq.) was then added to the flask containing the parent polymer via airtight syringe and the reaction was stirred for 16 h. It was then removed from heat, opened to atmosphere and immediately filtered through a plug of neutral alumina to remove the copper catalyst. The nanoparticle solution was concentrated under reduced pressure, taken up in a minimal volume of THF (2–5 mL), and precipitated into cold hexanes. The resulting white to light green powder product was recovered using vacuum filtration (30–60% yield). Spectra, GPC traces, and all other relevant characterization is available in Appendix A, below.

LIST OF REFERENCES

- (1) Chen, A. H.; Silver, P. A. Designing Biological Compartmentalization. *Trends Cell Biol.* **2012**, 22 (12), 662–670. <https://doi.org/10.1016/j.tcb.2012.07.002>.
- (2) Pieters, B. J. G. E.; van Eldijk, M. B.; Nolte, R. J. M.; Mecnovic, J. Natural Supramolecular Protein Assemblies. *Chem. Soc. Rev.* **2016**, 45 (1), 24–39. <https://doi.org/10.1039/C5CS00157A>.
- (3) Huo, M.; Wang, N.; Fang, T.; Sun, M.; Wei, Y.; Yuan, J. Single-Chain Polymer Nanoparticles: Mimic the Proteins. *Polymer (Guildf)*. **2015**, 66, A11.
- (4) Sanchez-Sanchez, A.; Akbari, S.; Etxeberria, A.; Arbe, A.; Gasser, U.; Moreno, A. J.; Colmenero, J.; Pomposo, J. A. "Michael" Nanocarriers Mimicking Transient-Binding Disordered Proteins. *ACS Macro Lett.* **2013**, 2, 491.
- (5) Boyer, C.; Corrigan, N. A.; Jung, K.; Nguyen, D.; Nguyen, T.-K.; Adnan, N. N. M.; Oliver, S.; Shanmugam, S.; Yeow, J. Copper-Mediated Living Radical Polymerization (Atom Transfer Radical Polymerization and Copper(0) Mediated Polymerization): From Fundamentals to Bioapplications. *Chem. Rev.* **2016**, 116 (4), 1803–1949.

<https://doi.org/10.1021/acs.chemrev.5b00396>.

- (6) Perrier, S. 50th Anniversary Perspective: RAFT Polymerization—A User Guide. *Macromolecules* **2017**, *50* (19), 7433–7447. <https://doi.org/10.1021/acs.macromol.7b00767>.
- (7) Erickson, H. P. Size and Shape of Protein Molecules at the Nanometer Level Determined by Sedimentation, Gel Filtration, and Electron Microscopy. *Biol. Proced. Online* **2009**, *11*, 32–51. <https://doi.org/10.1007/s12575-009-9008-x>.
- (8) Woodruff, S. R.; Davis, B. J.; Tsarevsky, N. V. Selecting the Optimal Reaction Conditions for Copper-Mediated Atom Transfer Radical Polymerization at Low Catalyst Concentration. In *Progress in Controlled Radical Polymerization: Mechanisms and Techniques*; ACS Symposium Series; American Chemical Society, 2019; Vol. 1100, pp 99–113. <https://doi.org/doi:10.1021/bk-2012-1100.ch007> [10.1021/bk-2012-1100.ch007](https://doi.org/10.1021/bk-2012-1100.ch007).
- (9) Perez-Baena, I.; Moreno, A. J.; Colmenero, J.; Pomposo, J. A. Single-Chain Nanoparticles vs. Star, Hyperbranched and Dendrimeric Polymers: Effect of the Nanoscopic Architecture on the Flow Properties of Diluted Solutions. *Soft Matter* **2014**, *10* (47), 9454–9459. <https://doi.org/10.1039/C4SM01991A>.
- (10) Rossner, C.; Tang, Q.; Glatter, O.; Müller, M.; Vana, P. Uniform Distance Scaling Behavior of Planet–Satellite Nanostructures Made by Star Polymers. *Langmuir* **2017**, *33* (8), 2017–

2026. <https://doi.org/10.1021/acs.langmuir.6b04473>.

- (11) Bosman, A. W.; Janssen, H. M.; Meijer, E. W. About Dendrimers: Structure, Physical Properties, and Applications. *Chem. Rev.* **1999**, *99* (7), 1665–1688. <https://doi.org/10.1021/cr970069y>.
- (12) Caminade, A.-M.; Yan, D.; Smith, D. K. Dendrimers and Hyperbranched Polymers. *Chem. Soc. Rev.* **2015**, *44* (12), 3870–3873. <https://doi.org/10.1039/C5CS90049B>.
- (13) Ren, J. M.; McKenzie, T. G.; Fu, Q.; Wong, E. H. H.; Xu, J.; An, Z.; Shanmugam, S.; Davis, T. P.; Boyer, C.; Qiao, G. G. Star Polymers. *Chem. Rev.* **2016**, *116* (12), 6743–6836. <https://doi.org/10.1021/acs.chemrev.6b00008>.
- (14) Verduzco, R.; Li, X.; Pesek, S. L.; Stein, G. E. Structure, Function, Self-Assembly, and Applications of Bottlebrush Copolymers. *Chem. Soc. Rev.* **2015**, *44* (8), 2405–2420. <https://doi.org/10.1039/C4CS00329B>.
- (15) Verduzco, R.; Li, X.; Pesek, S. L.; Stein, G. E. Structure, Function, Self-Assembly, and Applications of Bottlebrush Copolymers. *Chem. Soc. Rev.* **2015**, *44* (8), 2405–2420. <https://doi.org/10.1039/C4CS00329B>.
- (16) Keddie, D. J. A Guide to the Synthesis of Block Copolymers Using Reversible-Addition

- Fragmentation Chain Transfer (RAFT) Polymerization. *Chem. Soc. Rev.* **2014**, *43* (2), 496–505. <https://doi.org/10.1039/C3CS60290G>.
- (17) ter Huurne, G. M.; Gillissen, M. A. J.; Palmans, A. R. A.; Voets, I. K.; Meijer, E. W. The Coil-to-Globule Transition of Single-Chain Polymeric Nanoparticles with a Chiral Internal Secondary Structure. *Macromolecules* **2015**, *48* (12), 3949–3956. <https://doi.org/10.1021/acs.macromol.5b00604>.
- (18) Le Bailly, B. A. F.; Clayden, J. Dynamic Foldamer Chemistry. *Chem. Commun.* **2016**, *52* (27), 4852–4863. <https://doi.org/10.1039/C6CC00788K>.
- (19) Kumita, J. R.; Smart, O. S.; Woolley, G. A. Photo-Control of Helix Content in a Short Peptide. *Proc. Natl. Acad. Sci.* **2000**, *97* (8), 3803. <https://doi.org/10.1073/pnas.97.8.3803>.
- (20) Gutekunst, W. R.; Hawker, C. J. A General Approach to Sequence-Controlled Polymers Using Macrocyclic Ring Opening Metathesis Polymerization. *J. Am. Chem. Soc.* **2015**, *137* (25), 8038–8041. <https://doi.org/10.1021/jacs.5b04940>.
- (21) Schulz, M. D.; Wagener, K. B. Precision Polymers through ADMET Polymerization. *Macromol. Chem. Phys.* **2014**, *215* (20), 1936–1945. <https://doi.org/10.1002/macp.201400268>.

- (22) Martens, S.; Holloway, J. O.; Du Prez, F. E. Click and Click-Inspired Chemistry for the Design of Sequence-Controlled Polymers. *Macromol. Rapid Commun.* **2017**, *38* (24), 1700469. <https://doi.org/10.1002/marc.201700469>.
- (23) Wang, C.-H.; Song, Z.-Y.; Deng, X.-X.; Zhang, L.-J.; Du, F.-S.; Li, Z.-C. Combination of ATRA and ATRC for the Synthesis of Periodic Vinyl Copolymers. *Macromol. Rapid Commun.* **2014**, *35* (4), 474–478. <https://doi.org/10.1002/marc.201300721>.
- (24) Wang, C.-H.; Song, Z.-Y.; Deng, X.-X.; Zhang, L.-J.; Du, F.-S.; Li, Z.-C. Combination of ATRA and ATRC for the Synthesis of Periodic Vinyl Copolymers. *Macromol. Rapid Commun.* **2014**, *35* (4), 474–478. <https://doi.org/10.1002/marc.201300721>.
- (25) Crosslinking of Single Linear Macromolecules. *J. Polym. Sci.* **1962**, *57* (165), 311–319. <https://doi.org/10.1002/pol.1962.1205716524>.
- (26) Tuten, B. T.; Chao, D.; Lyon, C. K.; Berda, E. B. Single-Chain Polymer Nanoparticles via Reversible Disulfide Bridges. *Polym. Chem.* **2012**, *3* (11), 3068–3071. <https://doi.org/10.1039/C2PY20308A>.
- (27) Frank, P. G.; Tuten, B. T.; Prasher, A.; Chao, D.; Berda, E. B. Intra-Chain Photodimerization of Pendant Anthracene Units as an Efficient Route to Single-Chain Nanoparticle Fabrication. *Macromol. Rapid Commun.* **2014**, *35* (2), 249–253. <https://doi.org/10.1002/marc.201300677>.

- (28) Gillissen, M. A. J.; Voets, I. K.; Meijer, E. W.; Palmans, A. R. A. Single Chain Polymeric Nanoparticles as Compartmentalised Sensors for Metal Ions. *Polym. Chem.* **2012**, 3 (11), 3166–3174. <https://doi.org/10.1039/C2PY20350B>.
- (29) Hanlon, A. M.; Lyon, C. K.; Berda, E. B. What Is Next in Single-Chain Nanoparticles? *Macromolecules* **2016**, 49, 2.
- (30) Altintas, O.; Barner-Kowollik, C. Single Chain Folding of Synthetic Polymers by Covalent and Non-Covalent Interactions: Current Status and Future Perspectives. *Macromol. Rapid Commun.* **2012**, 33, 958.
- (31) Zimm, B. No Title. *J. Chem. Phys.* **1946**, 14, 164.
- (32) Debye, P. No Title. *J. Phys. Coll. Chem.* **1947**, 51, 18.
- (33) Lyon, C. K.; Prasher, A.; Hanlon, A. M.; Tuten, B. T.; Tooley, C. A.; Frank, P. G.; Berda, E. B. A Brief User's Guide to Single-Chain Nanoparticles. *Polym. Chem.* **2015**, 6, 181.
- (34) Hanlon, A. M.; Martin, I.; Bright, E. R.; Chouinard, J.; Rodriguez, K. J.; Patenotte, G. E.; Berda, E. B. Exploring the Effects of Internal versus External Cross-Linking in Single-Chain "Folding" via Thermal Diels-Alder Reactions. *Polym. Chem.* **2017**.

- (35) Pomposo, J. A.; Perez-Baena, I.; Lo Verso, F.; Moreno, A. J.; Arbe, A.; Colmenero, J. How Far Are Single-Chain Polymer Nanoparticles in Solution from the Globular State? *ACS Macro Lett.* **2014**, 3 (8), 767–772. <https://doi.org/10.1021/mz500354q>.
- (36) Arbe, A.; Pomposo, J. A.; Moreno, A. J.; LoVerso, F.; González-Burgos, M.; Asenjo-Sanz, I.; Iturrospe, A.; Radulescu, A.; Ivanova, O.; Colmenero, J. Structure and Dynamics of Single-Chain Nano-Particles in Solution. *Polymer (Guildf)*. **2016**, 105, 532–544. <https://doi.org/https://doi.org/10.1016/j.polymer.2016.07.059>.
- (37) Gonzalez-Burgos, M.; Latorre-Sanchez, A.; Pomposo, J. A. Advances in Single Chain Technology. *Chem. Soc. Rev.* **2015**, 44 (17), 6122–6142. <https://doi.org/10.1039/C5CS00209E>.
- (38) Moreno, A. J.; Arbe, A.; Pomposo, J. A.; Colmenero, J.; Lo, V. F. Concentrated Solutions of Single-Chain Nanoparticles: A Simple Model for Intrinsically Disordered Proteins under Crowding Conditions. *J Phys Chem Lett* **2016**, 7 (5), 838–844.
- (39) Altintas, O.; Barner-Kowollik, C. Single Chain Folding of Synthetic Polymers by Covalent and Non-Covalent Interactions: Current Status and Future Perspectives. *Macromol. Rapid Commun.* **2012**, 33 (11), 958–971. <https://doi.org/10.1002/marc.201200049>.
- (40) Chao, D.; Jia, X.; Tuten, B.; Wang, C.; Berda, E. B. Controlled Folding of a Novel Electroactive Polyolefin via Multiple Sequential Orthogonal Intra-Chain Interactions. *Chem.*

Commun. **2013**, *49* (39), 4178–4180. <https://doi.org/10.1039/C2CC37157J>.

- (41) Lyon, C. K.; Hill, E. O.; Berda, E. B. Zipping Polymers into Nanoparticles via Intrachain Alternating Radical Copolymerization. *Macromol. Chem. Phys.* **2016**, *217*, 501.
- (42) Cole, J. P.; Lessard, J. J.; Lyon, C. K.; Tuten, B. T.; Berda, E. B. Intra-Chain Radical Chemistry as a Route to Poly(Norbornene Imide) Single-Chain Nanoparticles: Structural Considerations and the Role of Adventitious Oxygen. *Polym. Chem.* **2015**, *6* (31), 5555–5559. <https://doi.org/10.1039/C5PY00265F>.
- (43) Debuigne, A.; Hurtgen, M.; Detrembleur, C.; Jérôme, C.; Barner-Kowollik, C.; Junkers, T. Interpolymer Radical Coupling: A Toolbox Complementary to Controlled Radical Polymerization. *Prog. Polym. Sci.* **2012**, *37*, 1004.
- (44) Liu, J.; Lian, X.; Zhao, F.; Zhao, H. Intramolecular Atom Transfer Radical Coupling of Macromolecular Brushes. *J. Polym. Sci. Part A Polym. Chem.* **2013**, *51* (17), 3567–3571. <https://doi.org/10.1002/pola.26760>.
- (45) Chen, R.; Benware, S. J.; Cawthern, S. D.; Cole, J. P.; Lessard, J. J.; Crawford-Eng, I. M.; Saxena, R.; Berda, E. B. Assessing Structure/Property Relationships and Synthetic Protocols in the Fabrication of Poly(Oxanorbornene Imide) Single-Chain Nanoparticles. *Eur. Polym. J.* **2019**, *112*, 206–213. <https://doi.org/https://doi.org/10.1016/j.eurpolymj.2018.12.046>.

- (46) Mecerreyes, D.; Lee, V.; Hawker, C. J.; Hedrick, J. L.; Wursch, A.; Volksen, W.; Magbitang, T.; Huang, E.; Miller, R. D. A Novel Approach to Functionalized Nanoparticles: Self-Crosslinking of Macromolecules in Ultradilute Solution. *Adv. Mater.* **2001**, *13*, 204.
- (47) Dirlam, P. T.; Kim, H. J.; Arrington, K. J.; Chung, W. J.; Sahoo, R.; Hill, L. J.; Costanzo, P. J.; Theato, P.; Char, K.; Pyun, J. Single Chain Polymer Nanoparticles via Sequential ATRP and Oxidative Polymerization. *Polym. Chem.* **2013**, *4* (13), 3765–3773. <https://doi.org/10.1039/C3PY00321C>.
- (48) Roy, R. K.; Lutz, J.-F. Compartmentalization of Single Polymer Chains by Stepwise Intramolecular Cross-Linking of Sequence-Controlled Macromolecules. *J. Am. Chem. Soc.* **2014**, *136* (37), 12888–12891. <https://doi.org/10.1021/ja507889x>.
- (49) P Cole, J.; Lessard, J.; Rodriguez, K.; Hanlon, A.; Reville, E.; Mancinelli, J.; Berda, E. *Single-Chain Nanoparticles Containing Sequence-Defined Segments: Using Primary Structure Control to Promote Secondary and Tertiary Structures in Synthetic Protein Mimics*; 2017; Vol. 8. <https://doi.org/10.1039/C7PY01133D>.
- (50) Lambert, R.; Wirotius, A.-L.; Taton, D. Intramolecular Quaternization as Folding Strategy for the Synthesis of Catalytically Active Imidazolium-Based Single Chain Nanoparticles. *ACS Macro Lett.* **2017**, *6* (5), 489–494. <https://doi.org/10.1021/acsmacrolett.7b00161>.
- (51) Stals, P. J. M.; Smulders, M. M. J.; Martín-Rapún, R.; Palmans, A. R. A.; Meijer, E. W.

- Asymmetrically Substituted Benzene-1,3,5-Tricarboxamides: Self-Assembly and Odd–Even Effects in the Solid State and in Dilute Solution. *Chem. – A Eur. J.* **2009**, *15* (9), 2071–2080. <https://doi.org/10.1002/chem.200802196>.
- (52) Stals, P. J. M.; Gillissen, M. A. J.; Paffen, T. F. E.; de Greef, T. F. A.; Lindner, P.; Meijer, E. W.; Palmans, A. R. A.; Voets, I. K. Folding Polymers with Pendant Hydrogen Bonding Motifs in Water: The Effect of Polymer Length and Concentration on the Shape and Size of Single-Chain Polymeric Nanoparticles. *Macromolecules* **2014**, *47* (9), 2947–2954. <https://doi.org/10.1021/ma500273g>.
- (53) Huerta, E.; Stals, P. J. M.; Meijer, E. W.; Palmans, A. R. A. Consequences of Folding a Water-Soluble Polymer Around an Organocatalyst. *Angew. Chem., Int. Ed.* **2013**, *52*, 2906.
- (54) Voter, A. F.; Tillman, E. S.; Findeis, P. M.; Radzinski, S. C. Synthesis of Macrocyclic Polymers Formed via Intramolecular Radical Trap-Assisted Atom Transfer Radical Coupling. *ACS Macro Lett.* **2012**, *1* (8), 1066–1070. <https://doi.org/10.1021/mz300311p>.
- (55) Debuigne, A.; Hurtgen, M.; Detrembleur, C.; Jérôme, C.; Barner-Kowollik, C.; Junkers, T. Interpolymer Radical Coupling: A Toolbox Complementary to Controlled Radical Polymerization. *Prog. Polym. Sci.* **2012**, *37* (7), 1004–1030. <https://doi.org/https://doi.org/10.1016/j.progpolymsci.2012.01.003>.
- (56) Lai, K.-Y.; Huang, Y.-S.; Chu, C.-Y.; Huang, C.-F. Synthesis of Poly(N-H Benzamide)-b-

- Poly(Lauryl Methacrylate)-b-Poly(N-H Benzamide) Symmetrical Triblock Copolymers by Combinations of CGCP, SARA ATRP, and SA ATRC. *Polymer (Guildf)*. **2018**, 137, 385–394. <https://doi.org/10.1016/j.polymer.2018.01.033>.
- (57) Yagci, Y. First Polyrecombination Reaction via Atom Transfer Radical Coupling (ATRC), a New Way for the Synthesis of Poly(p-Xylylene) AU - Cianga, Ioan. *Des. Monomers Polym.* **2007**, 10 (6), 575–584. <https://doi.org/10.1163/156855507782401178>.
- (58) Wrue, M. H.; McUmbert, A. C.; Anthamatten, M. Atom Transfer Radical Polymerization of End-Functionalized Hydrogen-Bonding Polymers and Resulting Polymer Miscibility. *Macromolecules* **2009**, 42 (23), 9255–9262. <https://doi.org/10.1021/ma901822k>.
- (59) Bunha, A. K.; Mangadlao, J.; Felipe, M. J.; Pangilinan, K.; Advincula, R. Catenated PS–PMMA Block Copolymers via Supramolecularly Templated ATRP Initiator Approach. *Macromol. Rapid Commun.* **2012**, 33 (14), 1214–1219. <https://doi.org/10.1002/marc.201200043>.
- (60) Sarbu, T.; Lin, K. Y.; Ell, J.; Siegwart, D. J.; Spanswick, J.; Matyjaszewski, K. Polystyrene with Designed Molecular Weight Distribution by Atom Transfer Radical Coupling. *Macromolecules* **2004**, 37, 3120.
- (61) Siegwart, D. J.; Jahed, N.; Sarbu, T.; Matyjaszewski, K. Characterization of α,ω -Dihydroxypolystyrene by Gradient Polymer Elution Chromatography and Two-Dimensional

- Liquid Chromatography AU - Gao, Haifeng. *Des. Monomers Polym.* **2005**, 8 (6), 533–546.
<https://doi.org/10.1163/156855505774597713>.
- (62) Yoshikawa, C.; Goto, A.; Fukuda, T. Reactions of Polystyrene Radicals in a Monomer-Free Atom Transfer Radical Polymerization System. *e-Polym.* **2002**, 2, 172.
- (63) Yurteri, S.; Cianga, I.; Yagci, Y. Synthesis and Characterization of α,ω -Telechelic Polymers by Atom Transfer Radical Polymerization and Coupling Processes. *Macromol. Chem. Phys.* **2003**, 204 (14), 1771–1783. <https://doi.org/10.1002/macp.200300030>.
- (64) Luo, X.; Wang, G.; Huang, J. Preparation of H-Shaped ABCAB Terpolymers by Atom Transfer Radical Coupling. *J. Polym. Sci. Part A Polym. Chem.* **2009**, 47 (1), 59–68.
<https://doi.org/10.1002/pola.23120>.
- (65) Wang, S.; Zhang, K.; Chen, Y.; Xi, F. Isomeric Dicyclic Polymers via Atom Transfer Radical Polymerization and Atom Transfer Radical Coupling Cyclization. *Macromolecules* **2014**, 47 (6), 1993–1998. <https://doi.org/10.1021/ma402335f>.
- (66) Pan, C. W.; Xia, K.; Parker, S. A.; Tillman, E. S. Identity of Low-Molecular-Weight Species Formed in End-To-End Cyclization Reactions Performed in THF. *Polym.* **2018**, 10 (8), N.PAG-N.PAG. <https://doi.org/10.3390/polym10080844>.

- (67) Arce, M. M.; Pan, C. W.; Thursby, M. M.; Wu, J. P.; Carnicom, E. M.; Tillman, E. S. Influence of Solvent on Radical Trap-Assisted Dimerization and Cyclization of Polystyrene Radicals. *Macromolecules* **2016**, *49* (20), 7804–7813. <https://doi.org/10.1021/acs.macromol.6b01794>.
- (68) Fischer, H. The Persistent Radical Effect: A Principle for Selective Radical Reactions and Living Radical Polymerizations. *Chem. Rev.* **2001**, *101* (12), 3581–3610. <https://doi.org/10.1021/cr990124y>.
- (69) Krys, P.; Ribelli, T. G.; Matyjaszewski, K.; Gennaro, A. Relation between Overall Rate of ATRP and Rates of Activation of Dormant Species. *Macromolecules* **2016**, *49* (7), 2467–2476. <https://doi.org/10.1021/acs.macromol.6b00058>.
- (70) Jakubowski, W.; Min, K.; Matyjaszewski, K. Activators Regenerated by Electron Transfer for Atom Transfer Radical Polymerization of Styrene. *Macromolecules* **2006**, *39* (1), 39–45. <https://doi.org/10.1021/ma0522716>.
- (71) Hanlon R., A. M. C.; Rodriguez, K. J.; Willis, C.; Dickinson, J. G.; Cashman, M.; Berda, E. B. Scalable Synthesis of Single-Chain Nanoparticles under Mild Conditions. **2017**.
- (72) Bleach, R.; Karagoz, B.; Prakash, S. M.; Davis, T. P.; Boyer, C. In Situ Formation of Polymer–Gold Composite Nanoparticles with Tunable Morphologies. *ACS Macro Lett.* **2014**, *3* (7), 591–596. <https://doi.org/10.1021/mz500195u>.

- (73) Matyjaszewski, K.; Coca, S.; Gaynor, S. G.; Wei, M.; Woodworth, B. E. Zerovalent Metals in Controlled/"Living" Radical Polymerization. *Macromolecules* **1997**, *30*, 7348. <https://doi.org/10.1021/ma971258l>.
- (74) Tang, W.; Kwak, Y.; Braunecker, W.; Tsarevsky, N. V.; Coote, M. L.; Matyjaszewski, K. Understanding Atom Transfer Radical Polymerization: Effect of Ligand and Initiator Structures on the Equilibrium Constants. *J. Am. Chem. Soc.* **2008**, *130* (32), 10702–10713. <https://doi.org/10.1021/ja802290a>.
- (75) Carmo dos Santos, N. A.; Lorandi, F.; Badetti, E.; Wurst, K.; Isse, A. A.; Gennaro, A.; Licini, G.; Zonta, C. Tuning the Reactivity and Efficiency of Copper Catalysts for Atom Transfer Radical Polymerization by Synthetic Modification of Tris(2-Methylpyridyl)Amine. *Polymer (Guildf)*. **2017**, *128* (Supplement C), 169–176. <https://doi.org/https://doi.org/10.1016/j.polymer.2017.09.018>.
- (76) Gurr, P. A.; Mills, M. F.; Qiao, G. G.; Solomon, D. H. Initiator Efficiency in ATRP: The Tosyl Chloride/CuBr/PMDETA System. *Polymer (Guildf)*. **2005**, *46* (7), 2097–2104. <https://doi.org/http://dx.doi.org/10.1016/j.polymer.2005.01.015>.
- (77) Borguet, Y. P.; Tsarevsky, N. V. Low-Catalyst Concentration Atom Transfer Radical Polymerization of a Phosphonium Salt-Type Monomer. *Polym. Chem.* **2012**, *3* (9), 2487–2494. <https://doi.org/10.1039/C2PY20303K>.

- (78) Soerensen, N.; Schroeder, H.; Buback, M. SP–PLP–EPR Measurement of CuI-Mediated ATRP Deactivation and CuI-Mediated Organometallic Reactions in Butyl Acrylate Polymerization. *Macromolecules* **2016**, *49* (13), 4732–4738. <https://doi.org/10.1021/acs.macromol.6b00760>.
- (79) Nakamura, Y.; Yamago, S. Termination Mechanism in the Radical Polymerization of Methyl Methacrylate and Styrene Determined by the Reaction of Structurally Well-Defined Polymer End Radicals. *Macromolecules* **2015**, *48* (18), 6450–6456. <https://doi.org/10.1021/acs.macromol.5b01532>.
- (80) Li, W.; Chung, H.; Daeffler, C.; Johnson, J. A.; Grubbs, R. H. Application of ¹H DOSY for Facile Measurement of Polymer Molecular Weights. *Macromolecules* **2012**, *45*, 9595.
- (81) Chen, A.; Wu, D.; Johnson, C. S. Determination of Molecular Weight Distributions for Polymers by Diffusion-Ordered NMR. *J. Am. Chem. Soc.* **1995**, *117* (30), 7965–7970. <https://doi.org/10.1021/ja00135a015>.
- (82) Johnson, C. S. Diffusion Ordered Nuclear Magnetic Resonance Spectroscopy: Principles and Applications. *Prog. Nucl. Magn. Reson. Spectrosc.* **1999**, *34* (3), 203–256. [https://doi.org/https://doi.org/10.1016/S0079-6565\(99\)00003-5](https://doi.org/https://doi.org/10.1016/S0079-6565(99)00003-5).
- (83) Harth, E.; Van Horn, B.; Lee, V. Y.; Germack, D. S.; Gonzales, C. P.; Miller, R. D.; Hawker, C. J. A Facile Approach to Architecturally Defined Nanoparticles via Intramolecular Chain

Collapse. *J. Am. Chem. Soc.* **2002**, *124*, 8653.

- (84) Liu, J.; Lian, X.; Zhao, F.; Zhao, H. Intramolecular Atom Transfer Radical Coupling of Macromolecular Brushes. *J. Polym. Sci. Part A Polym. Chem.* **2013**, *51* (17), 3567–3571. <https://doi.org/10.1002/pola.26760>.
- (85) Lu, Y.; Debnath, D.; Weiss, R. A.; Pugh, C. Synthesis and Crosslinking of Hyperbranched Poly(N-nonyl Acrylate) to Form Organogels. *J. Polym. Sci. Part A Polym. Chem.* **2015**, *53* (20), 2399–2410. <https://doi.org/10.1002/pola.27700>.
- (86) Wang, G.; Huang, J. Versatility of Radical Coupling in Construction of Topological Polymers. *Polym. Chem.* **2014**, *5* (2), 277–308. <https://doi.org/10.1039/C3PY00872J>.
- (87) Nakamura, Y.; Ogihara, T.; Yamago, S. Mechanism of Cu(I)/Cu(0)-Mediated Reductive Coupling Reactions of Bromine-Terminated Polyacrylates, Polymethacrylates, and Polystyrene. *ACS Macro Lett.* **2016**, *5*, 248.
- (88) Bachler, P. R.; Forry, K. E.; Sparks, C. A.; Schulz, M. D.; Wagener, K. B.; Sumerlin, B. S. Modular Segmented Hyperbranched Copolymers. *Polym. Chem.* **2016**, *7* (25), 4155–4159. <https://doi.org/10.1039/C6PY00819D>.
- (89) Sarbu, T.; Lin, K.-Y.; Spanswick, J.; Gil, R. R.; Siegwart, D. J.; Matyjaszewski, K. Synthesis

- of Hydroxy-Telechelic Poly(Methyl Acrylate) and Polystyrene by Atom Transfer Radical Coupling. *Macromolecules* **2004**, 37 (26), 9694–9700. <https://doi.org/10.1021/ma0484375>.
- (90) Carnicom, E. M.; Coyne, W. E.; Myers, K. D.; Tillman, E. S. One Pot, Two Step Sequence Converting Atom Transfer Radical Polymerization Directly to Radical Trap-Assisted Atom Transfer Radical Coupling. *Polymer (Guildf)*. **2013**, 54 (21), 5560–5567. <https://doi.org/http://dx.doi.org/10.1016/j.polymer.2013.08.054>.
- (91) Wang, G.; Huang, J. Versatility of Radical Coupling in Construction of Topological Polymers. *Polym. Chem.* **2014**, 5 (2), 277–308. <https://doi.org/10.1039/C3PY00872J>.
- (92) Brandt, J.; Lenz, J.; Pahnke, K.; Schmidt, F. G.; Barner-Kowollik, C.; Lederer, A. Investigation of Thermoreversible Polymer Networks by Temperature Dependent Size Exclusion Chromatography. *Polym. Chem.* **2017**, 8 (43), 6598–6605. <https://doi.org/10.1039/C7PY01262D>.
- (93) Altintas, O.; Willenbacher, J.; Wuest, K. N. R.; Oehlenschlaeger, K. K.; Krolla-Sidenstein, P.; Gliemann, H.; Barner-Kowollik, C. A Mild and Efficient Approach to Functional Single-Chain Polymeric Nanoparticles via Photoinduced Diels–Alder Ligation. *Macromolecules* **2013**, 46 (20), 8092–8101. <https://doi.org/10.1021/ma4015033>.
- (94) Wedler-Jasinski, N.; Lueckerath, T.; Mutlu, H.; Goldmann, A. S.; Walther, A.; Stenzel, M. H.; Barner-Kowollik, C. Dynamic Covalent Single Chain Nanoparticles Based on Hetero

Diels-Alder Chemistry. *Chem. Commun.* **2017**, 53 (1), 157–160.

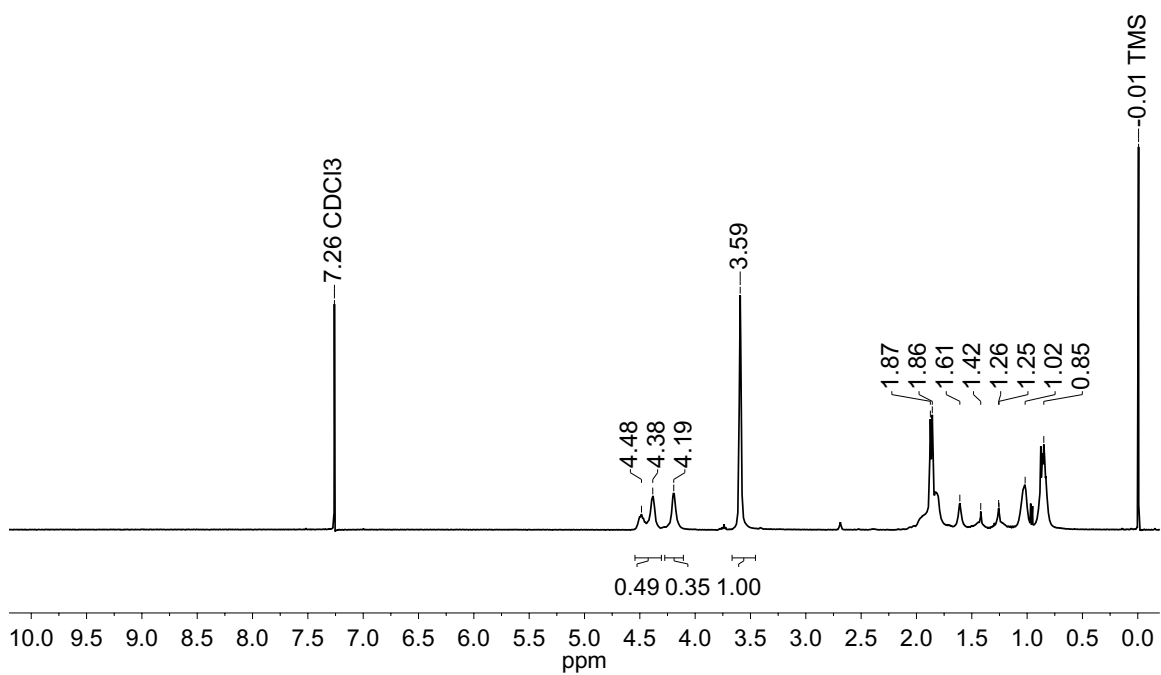
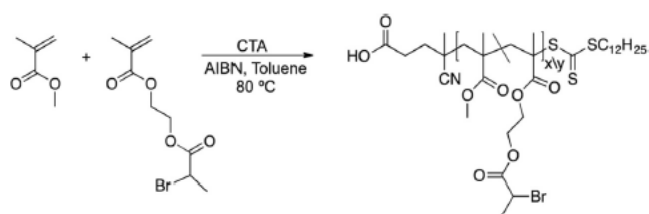
<https://doi.org/10.1039/C6CC07427H>.

Appendices

Appendix A: Characterization

Polymer Samples

PA₉₀



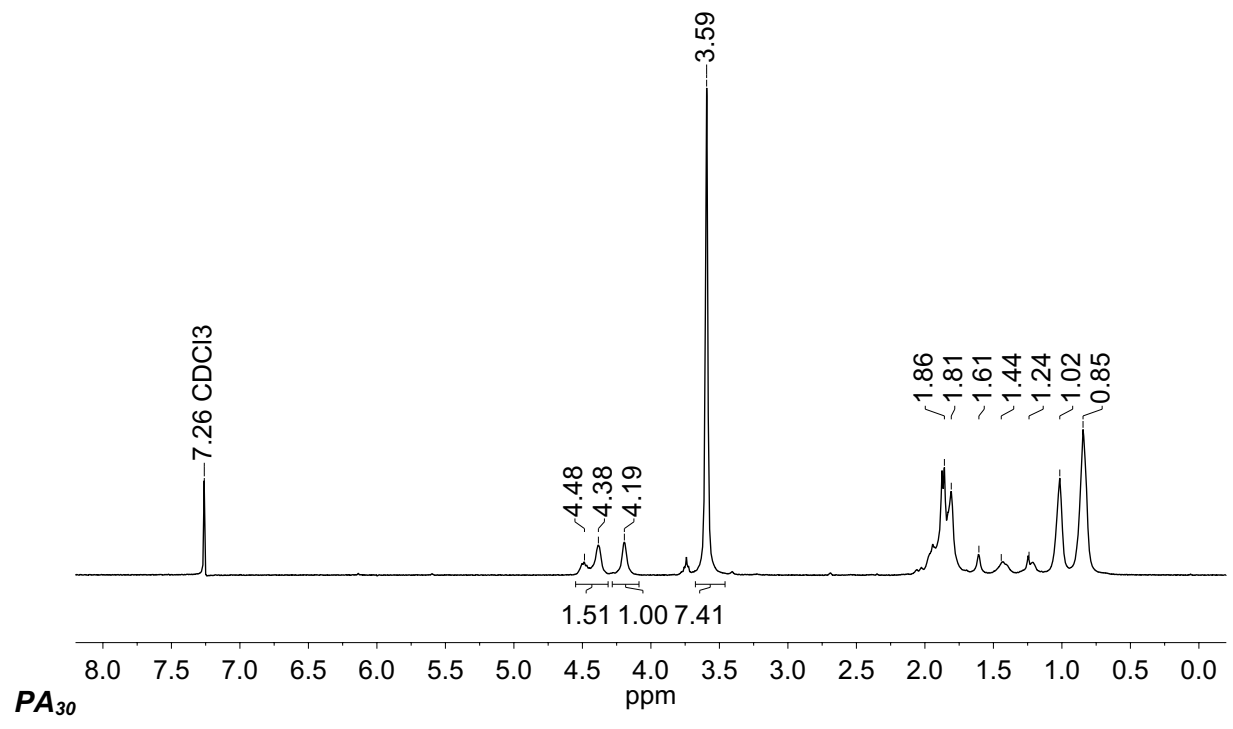
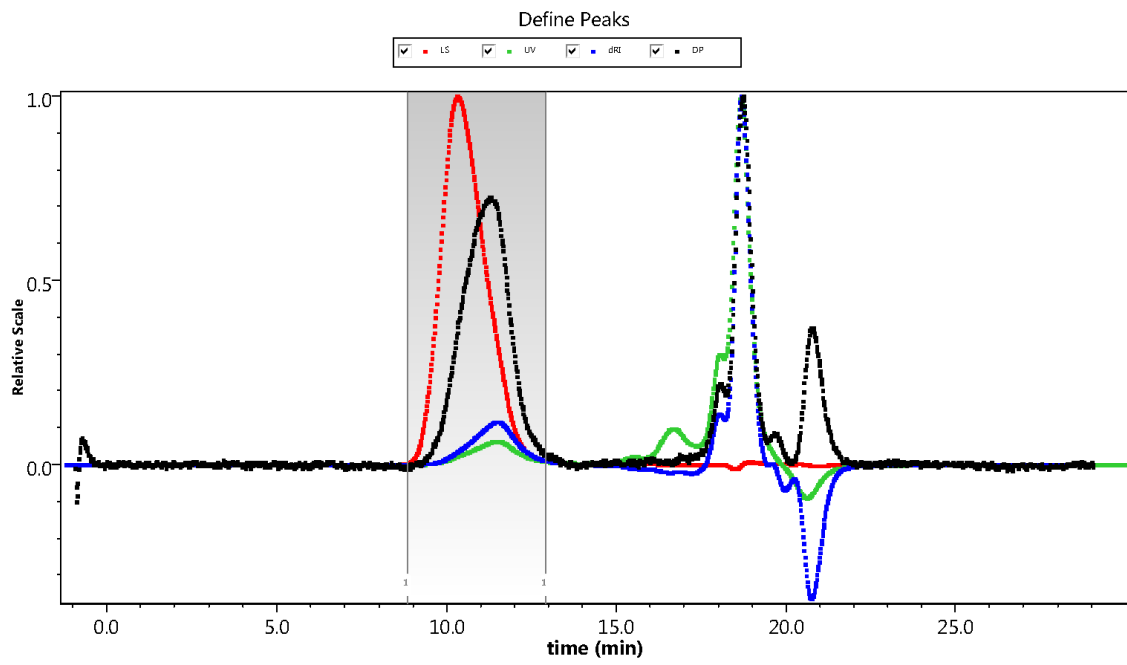


Figure SI 3. ¹H NMR of PA₃₀ (2).

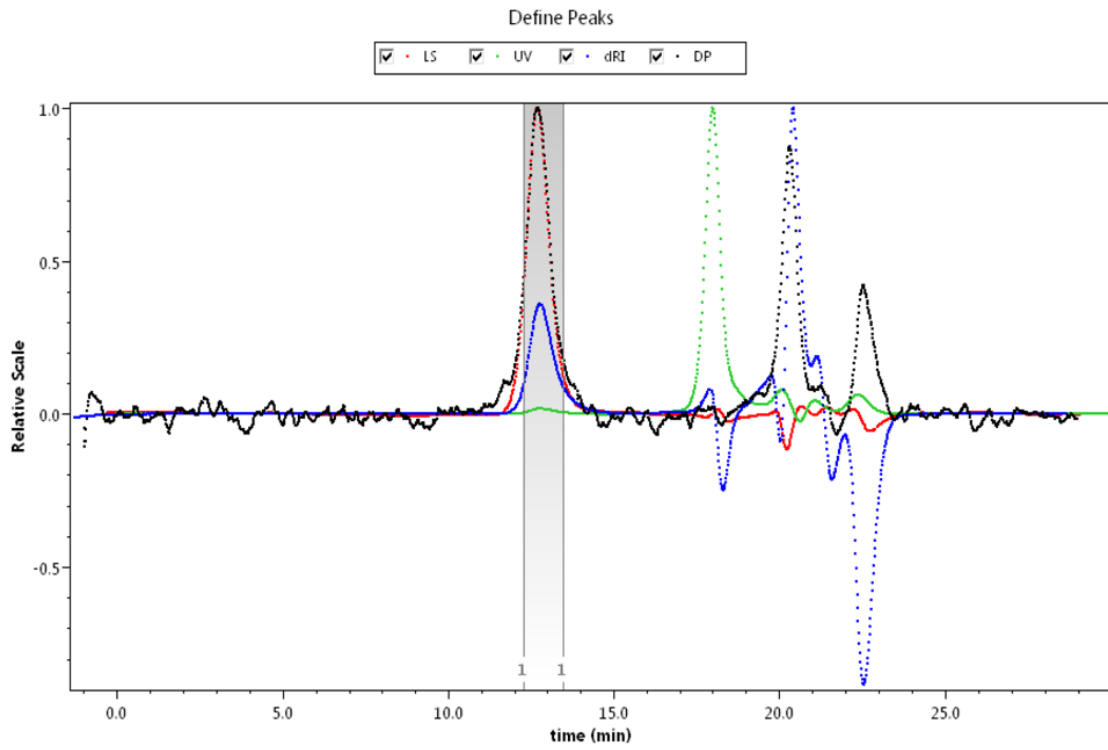
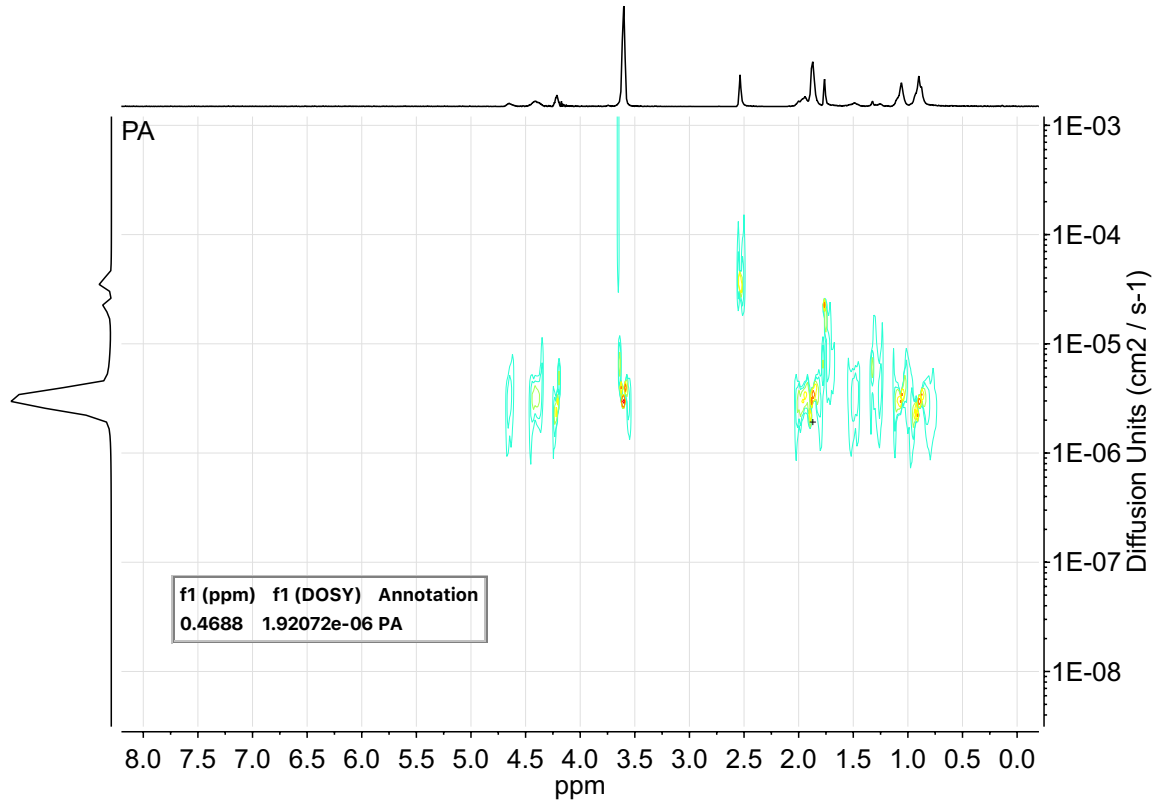


Figure SI 4

Mark-Houwink-Sakurada Plot

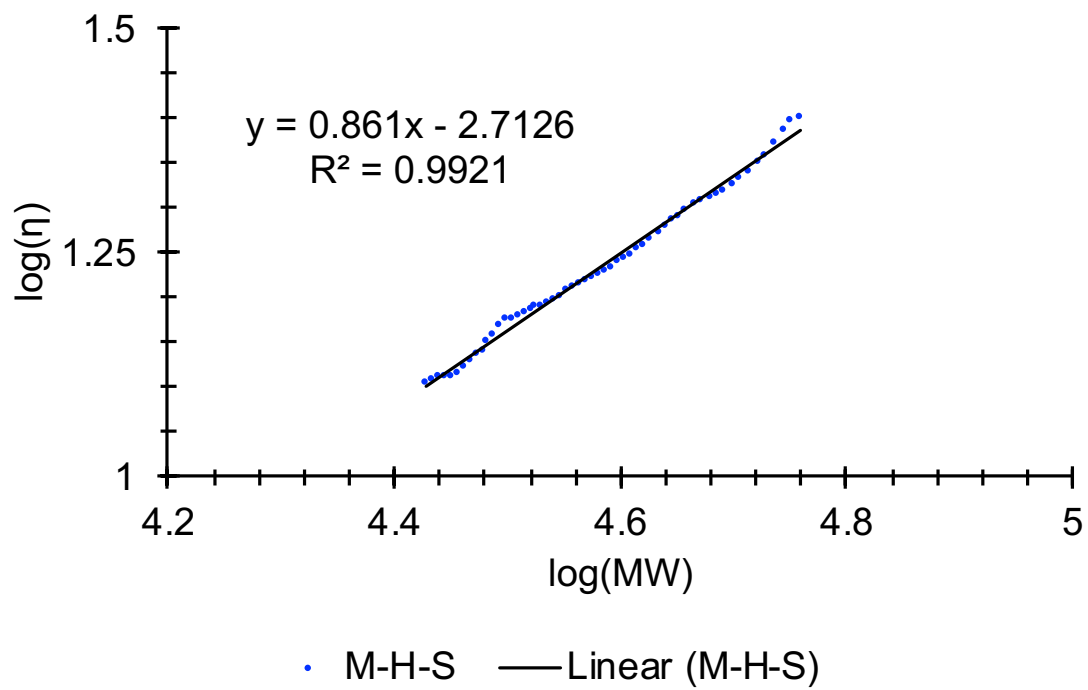
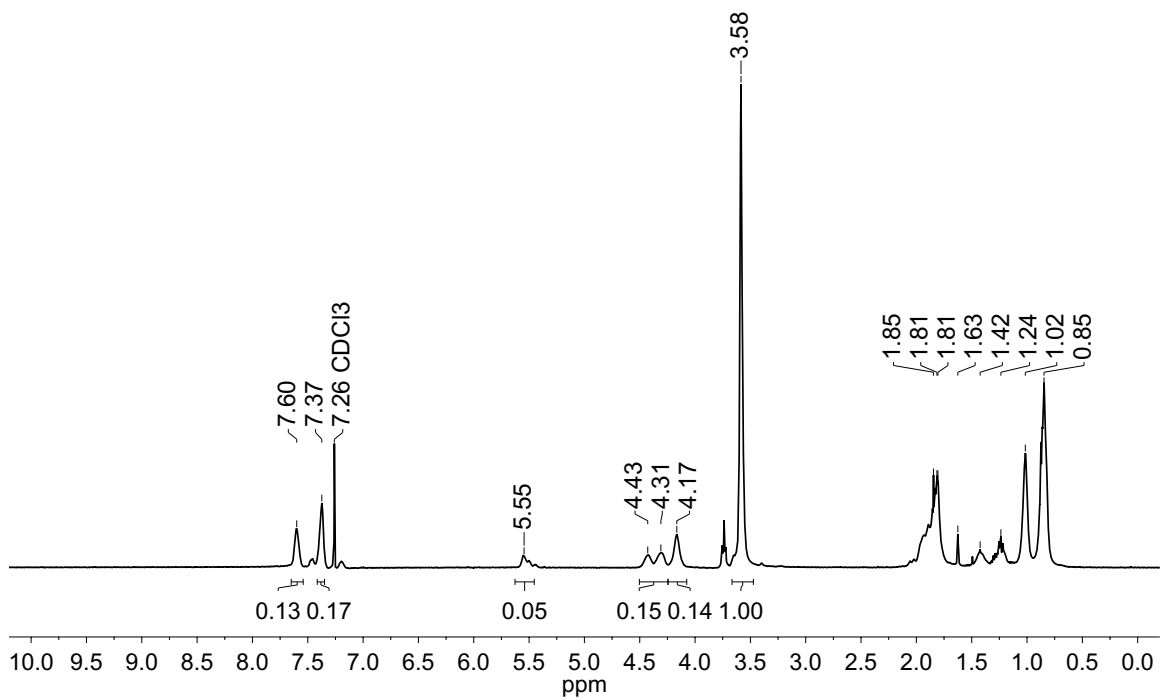
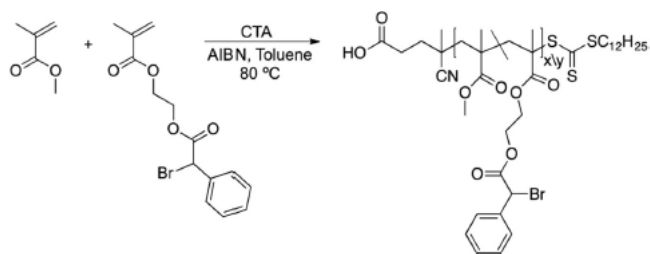


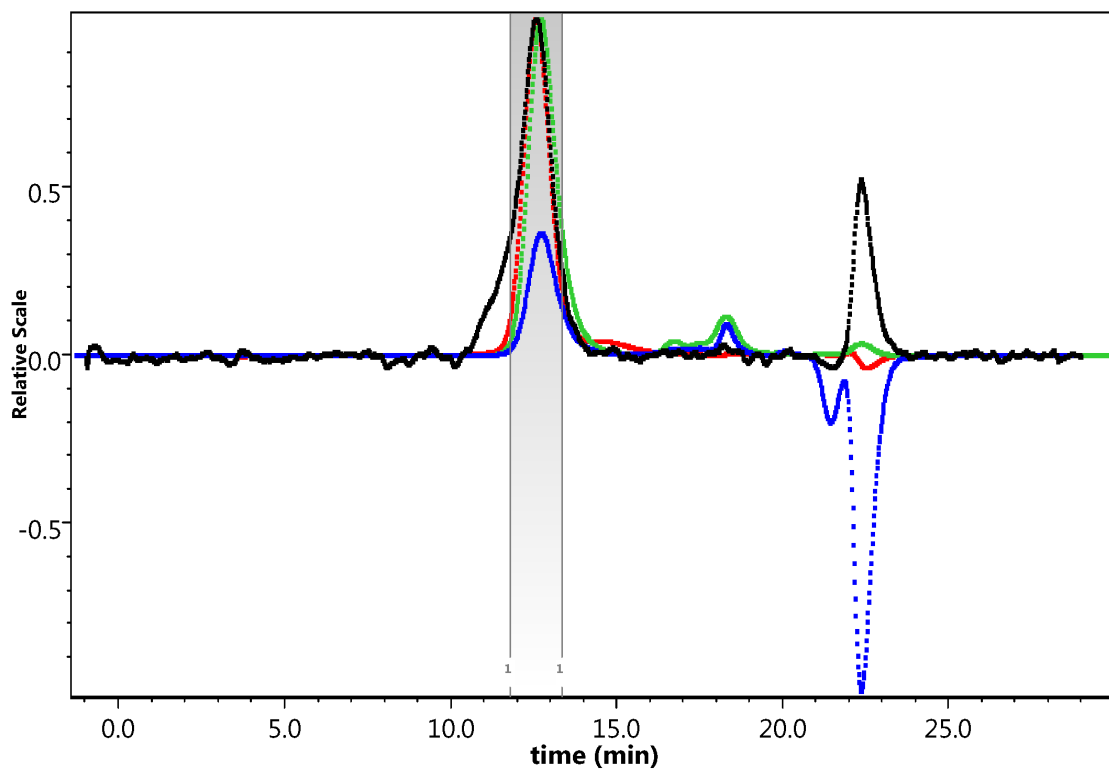
Figure SI 5

PB₄₀



Define Peaks

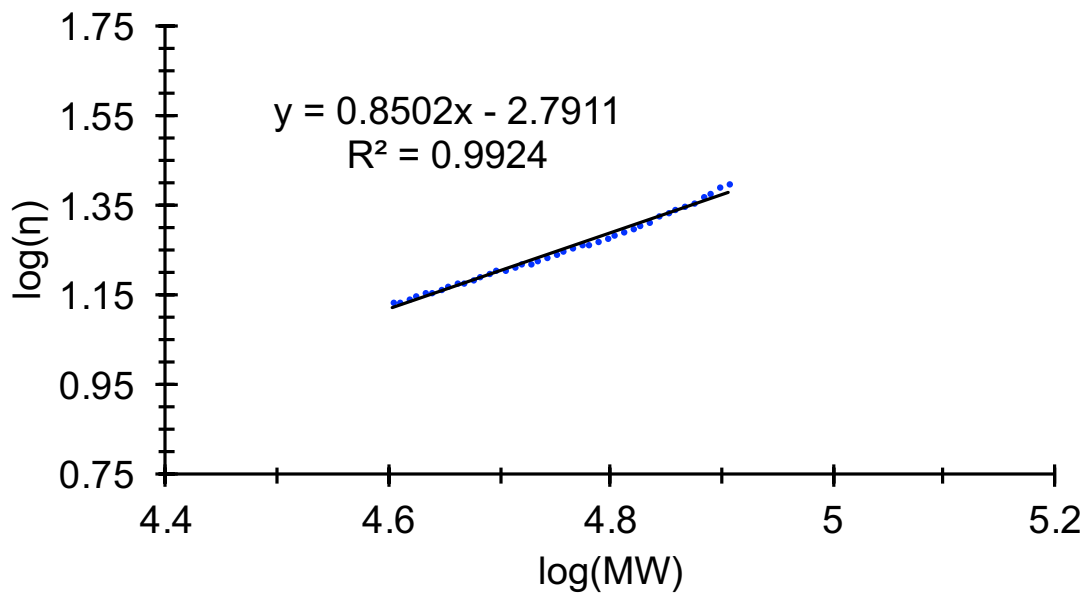
LS UV dRI DP



D = 0.613E-11

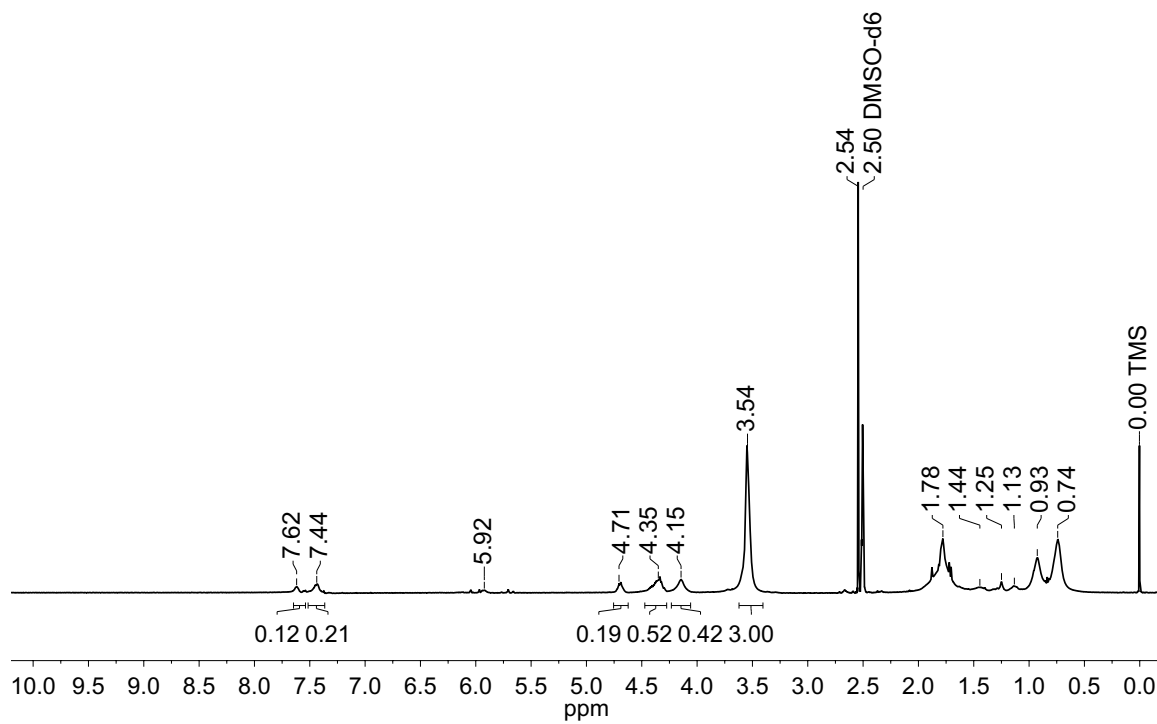
Solvent = DMF

Mark-Houwink-Sakurada Plot



• M-H-S — Linear (M-H-S)

PAB₁₅



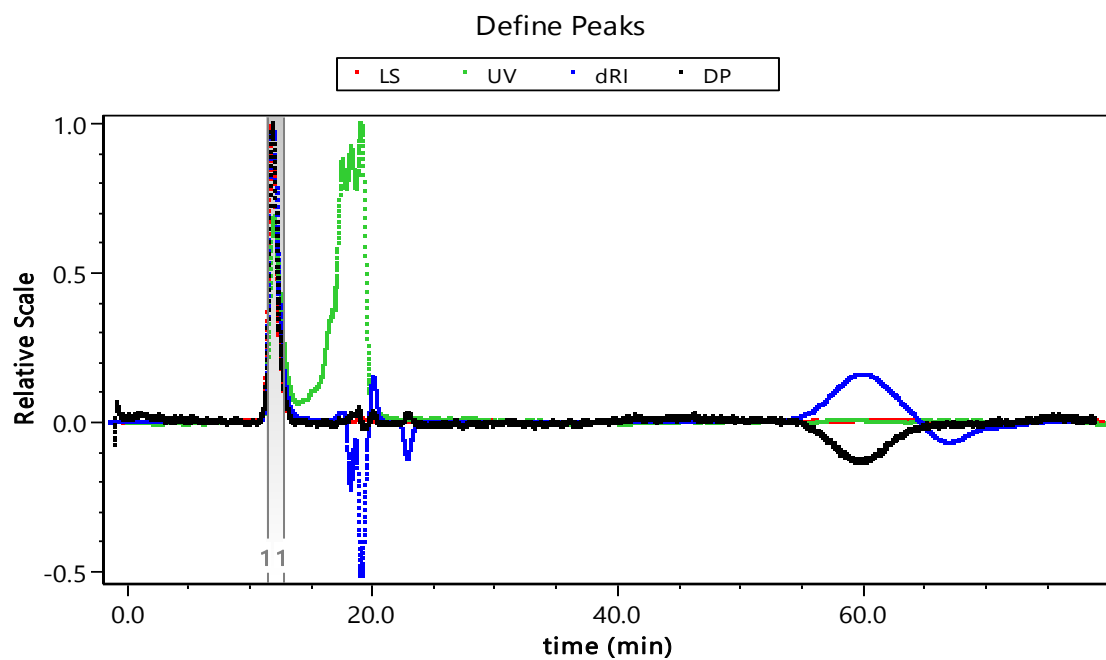
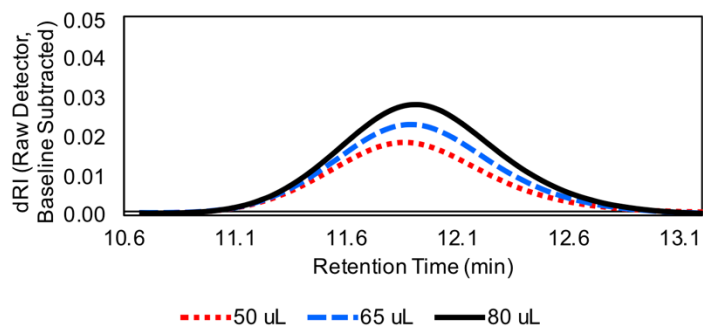
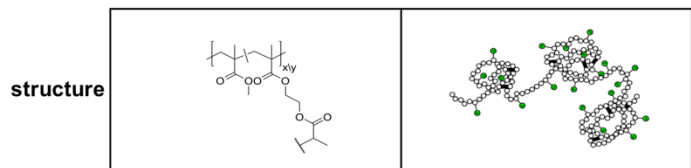


Figure SI 6

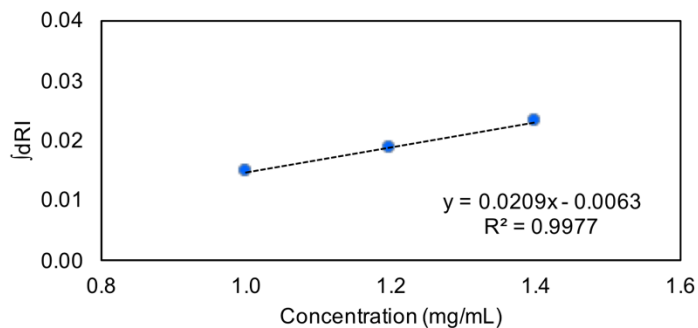
ATRC Products

NPA Series dn/dc

description SCNP; p(MMA-co-MeBrema)



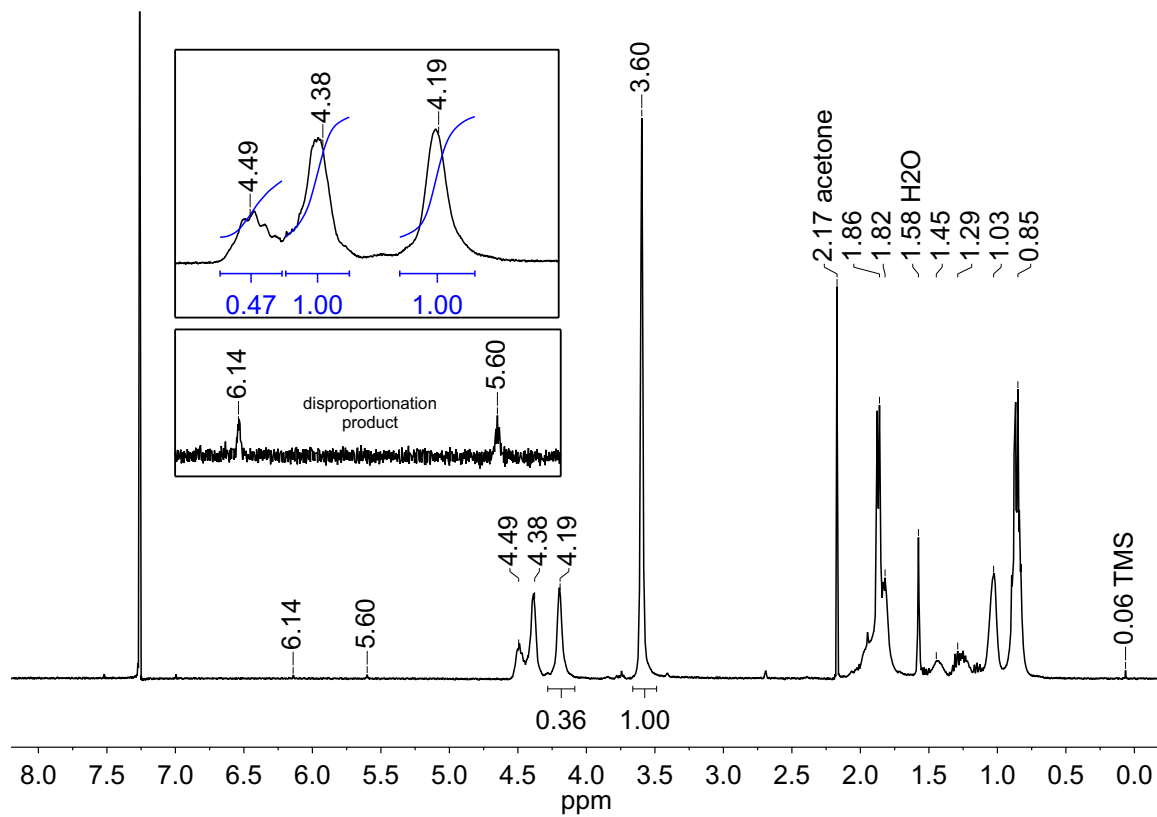
c (mg/mL)	area dRI curve
1.0	1.479E-02
1.2	1.863E-02
1.4	2.316E-02



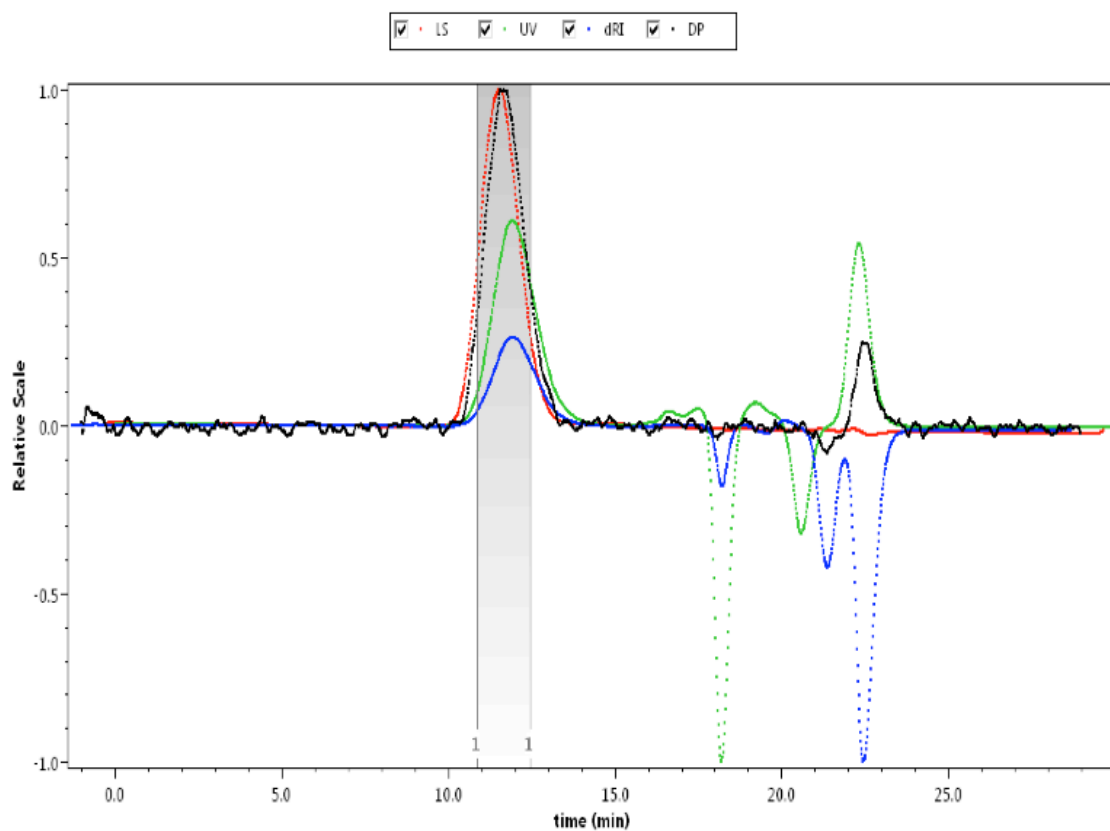
detector constant	2.64E-01
slope (linear)	2.09E-02
dn/dc	0.0792

Figure SI 7. The multiple injection volume method was used to determine refractive index increment for SCNP products made with p(MMA-co-MeBrema); $dn/dc = 0.0792$.

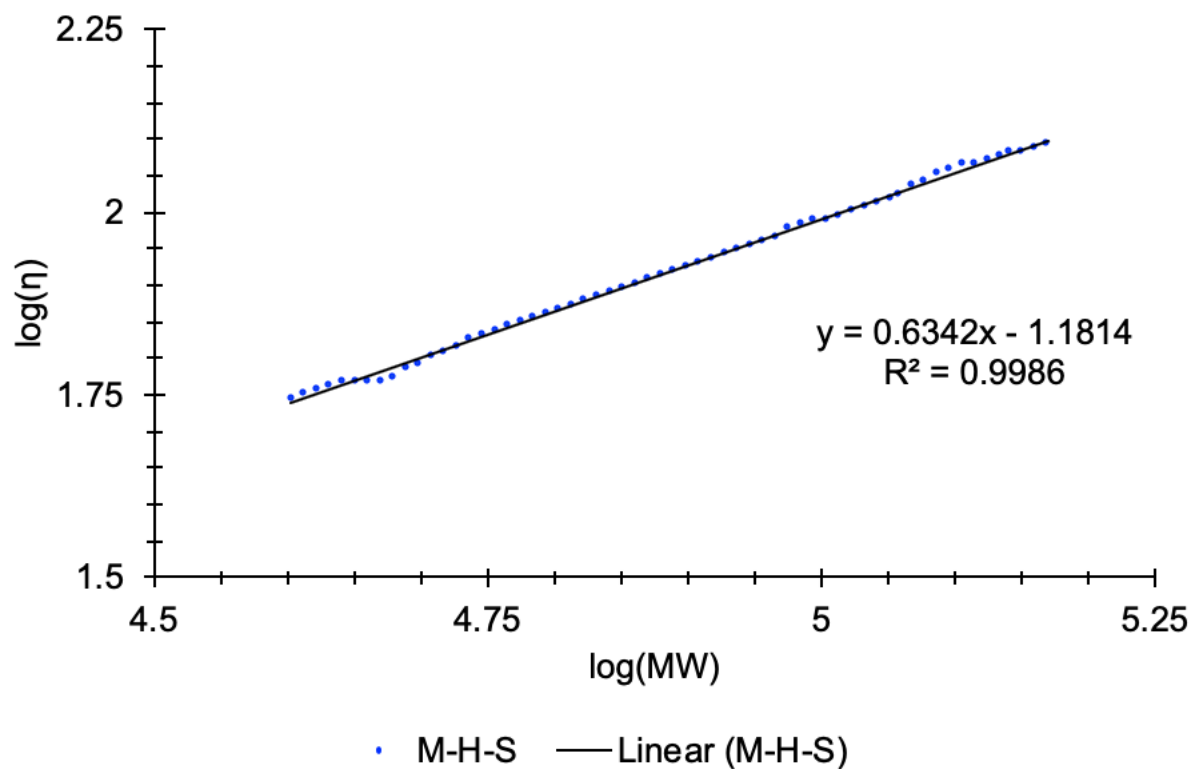
NPA-1



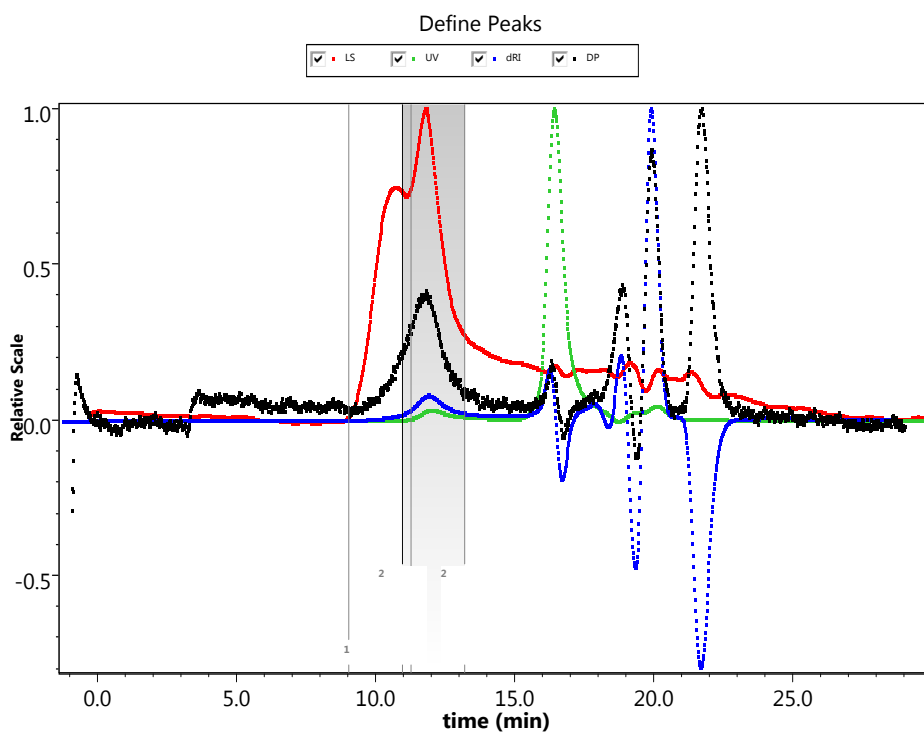
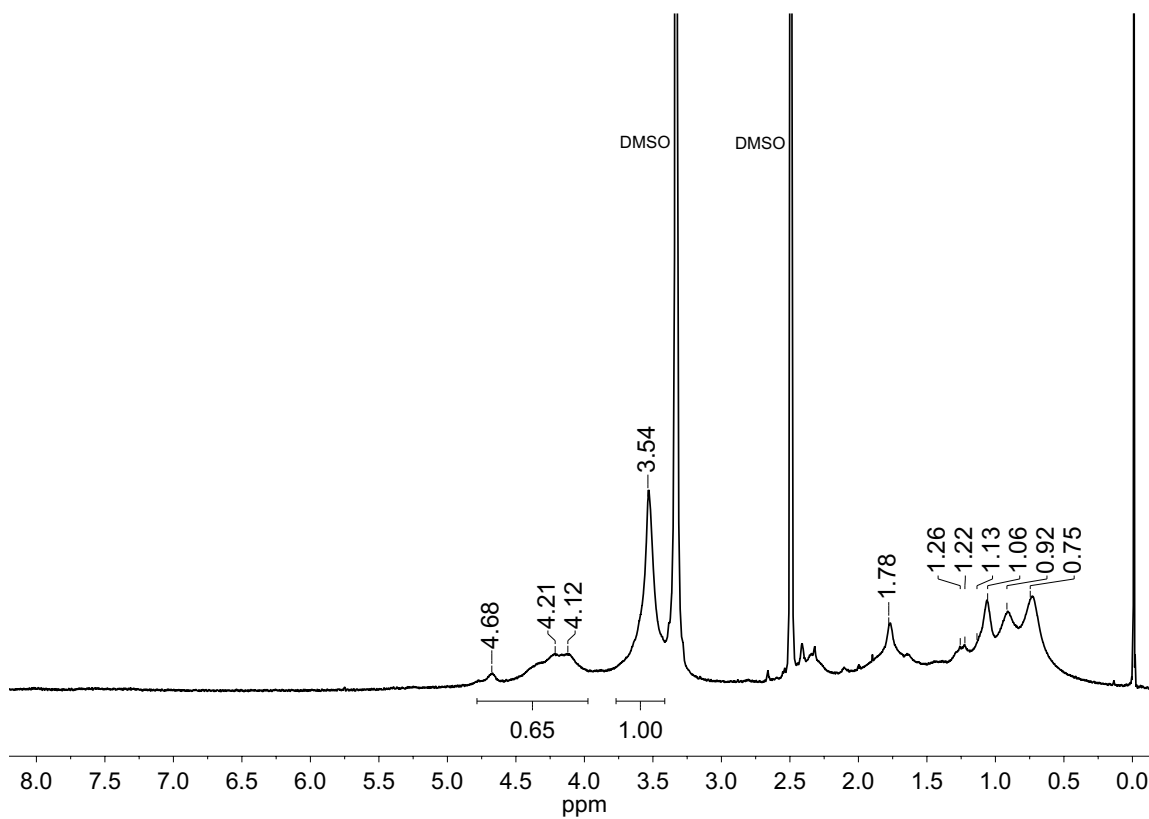
Define Peaks



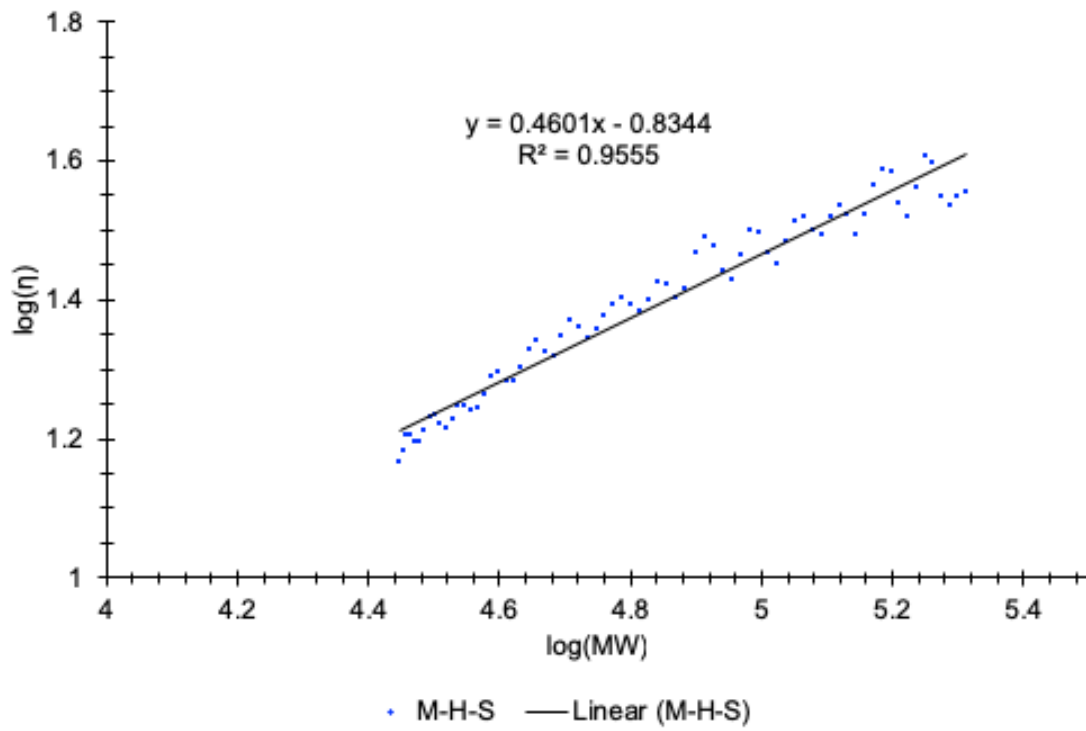
Mark-Houwink-Sakurada Plot



p(MMA-co-MeBrema) EB-4-7



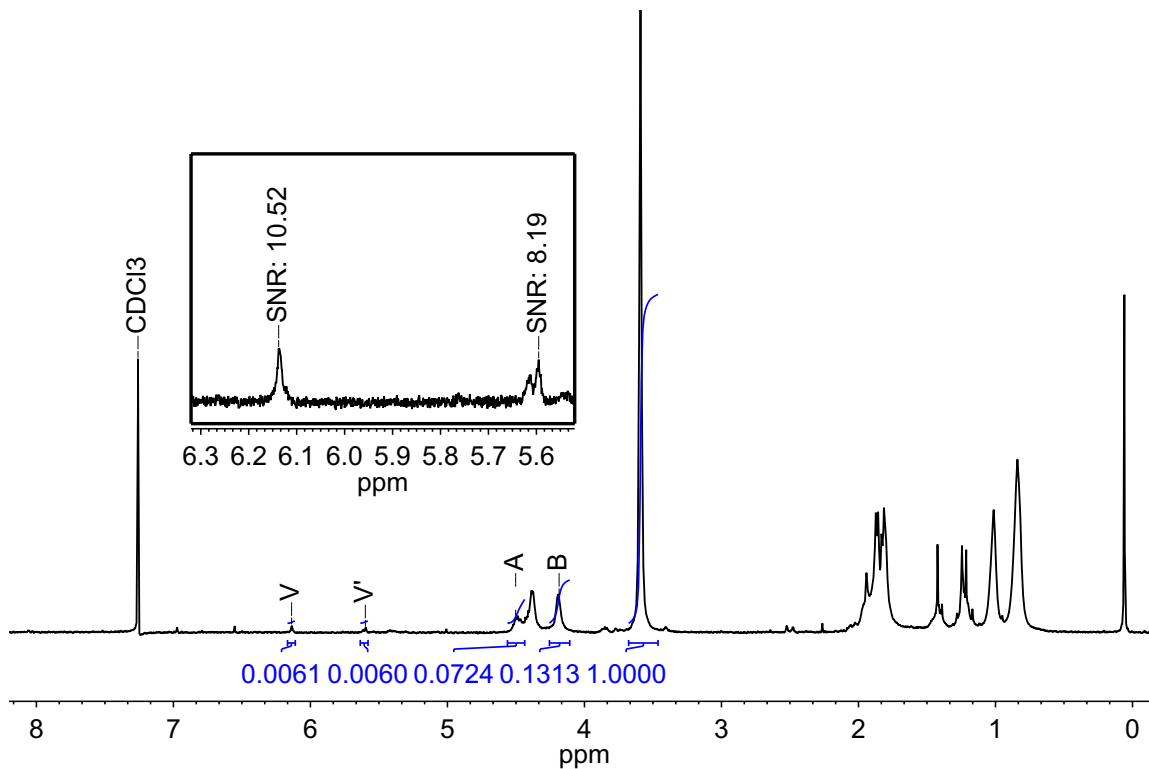
Mark-Houwink-Sakurada Plot



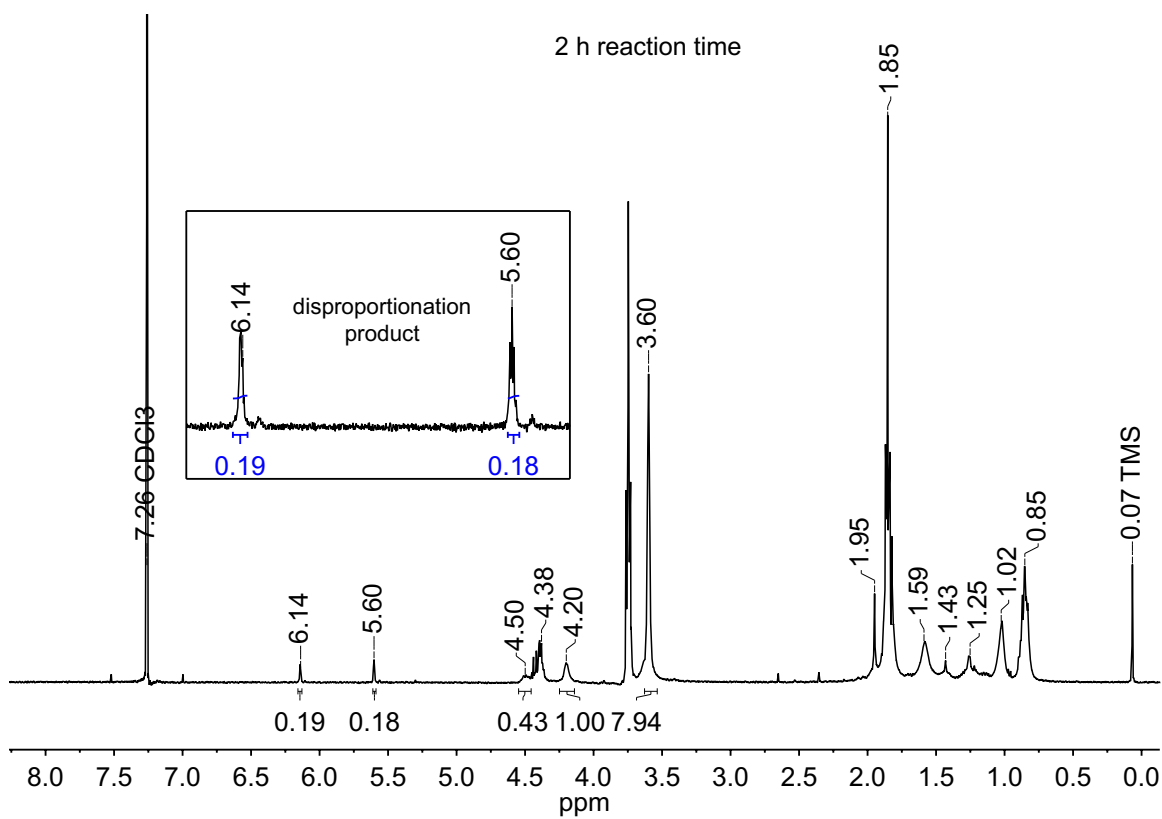
Reaction Progress of NPA-2

NPA-2-1h

NPA-2-1h

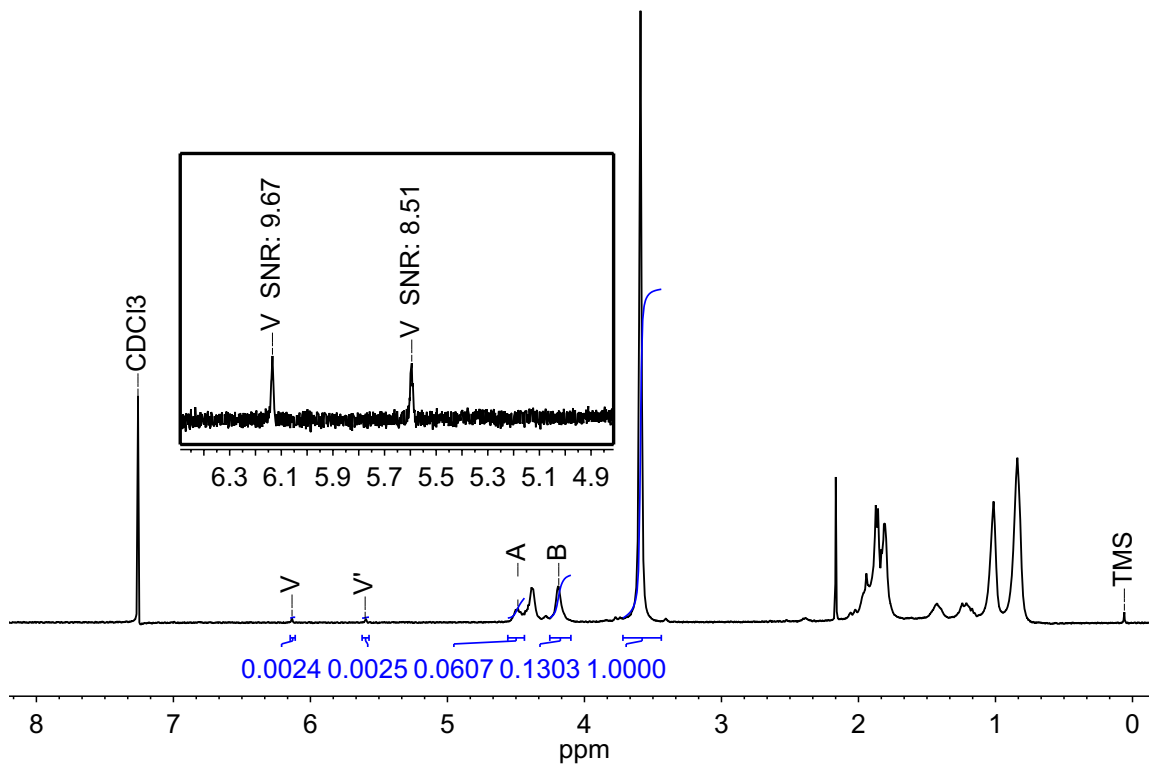


NPA-2-2h



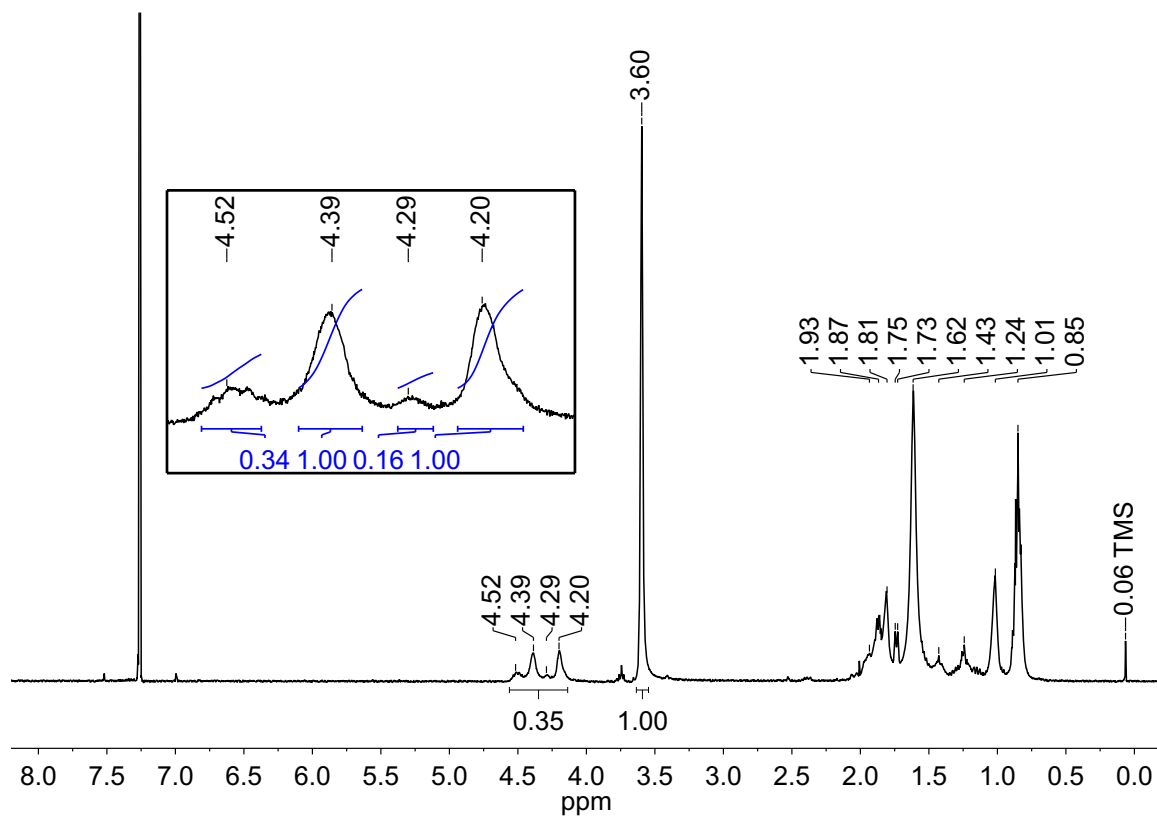
NPA-2-3h

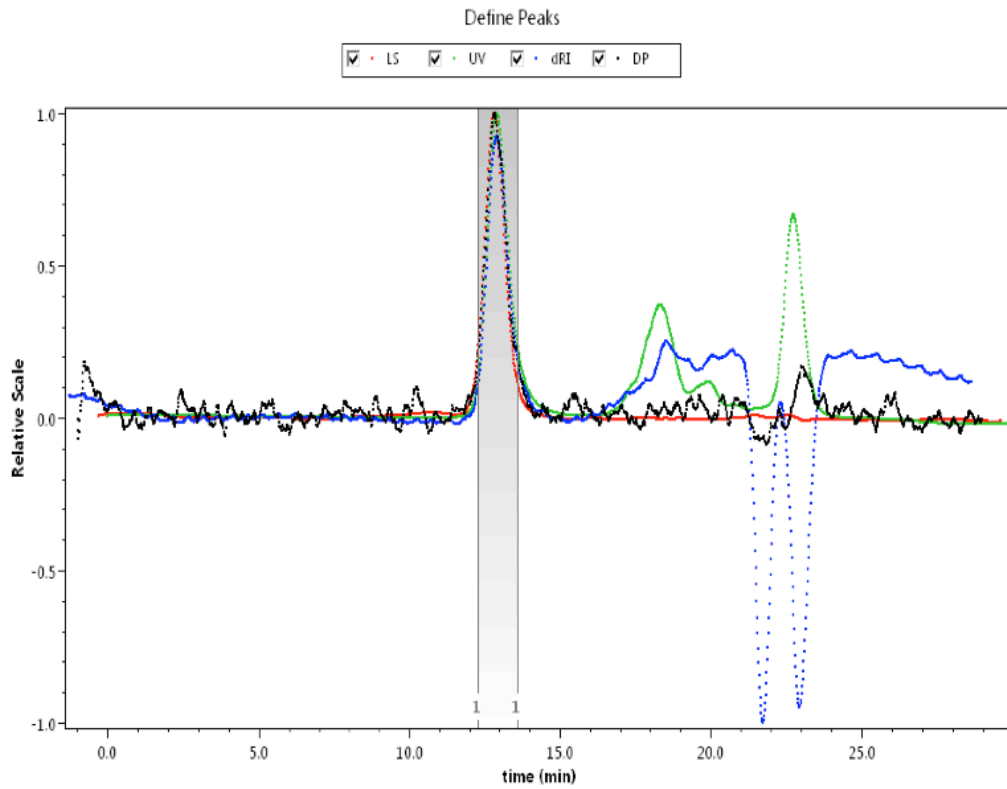
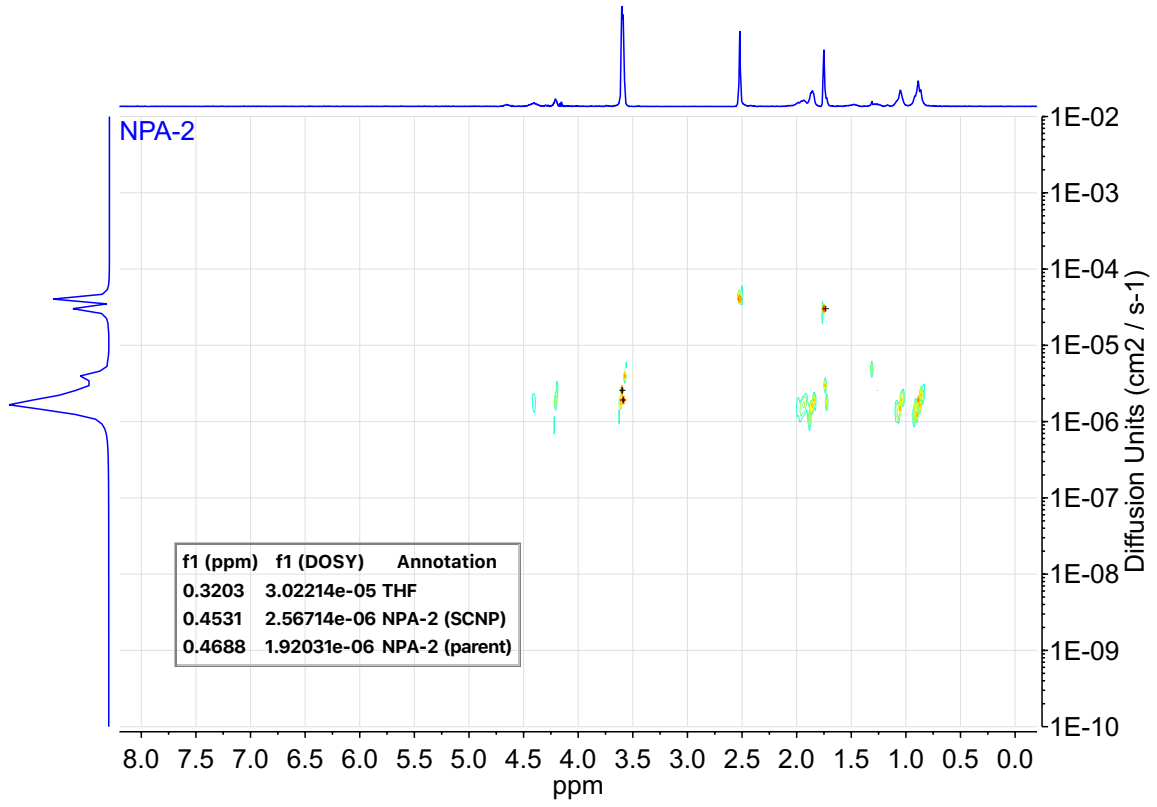
NPA-2-3h



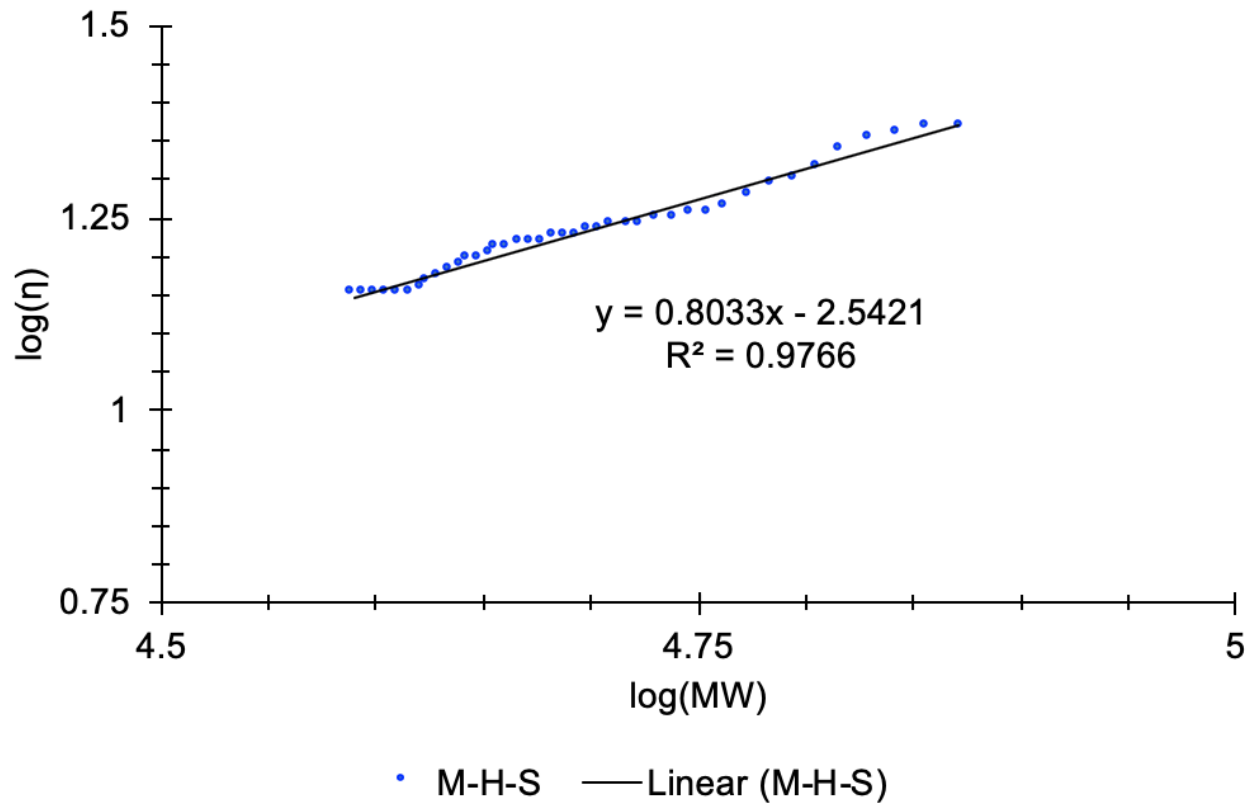
Series A: Variations in L

NPA-2

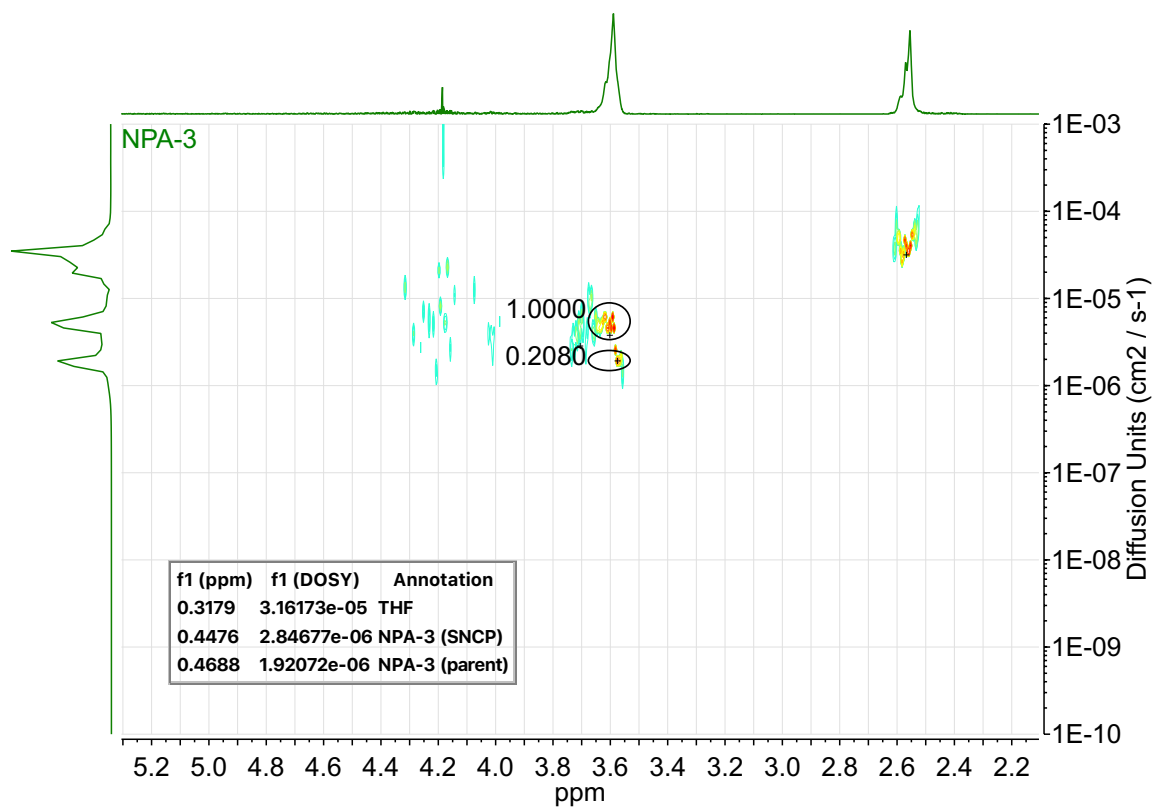
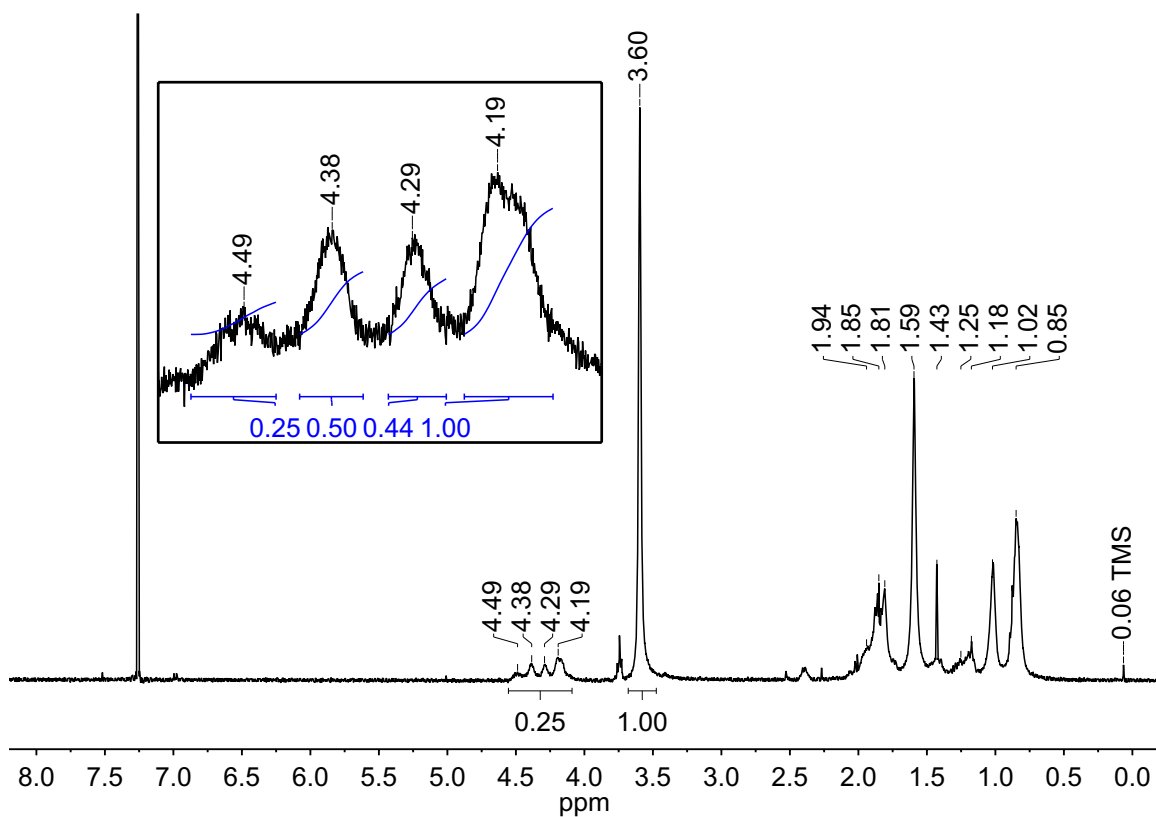


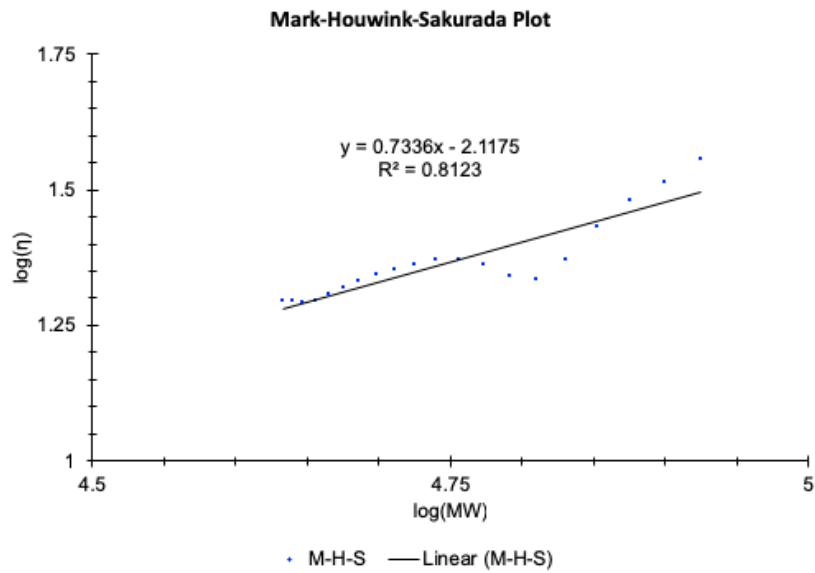
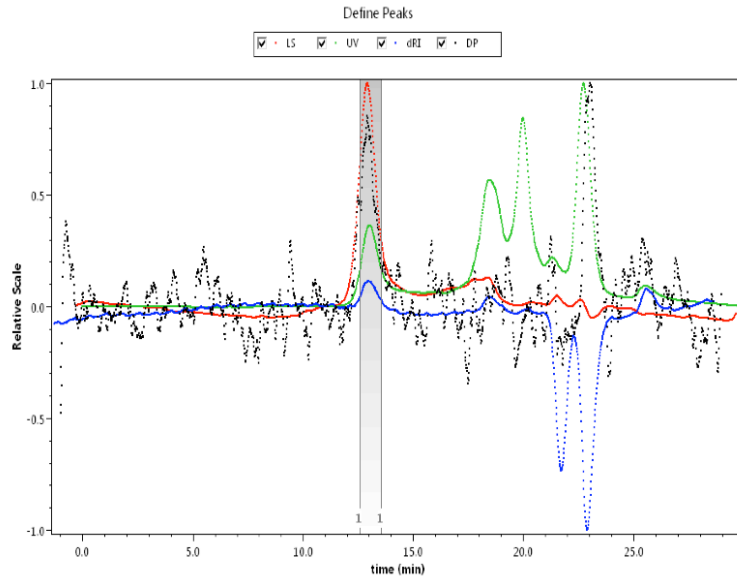


Mark-Houwink-Sakurada Plot

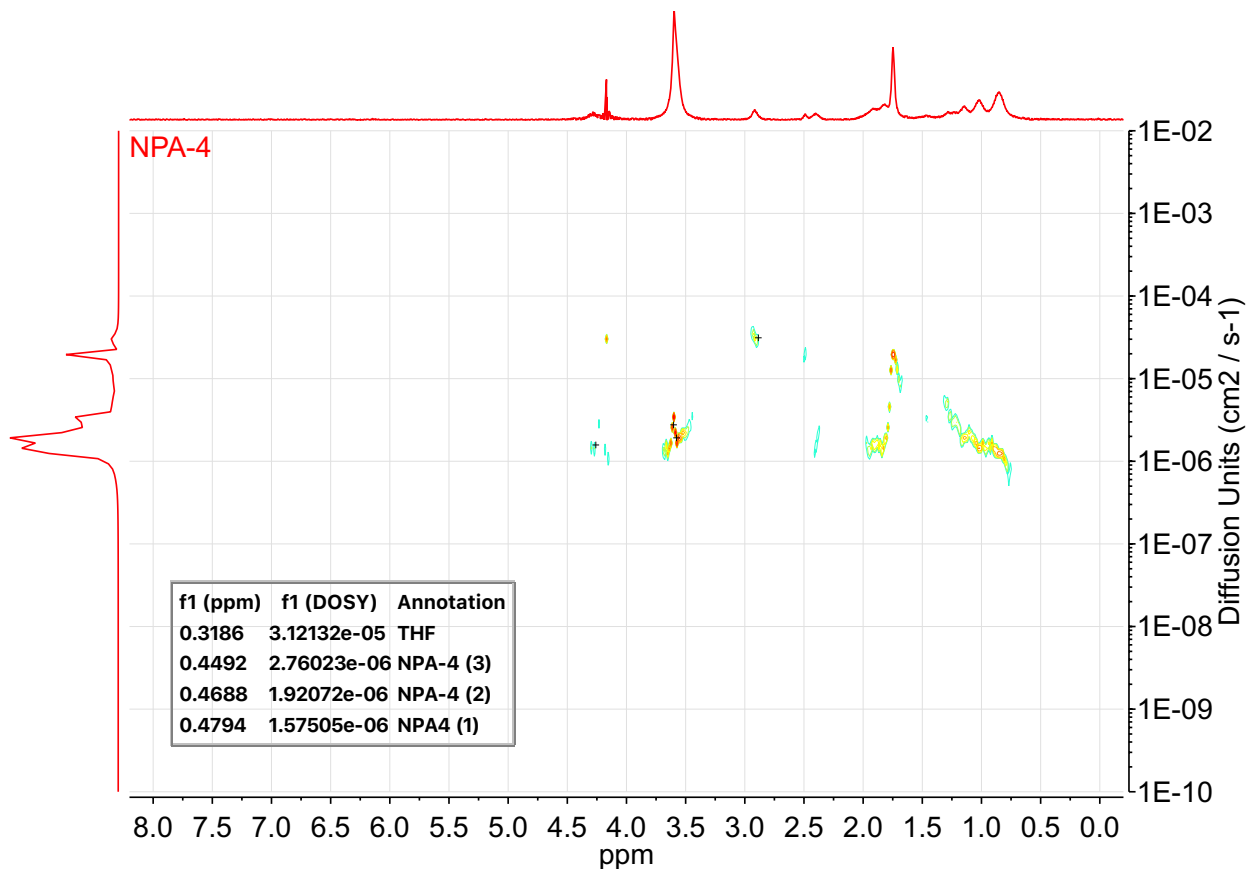
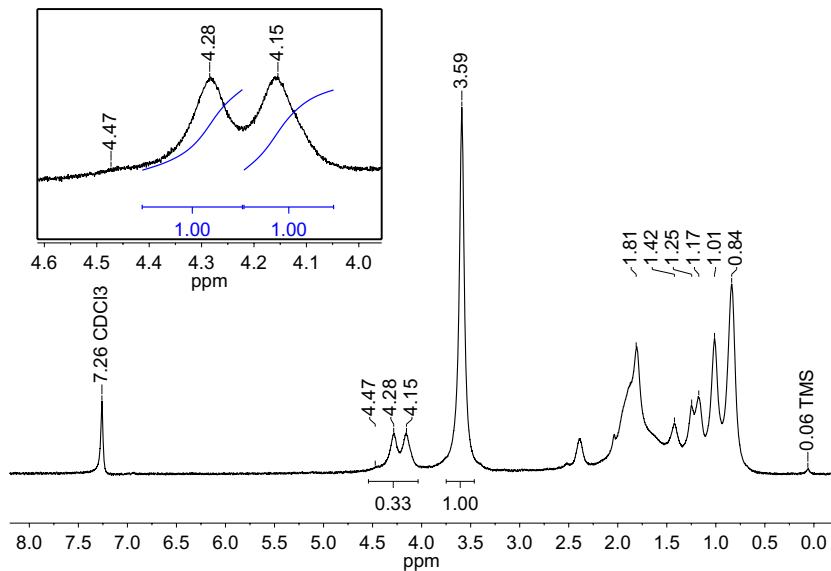


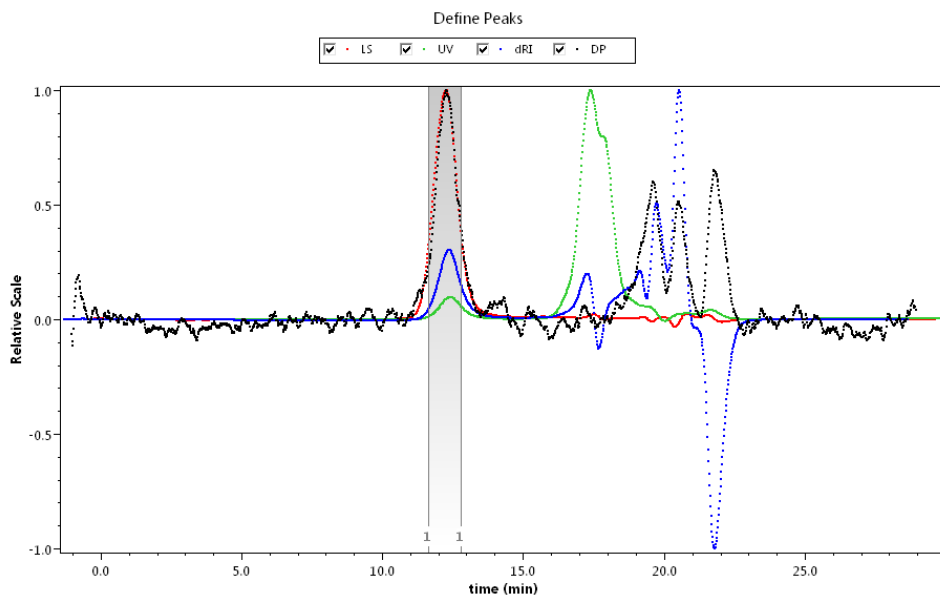
NPA-3



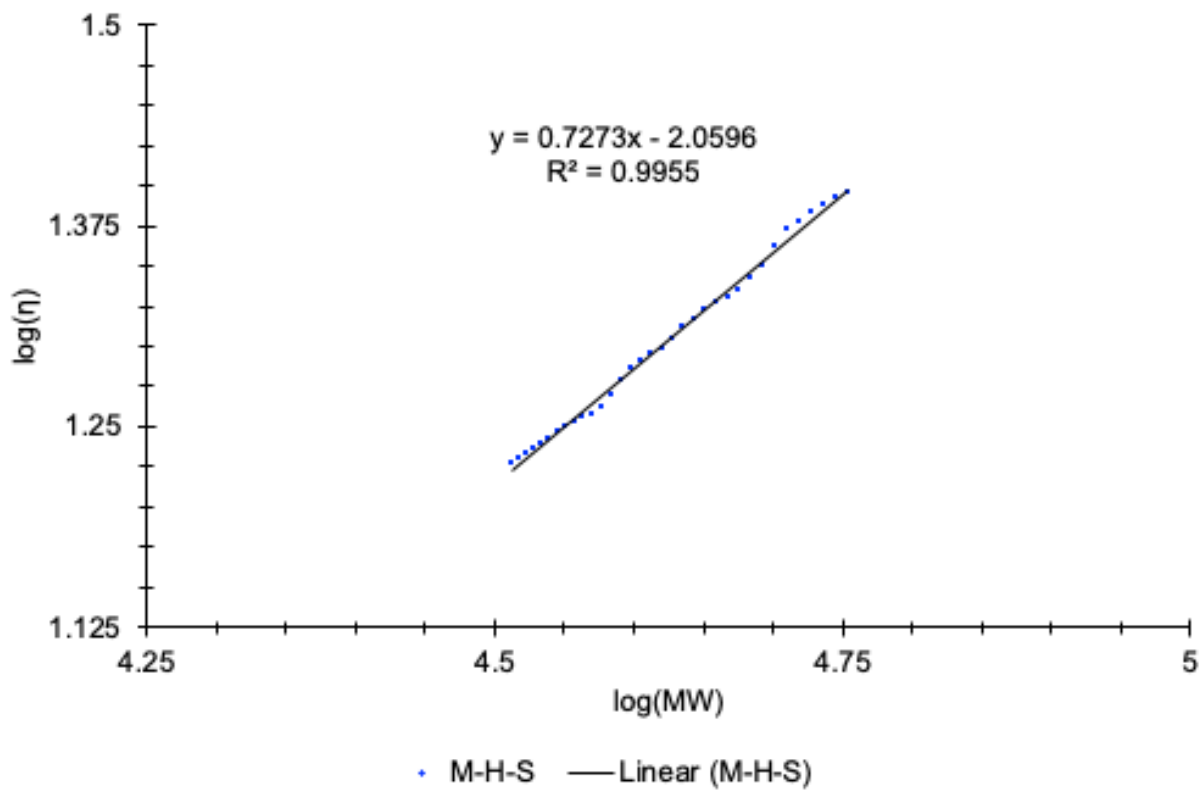


NPA-4



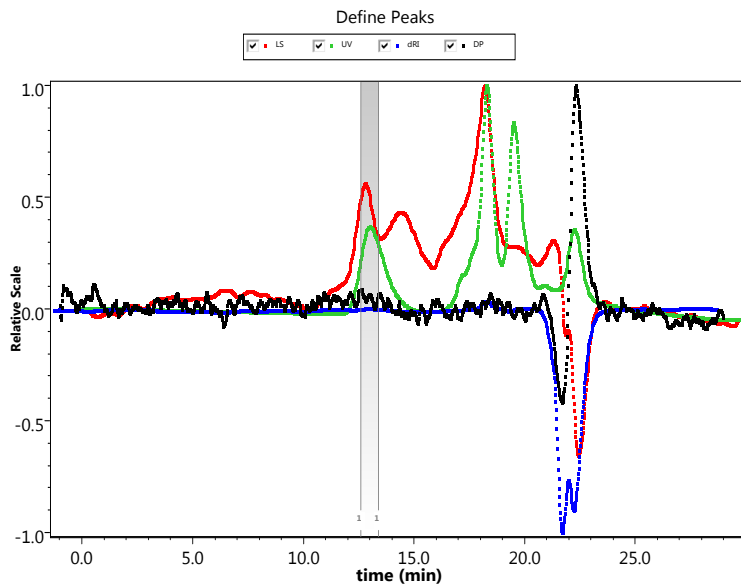
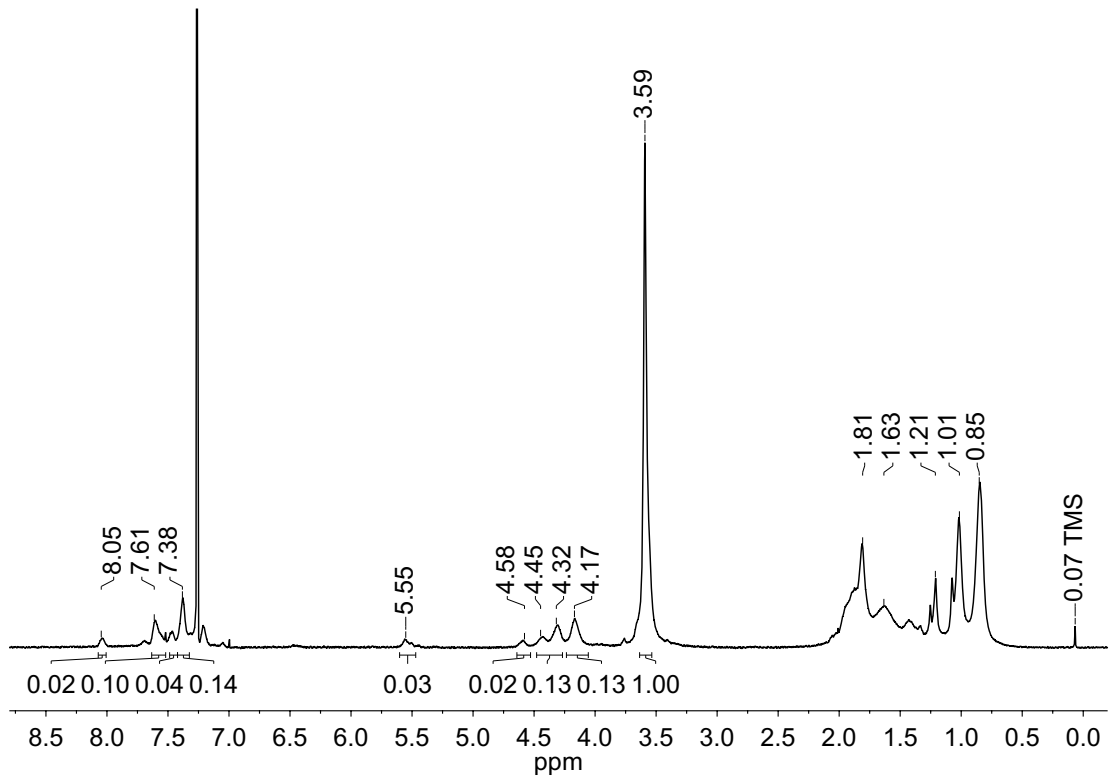


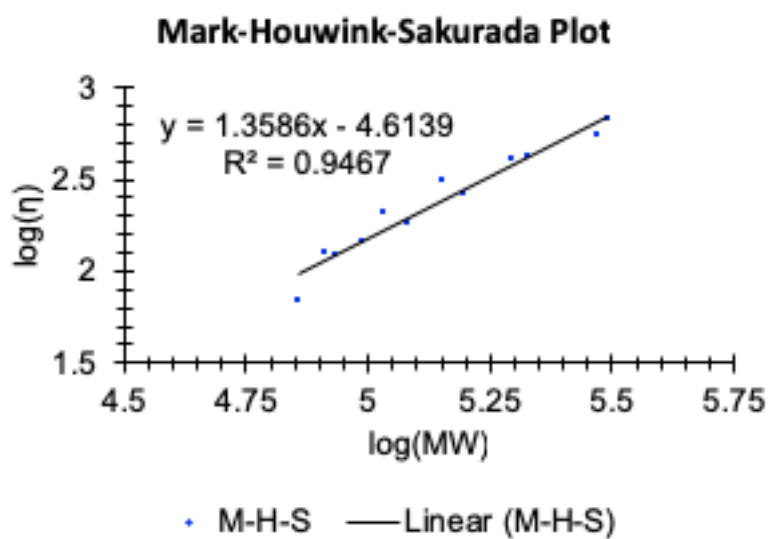
Mark-Houwink-Sakurada Plot

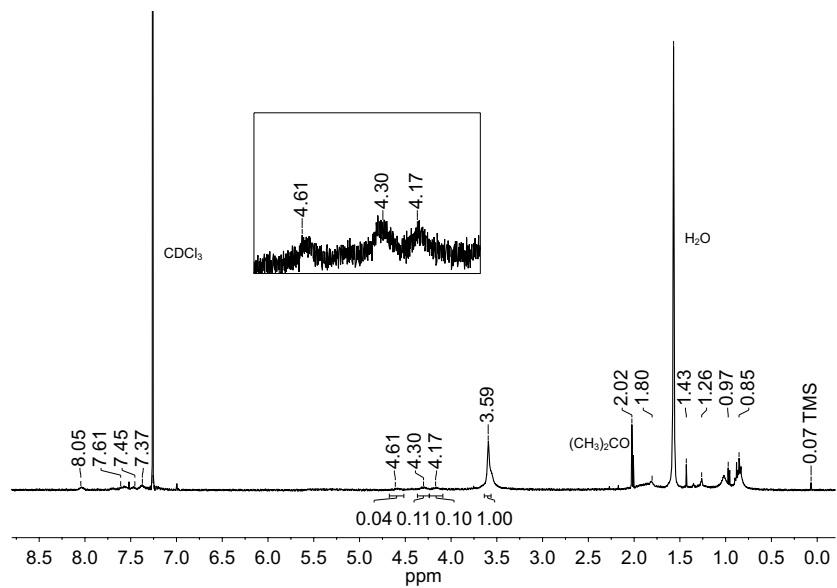


Series B: Variations in L, Continuous Addition

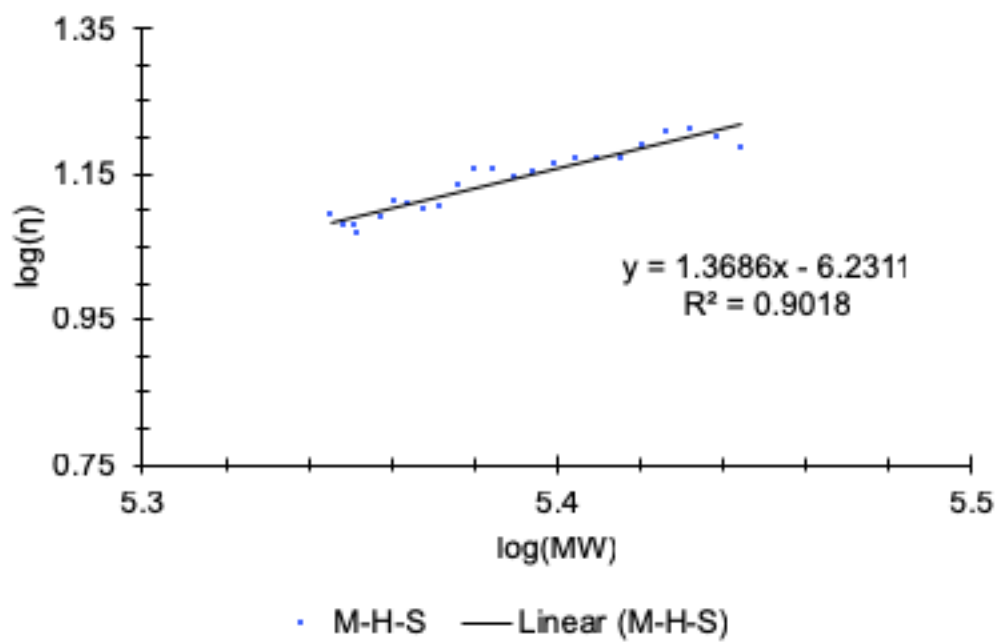
NPB-2



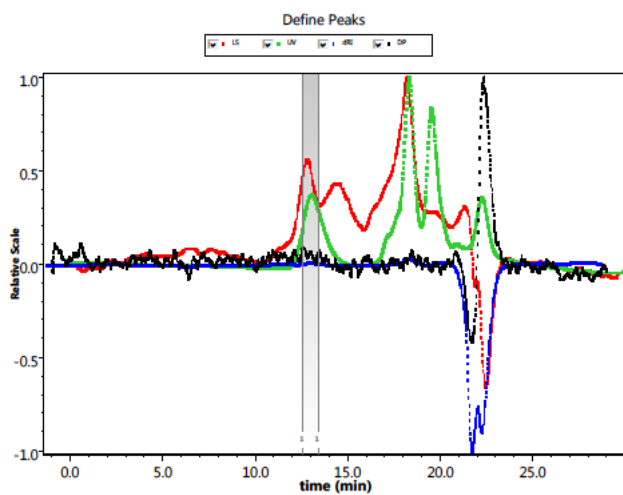




Mark-Houwink-Sakurada Plot



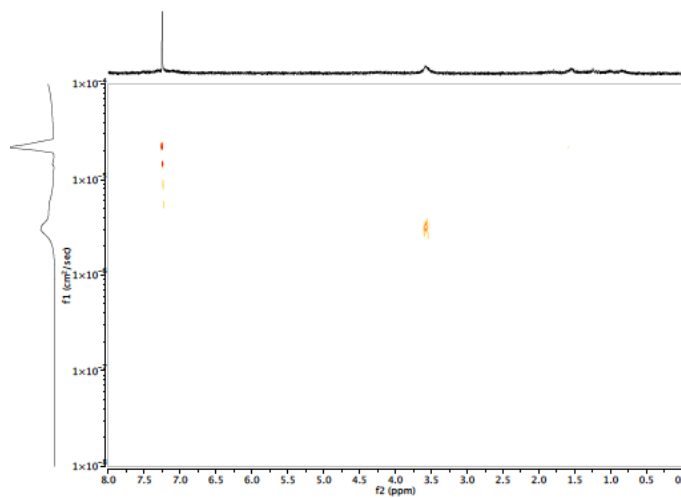
NPB-2



$D = 0.743e-10 \text{ m}^2/\text{s}$

Solvent = DMF

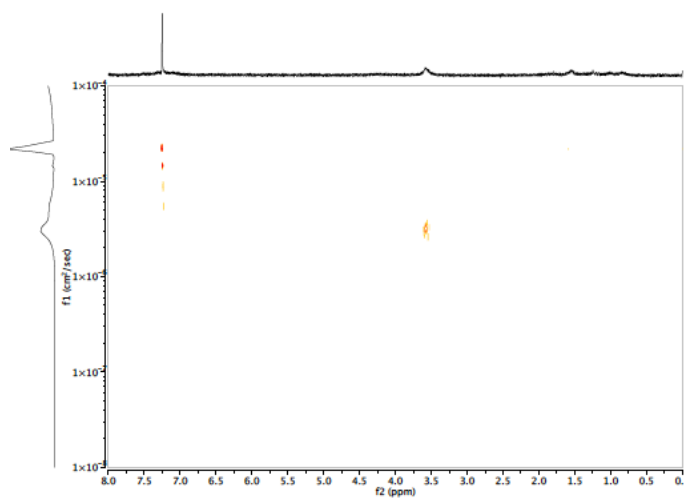
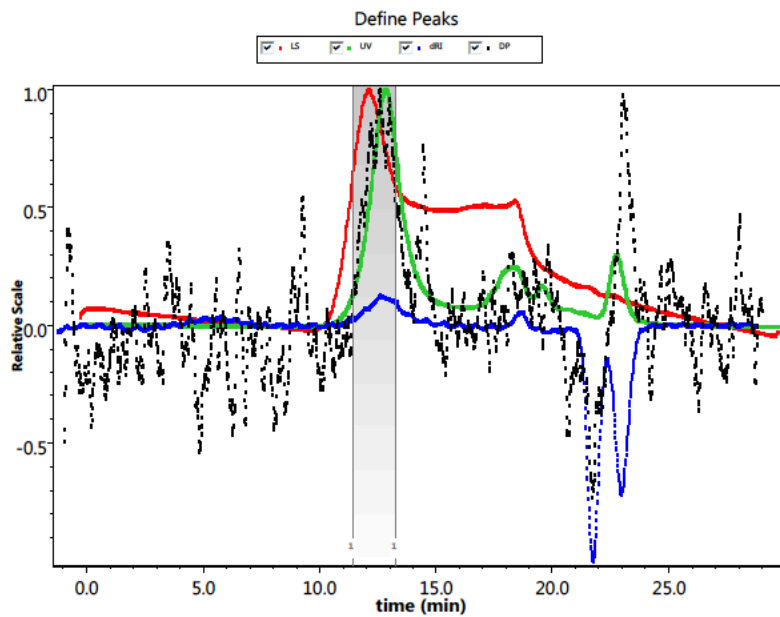
$R_H = 1.295 \text{ nm}$



$D = 0.667e-10 \text{ m}^2/\text{s}$

Solvent = DMF

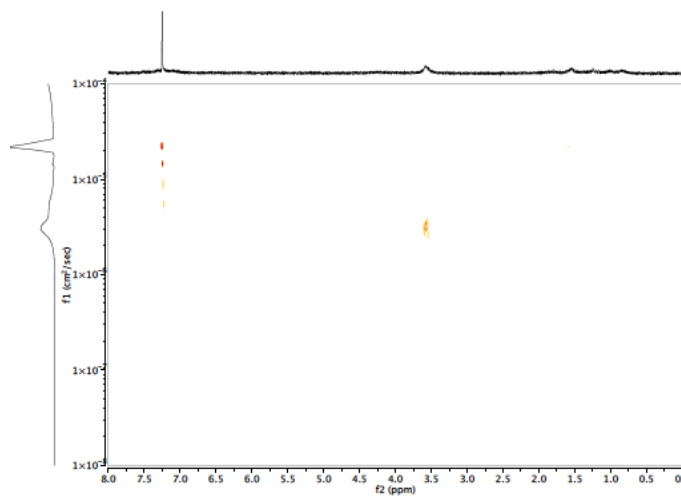
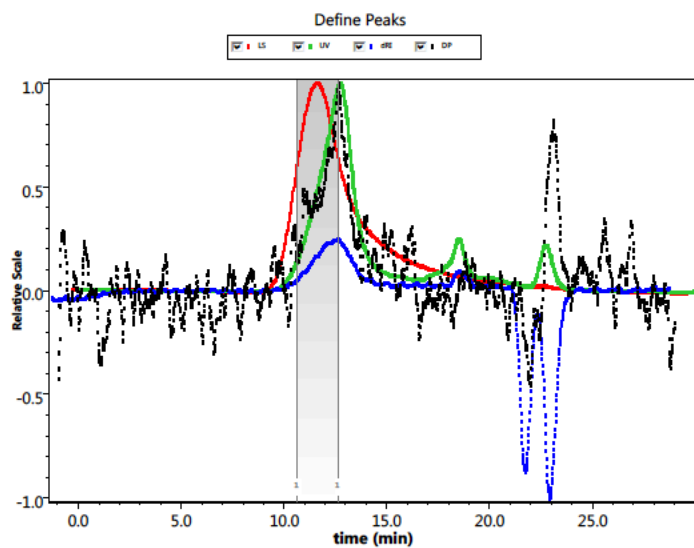
NPB-3



$$D = 0.211e-10 \text{ m}^2/\text{s}$$

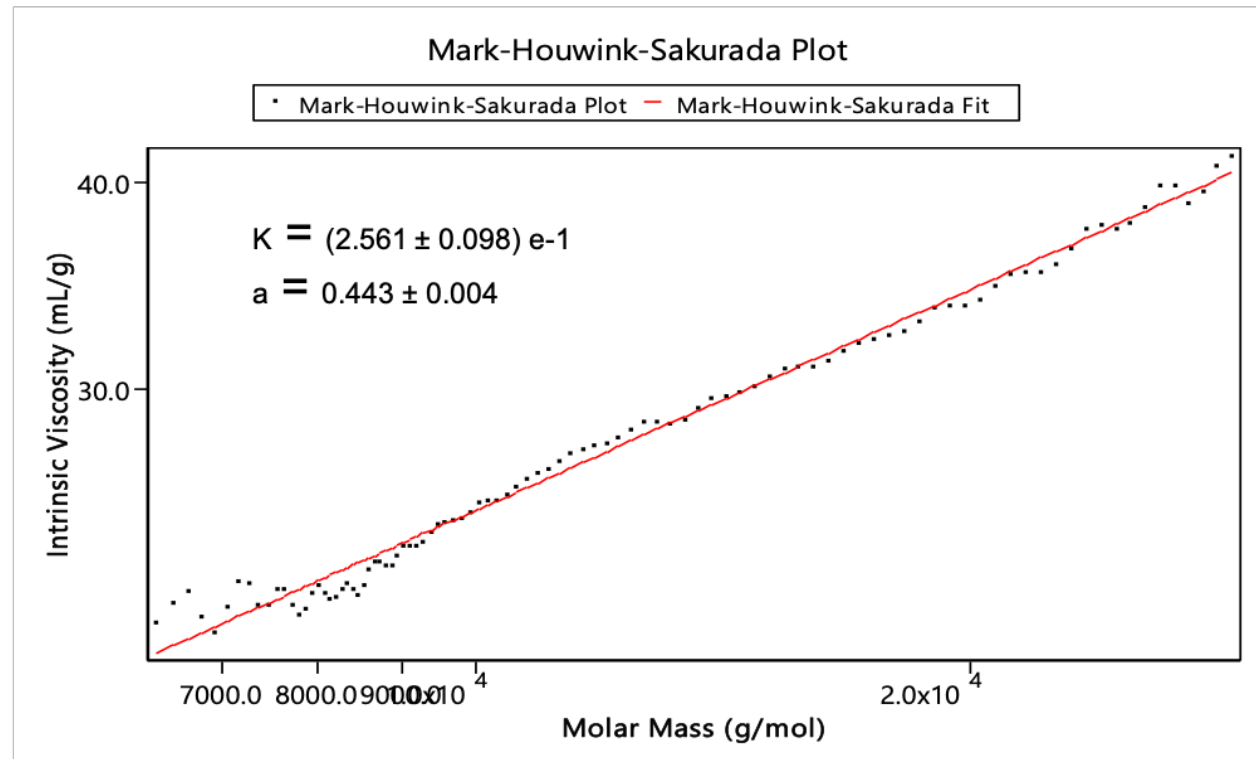
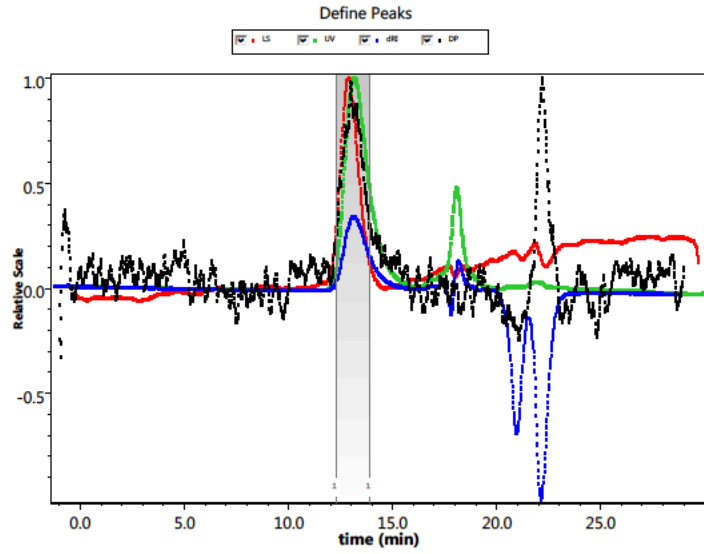
Solvent = DMF

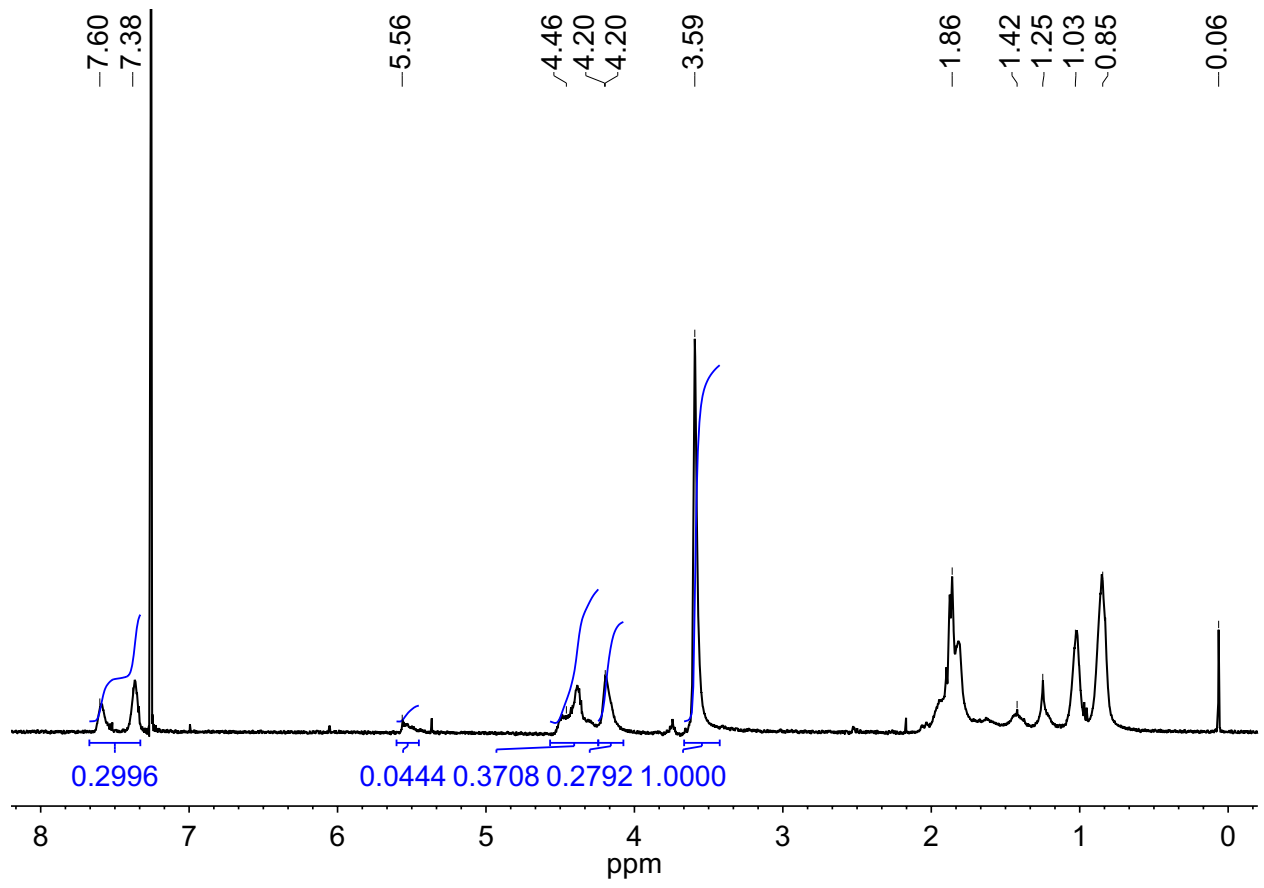
NPB-4



$D = 2.35e-10 \text{ m}^2/\text{s}$

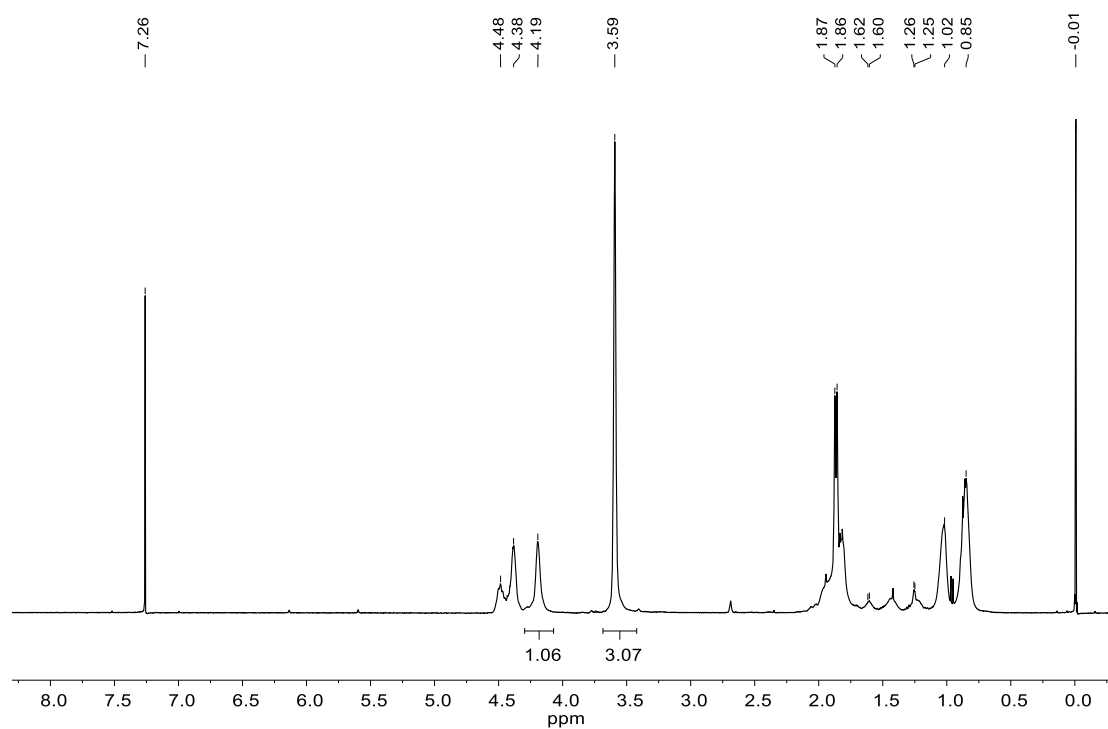
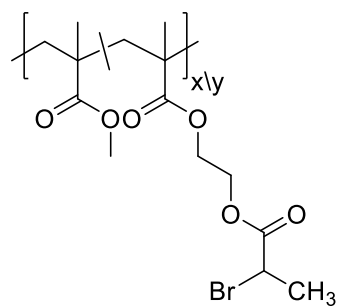
Solvent = DMF



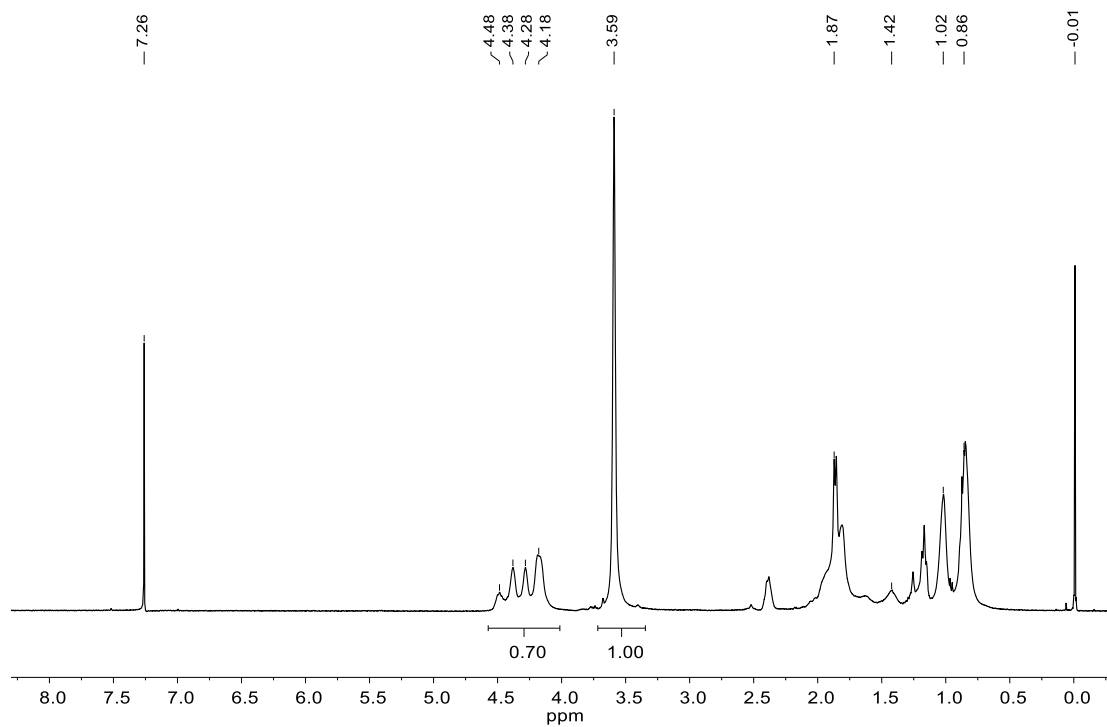
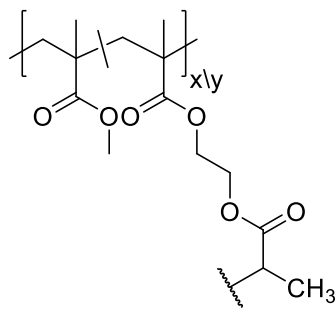


Hyperbranched and Brush Architectures

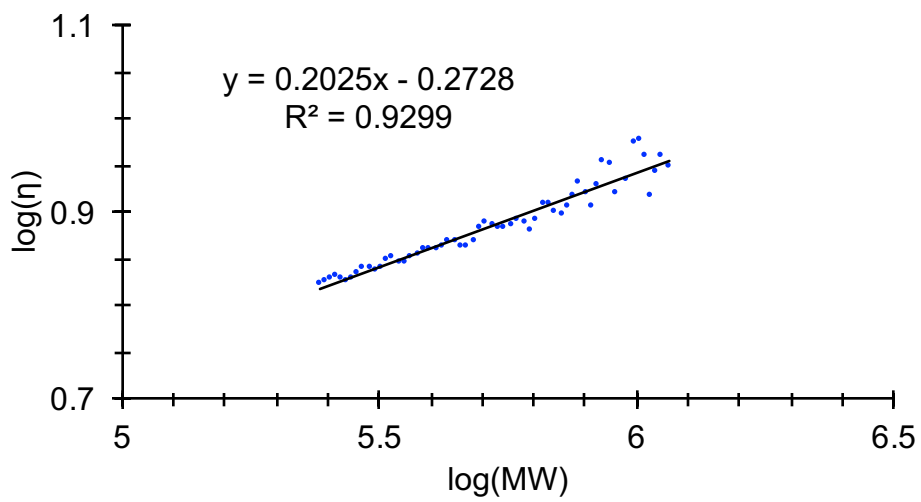
PA-1 *p*(MMA-co-MeBrema)



NPA-1

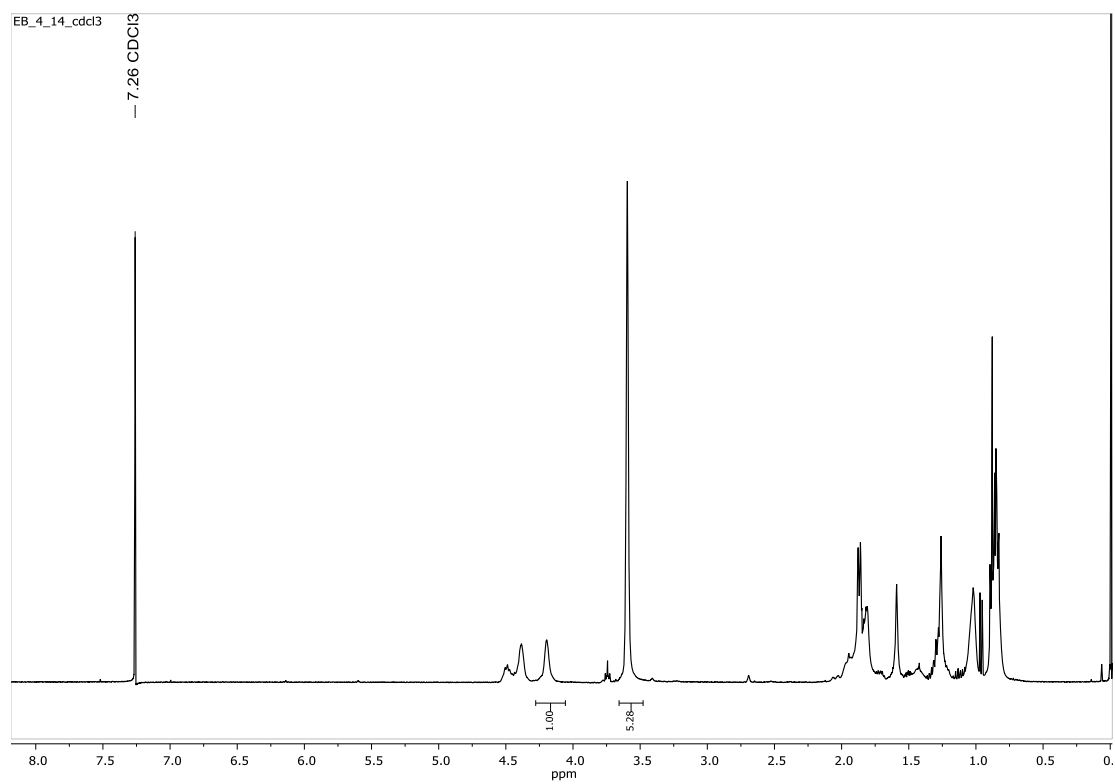
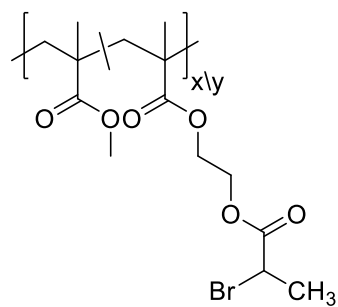


Mark-Houwink-Sakurada Plot

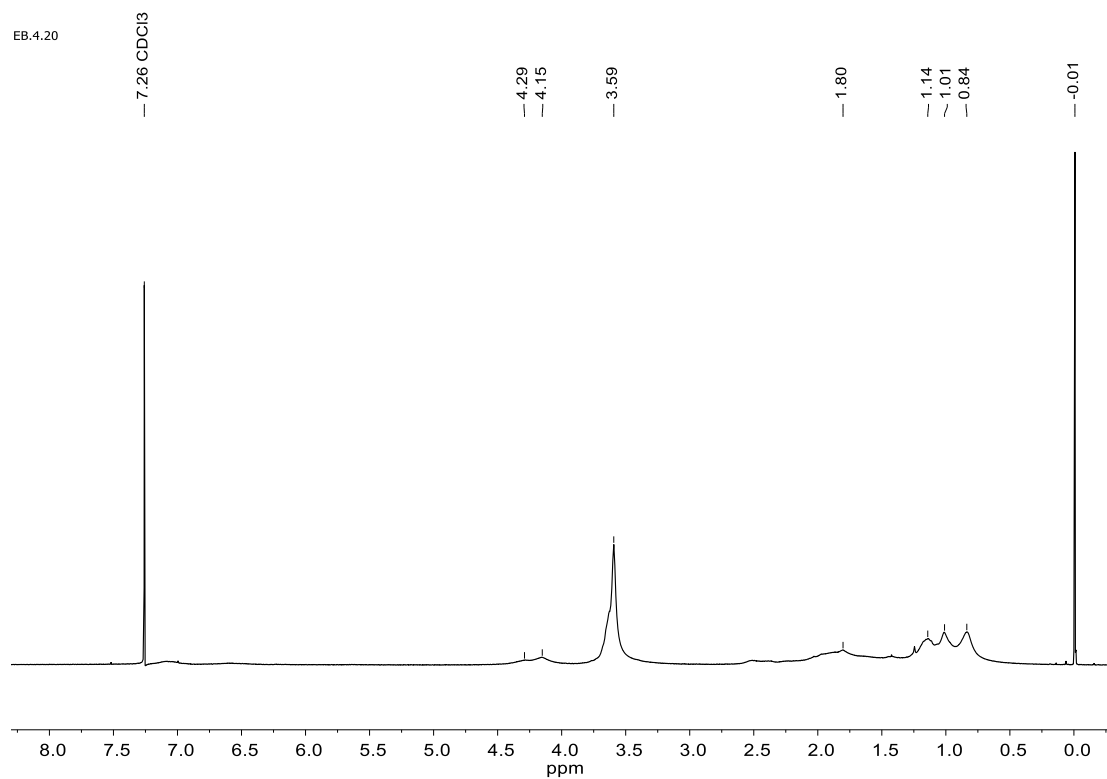
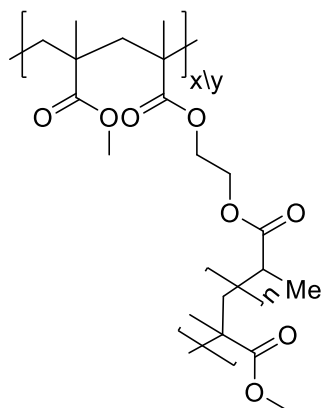


• M-H-S — Linear (M-H-S)

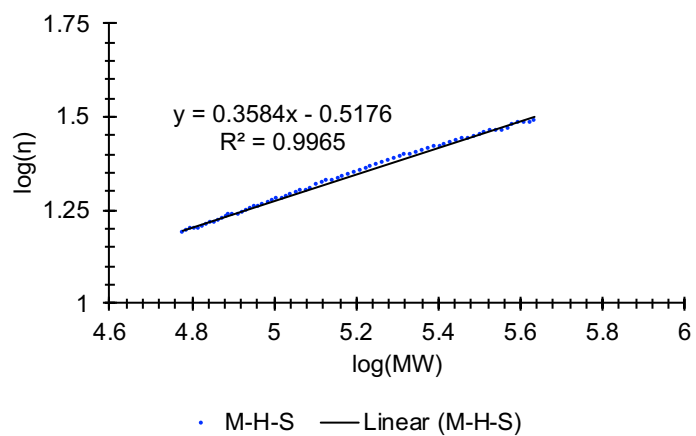
PA-2 p(MMA-co-MeBrema)



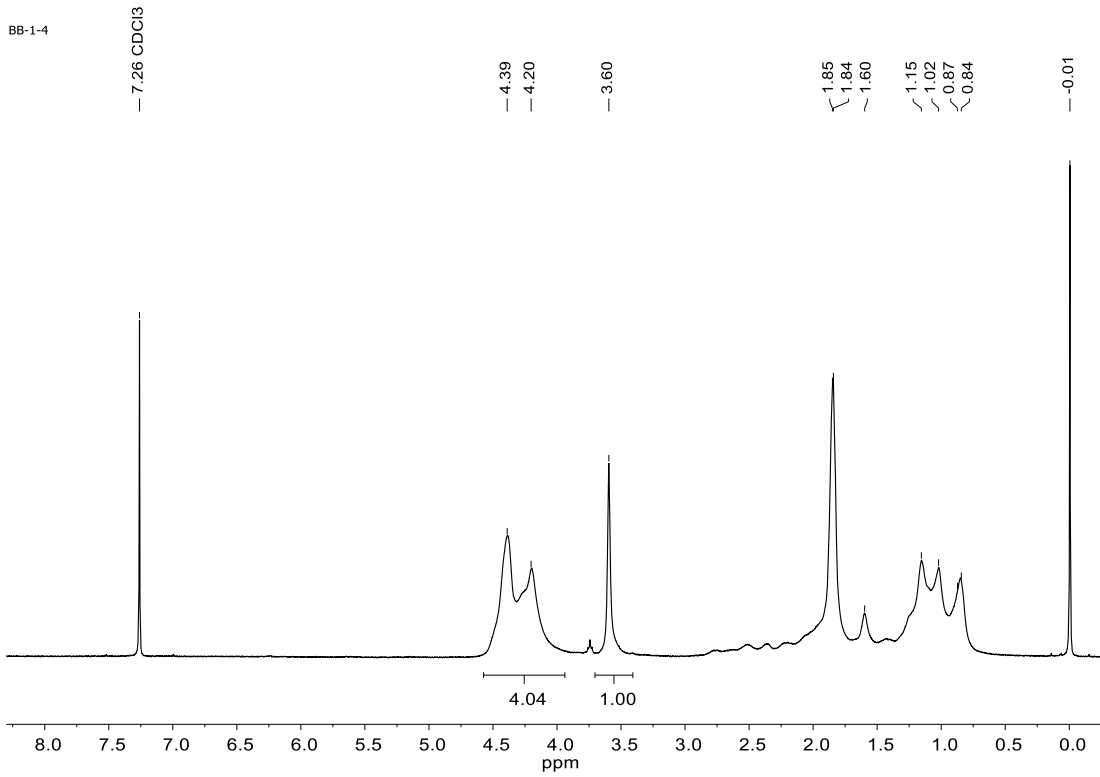
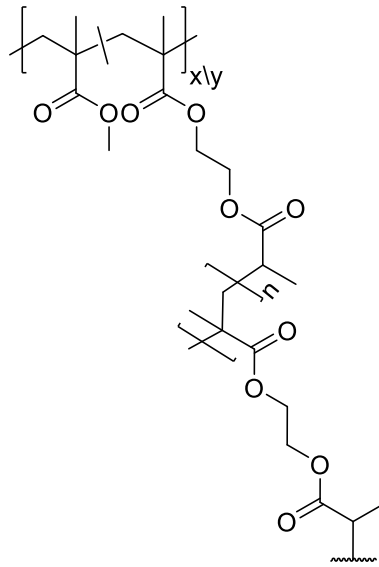
NPA-20



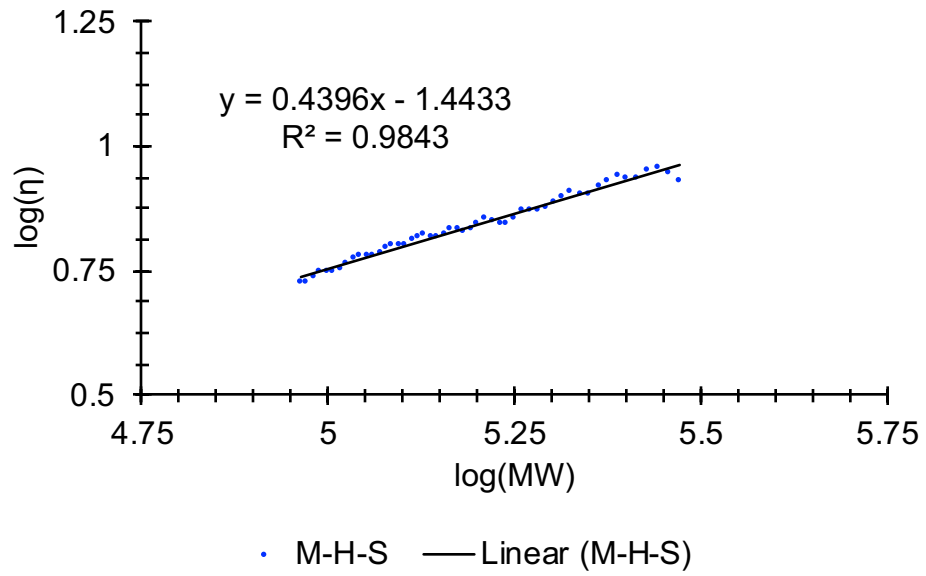
Mark-Houwink-Sakurada Plot



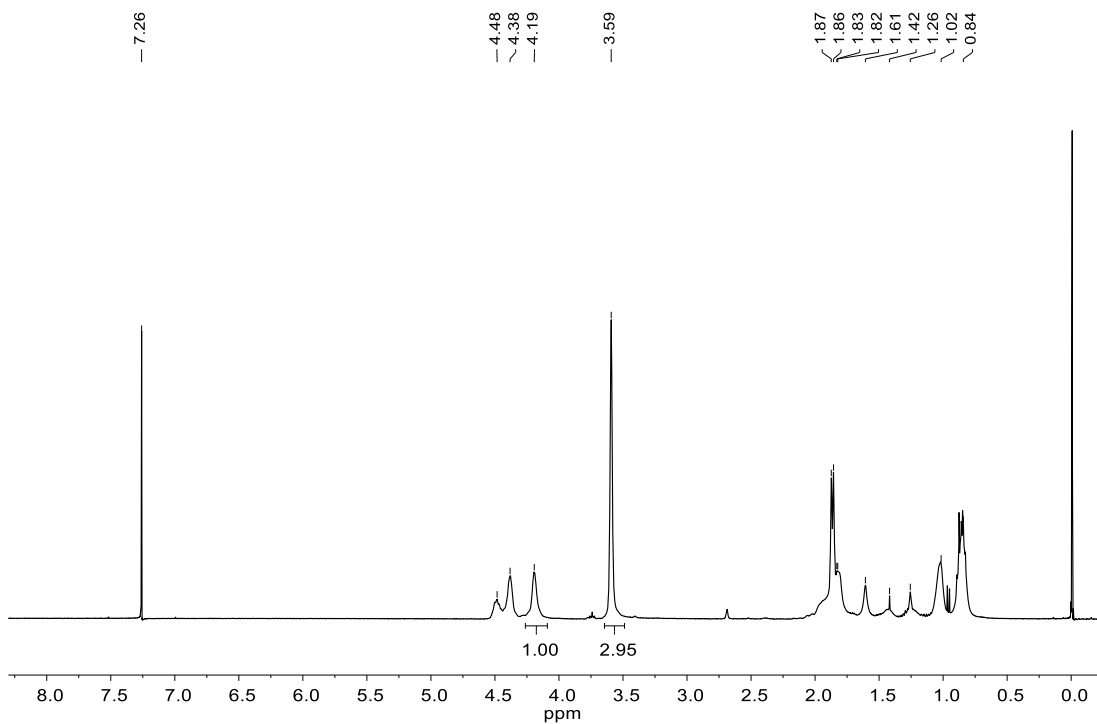
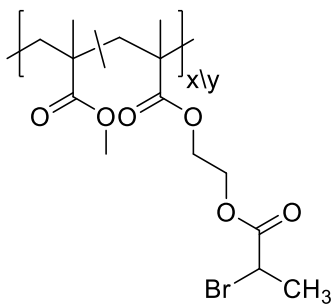
PA-2-MeBrema



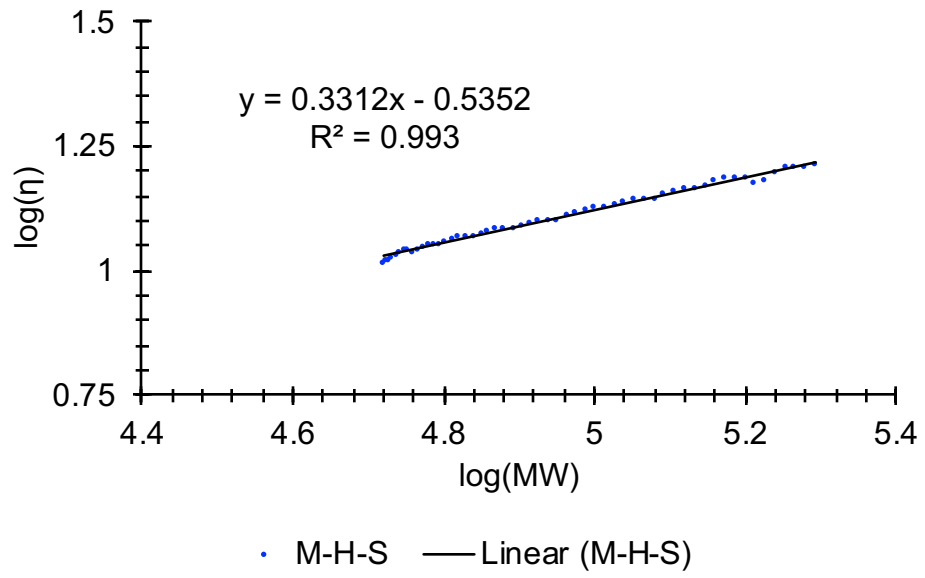
Mark-Houwink-Sakurada Plot



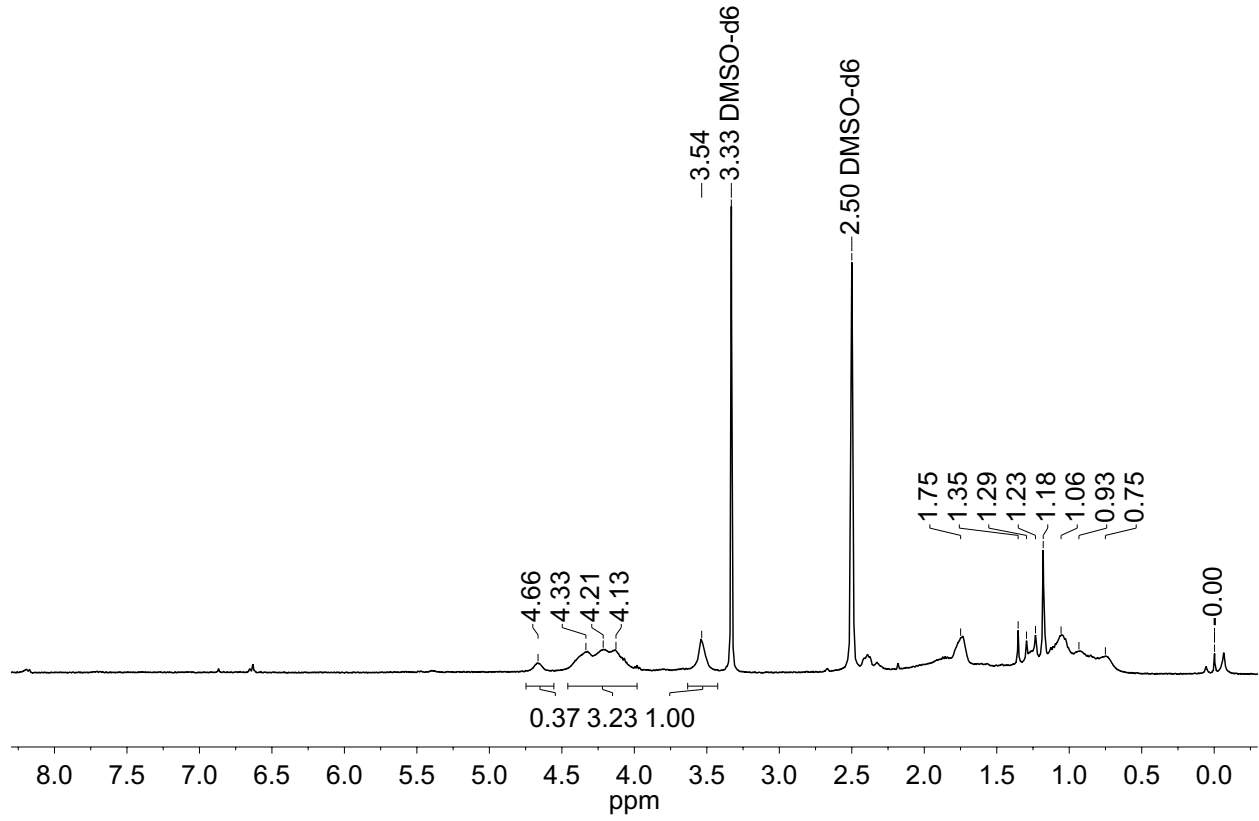
PA-3 p(MMA-co-MeBrema)



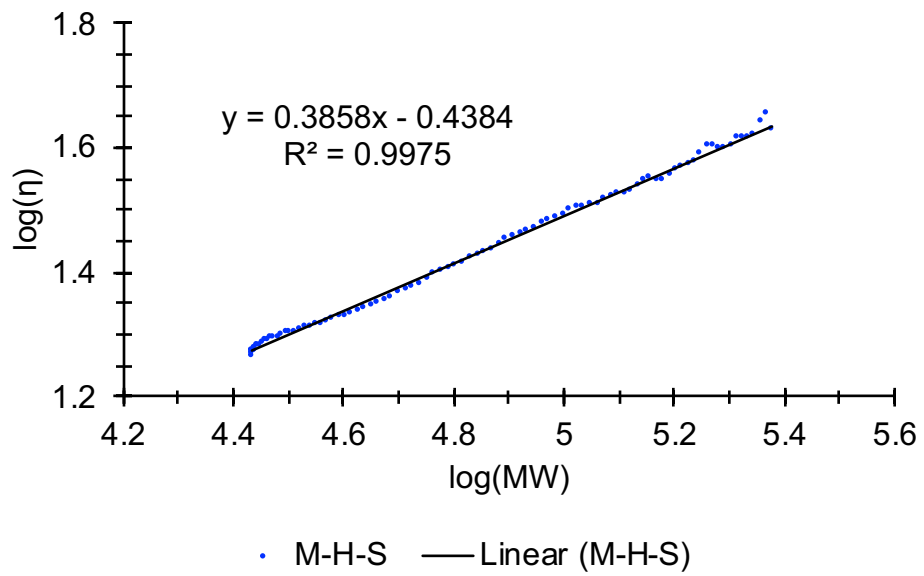
Mark-Houwink-Sakurada Plot



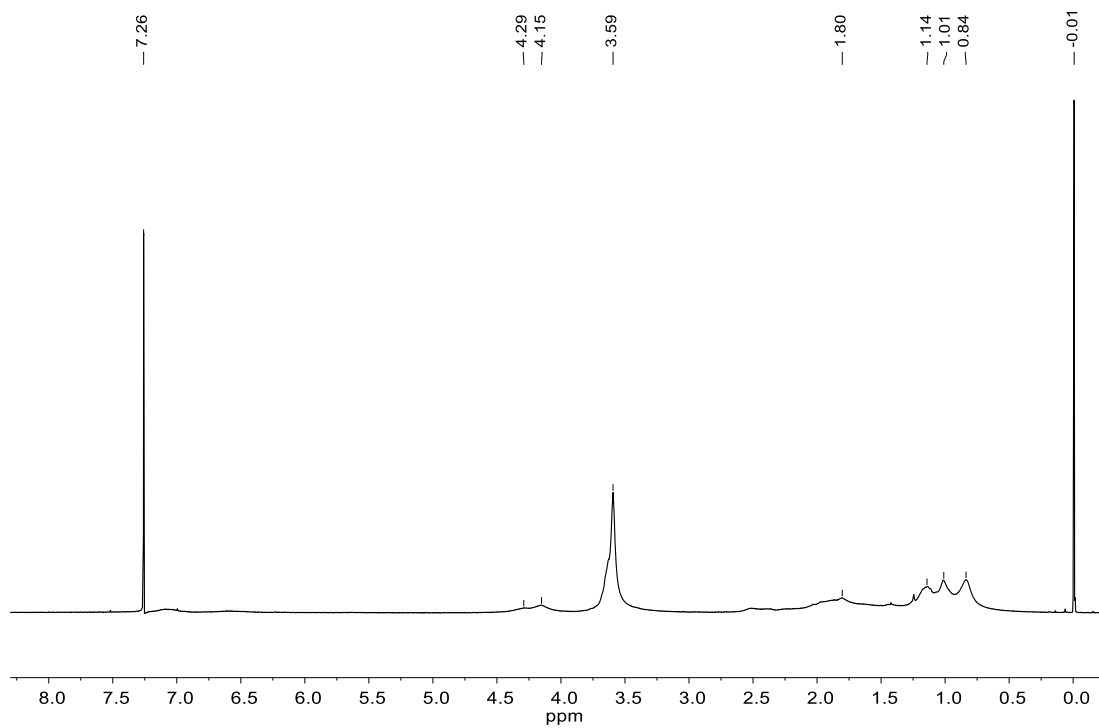
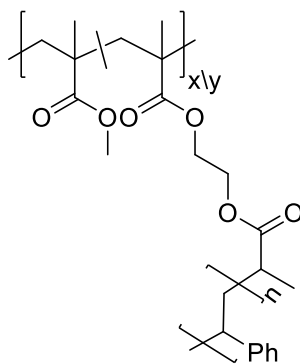
PA-3-MeBrema



Mark-Houwink-Sakurada Plot

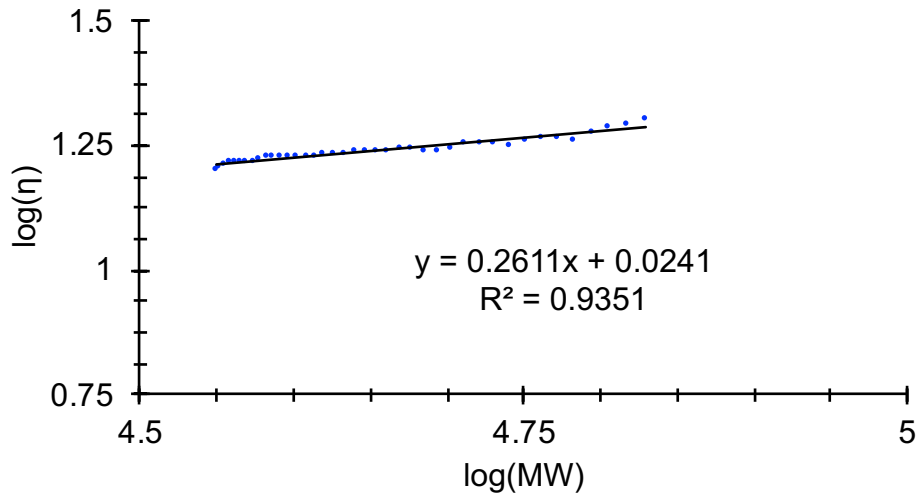


PA-3-STY



Sample 1.

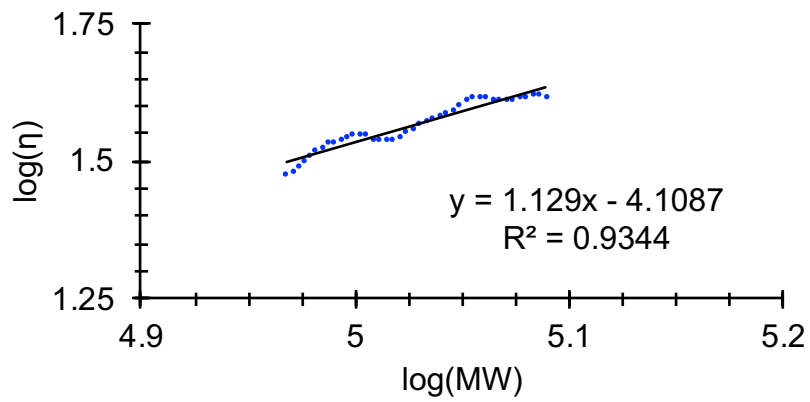
Mark-Houwink-Sakurada Plot



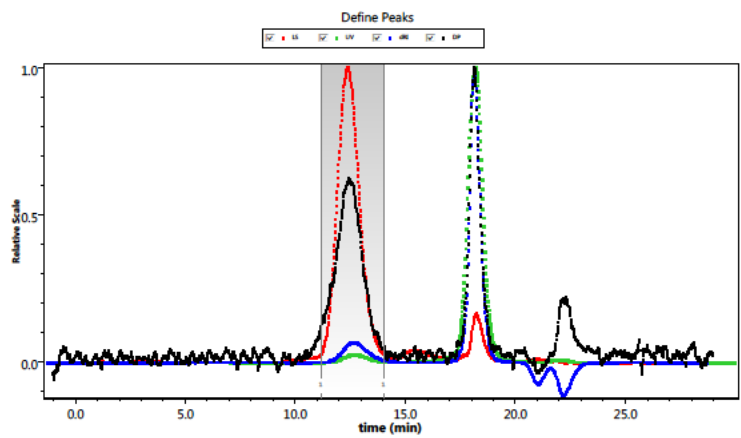
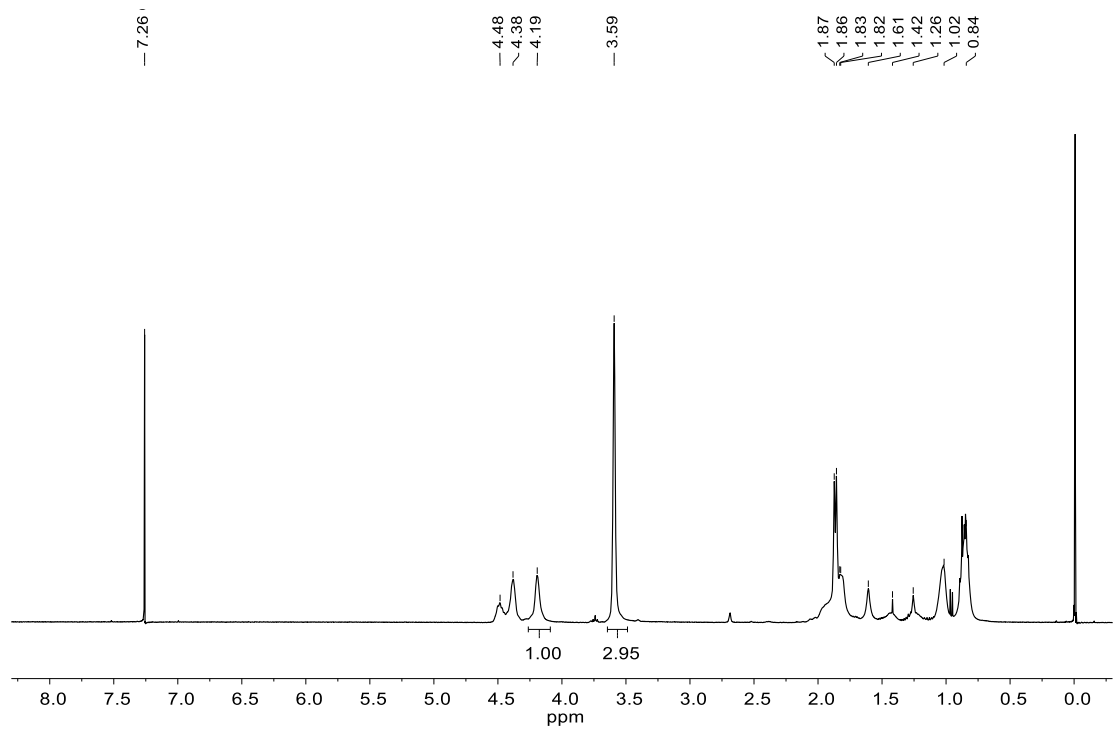
• M-H-S — Linear (M-H-S)

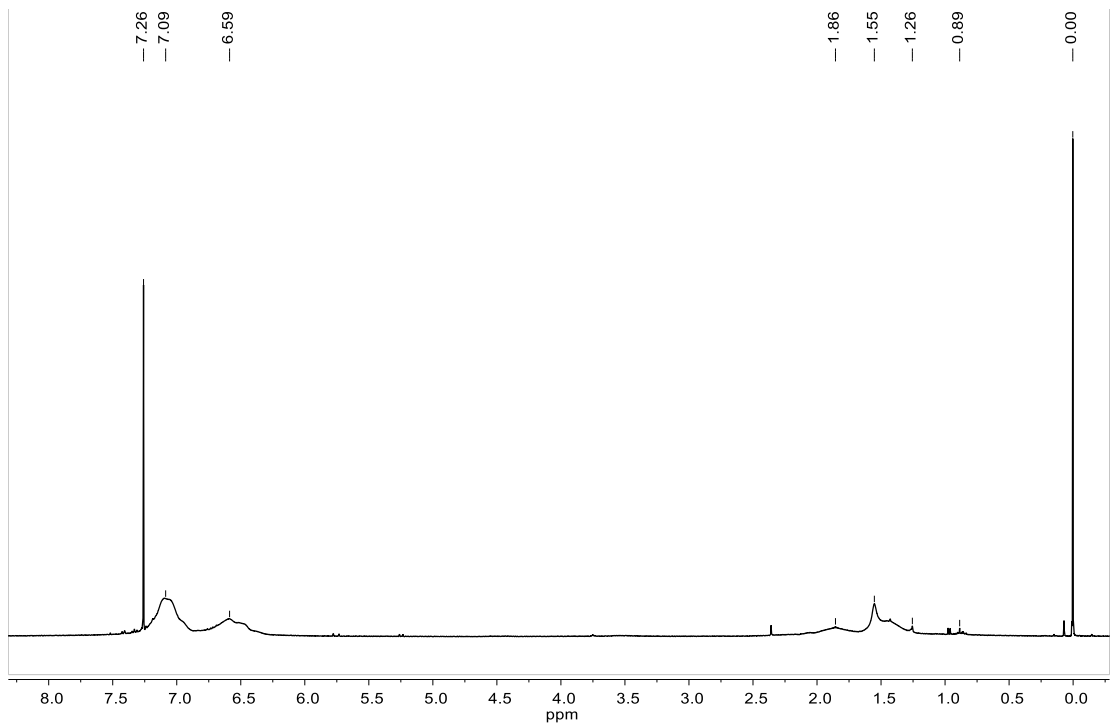
Sample 2.

Mark-Houwink-Sakurada Plot

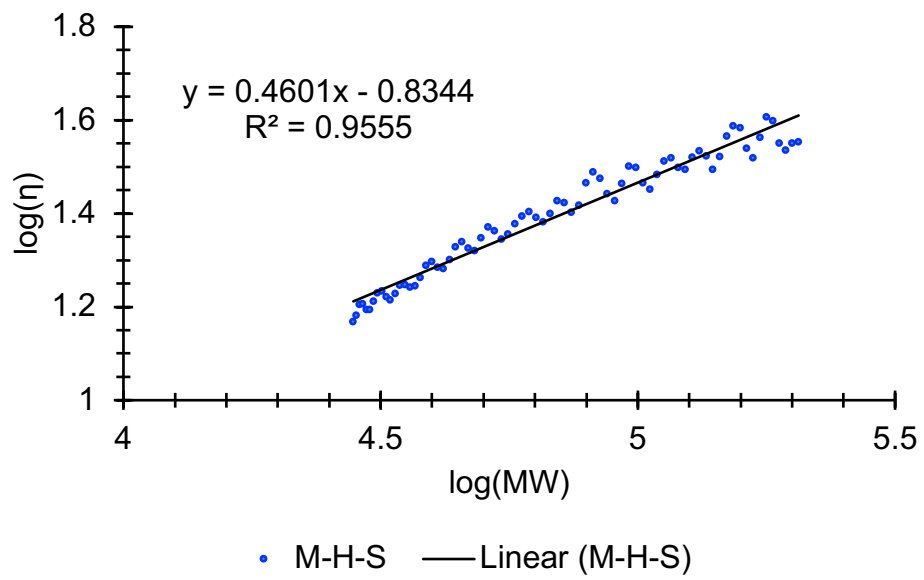


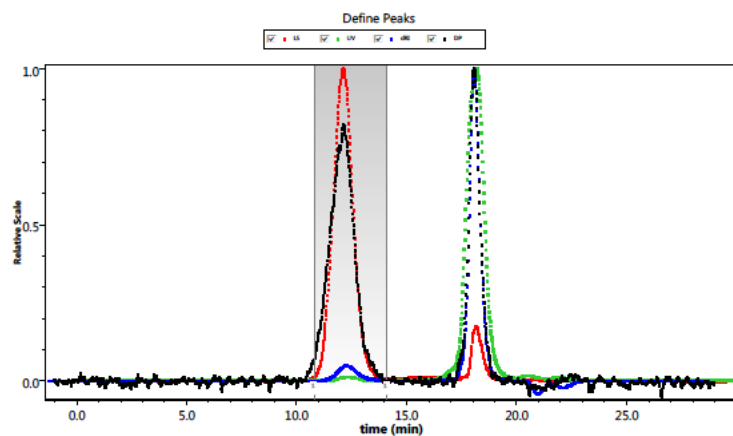
• M-H-S — Linear (M-H-S)





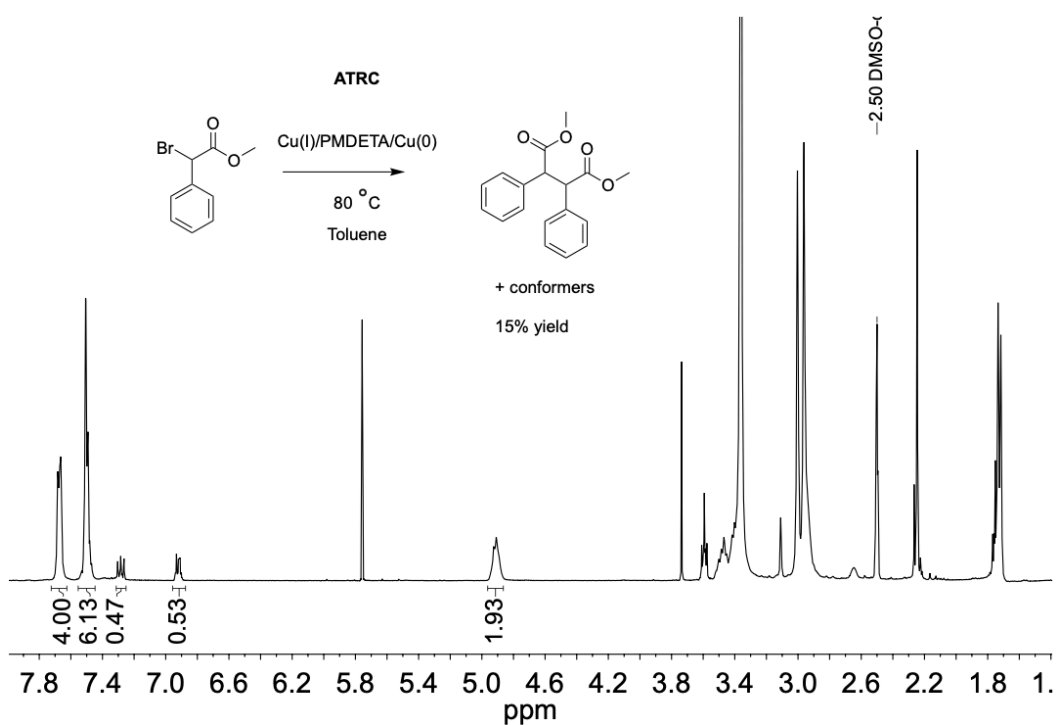
Mark-Houwink-Sakurada Plot





Appendix B: Additional Reactions Not Described in this Dissertation

Dimerization by ATRC



SCNP *via* Thermal Diels-Alder Chemistry

Introduction

Due to its reliability, versatility, and accessibility, the Diels-Alder reaction between furans and maleimide is commonly used to form and cross-link materials such as self-healing polymers, dendrimer formation, and SCNP.^{22,92-94} Its efficient, favorable reactivity is a result the combination of electron-deficiency in the maleimide dienophile with the favorable S-cis constrained conformation of the furan diene. In this experimental design, copolymers of methyl methacrylate (MMA) and furfuryl methacrylate (FMA) are cross-linked through multi-functional maleimide external cross-linkers. The system provides a readily-accessible platform to examine the details and optimize the conditions of the cross-linking reactions. We have recently established a user-friendly externally cross-linked SCNP synthesis using this chemistry.³⁴

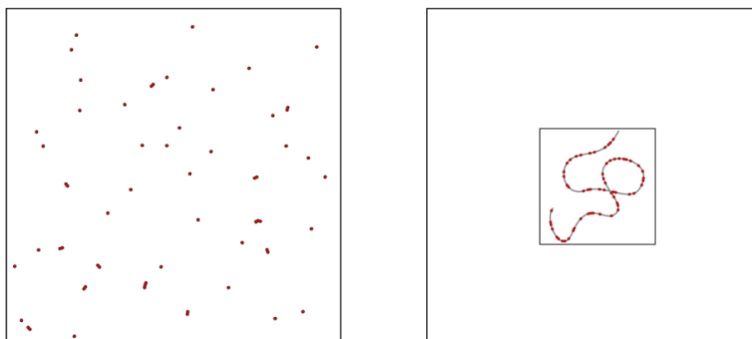


Figure 47. An illustration of the substantial physical difference between freely diffusing functional groups (left) and those tethered to a polymer backbone (right). When external cross-linkers are used for systems like that on the right, they should be used in a 2 to 3 fold excess to adjust their stoichiometry to account for the local concentration.

The ease of this model system provided the opportunity to study the effect of several variables on morphology. For example, during the optimization process, we discovered that a molar excess of external cross-linkers was required to promote efficient folding can efficiently proceed in dilute solution. This result was unexpected due to the highly efficient DA reaction

between this pair. This accounts for the significant difference between local and global concentration of functional groups tethered to polymer chains in ultra-dilute solutions (Figure 47).

The goals of the present study were to establish an ideal percent incorporation of FMA monomer, changing chemical properties and degree of functionality of the external cross-linker, and developing a methodology that does not require dilute solutions (Figure 48). The results of this experiment are especially valuable because they can be directly related to an internally cross-linked DA SCNP system.³⁴

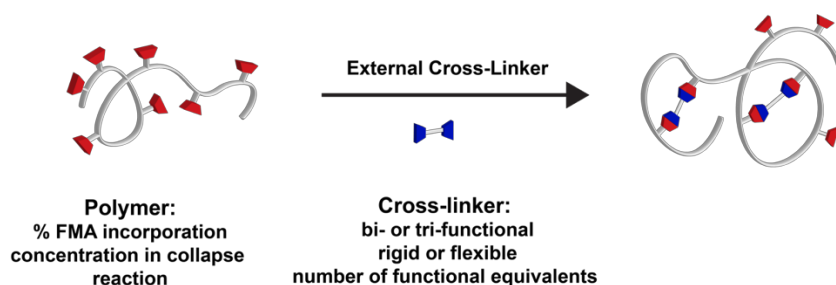
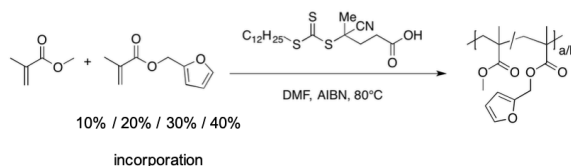


Figure 48. Key variables in the design of SCNP via thermal Diels-Alder reactions.

We demonstrated the synthesis and characterization of a range of SCNP prepared using Diels-Alder chemistry. Parent polymers were prepared using RAFT polymerization with a FMA incorporation of 10, 20, 30, and 40% (Scheme 9) and reacted with one of three multi-functional maleimide cross-linkers to afford SCNP as indicated in Scheme 10. Structure and percent incorporation of the parent polymer was verified by ¹H NMR (Figure 49), and while the resultant

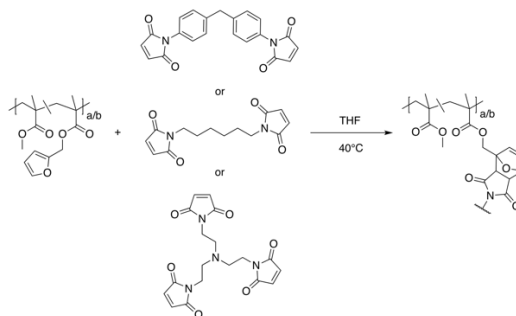
nanoparticles were insoluble in NMR solvents, the collapse was monitored by gel permeation chromatography, multi-angle light scattering, and viscometric data.

Experimental



Scheme 9. The preparation of furan-incorporated Diels-Alder active *via* RAFT.

Poly(methyl methacrylate-co-furfuryl methacrylate). Methyl methacrylate and furfuryl methyl methacrylate were added in the appropriate ratio to a stirring solution of 4-Cyano-4-[(dodecylsulfanylthiocarbonyl)sulfanyl]pentanoic acid (0.336 mL of a 0.02 g/mL stock solution), and azobisisobutyronitrile (0.137 mL of a 0.002 g/mL stock solution) in DMF (0.527mL) at 0 °C. The reaction mixture was sparged with argon for 30 minutes, then allowed to stir at 80 °C for 24 hours. The crude product was precipitated into cold methanol and recovered by vacuum filtration. GPC: $M_n = 2.906 \times 10^4$ ($\pm 0.966\%$), and $M_w/M_n = 1.252$ ($\pm 1.216\%$). $^1\text{H NMR}$ (400 MHz, CDCl_3) δ 7.44 (s), 6.41 (s), 6.36 (s), 4.98 (s), 3.60 (s), 1.81- 0.83 (m).



Scheme 10. An intrachain thermal Diels-Alder reaction between furan functionalized parent polymers and bi- or tri-functional external cross-linkers was used to form SCNP.

SCNP of the above (standard method). In an oil bath stirring at 40°C, 100 mg of the appropriate polymer was added to 100 mL of THF. Once dissolved, the appropriate maleimide (9 eq.) was added. The mixture was brought to a reflux and monitored every 24 hours by GPC. After 72 hours,

the mixture was concentrated in vacuo to approximately 2 mL and pipetted into a cellulose dialysis bag, which was allowed to stir at room temperature in 500 mL THF for three days to remove excess cross-linker. The dialysis solvent was changed twice daily for up to 3 days. The SCNP solution was then concentrated by rotary evaporation. The resulting SCNP display poor solubility in NMR solvents.

SCNP (continuous addition method). In an oil bath stirring at 40°C, 100 mg of the appropriate polymer was added to 49, 19, or 9 mL of THF. Once dissolved, a solution of the appropriate maleimide (9 eq.) in 1 mL THF was added over one hour by syringe pump. The mixture was brought to a reflux and monitored every 24 hours by GPC. After 72 hours, the majority of solvent was removed in vacuo and the resultant solution, approximately 2 mL, was pipetted into a cellulose dialysis bag, which was allowed to stir at room temperature in 500 mL THF for three days to remove excess cross-linker. The dialysis solvent was changed twice daily for up to 3 days. The SCNP solution was then concentrated by rotary evaporation. The resulting SCNP display poor solubility in NMR solvents.

Results and Discussion

The combination of the four parent polymers with varying FMA incorporation with the three external cross-linkers resulted in a matrix of twelve SCNP results, which are represented in the shift in retention time by MALS, demonstrated in Figure 51. In each case, collapse with nine-functional equivalents of cross-linker resulted in an increase in retention time corresponding to the expected decrease in hydrodynamic radius a polymer would experience during collapse. The degree of collapse, however, varied by both cross-linker and FMA incorporation in the parent polymer.

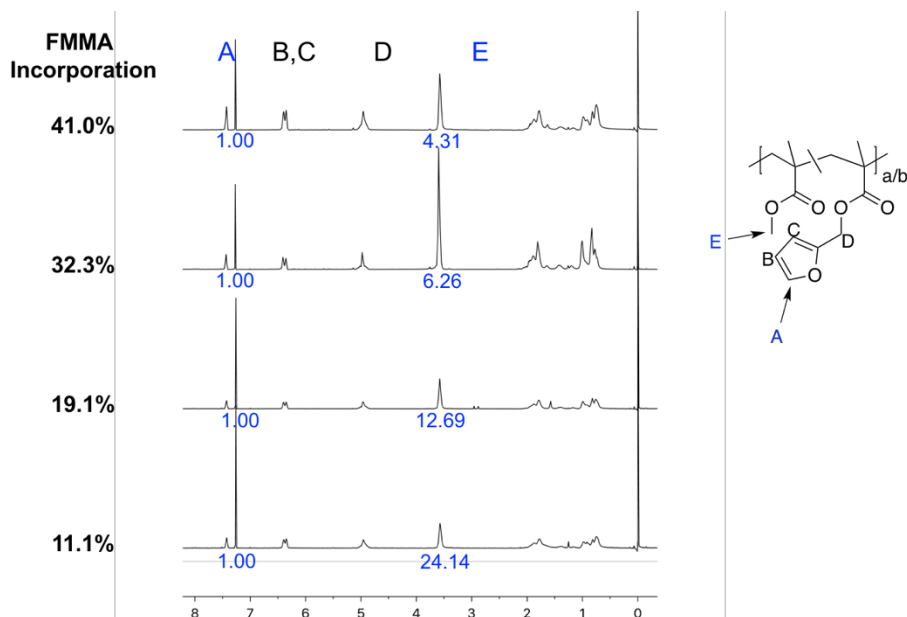


Figure 49. FMA incorporation of the parent chains was calculated by comparing the integrations of the ^1H NMR signals for peak E representing methyl protons in the MMA moieties and A representing a furfuryl proton in the FMA moieties.

Notably, a greater degree of collapse was seen in SCNP formed with the trifunctional cross-linker, even at the same number of functional equivalents. This is consistent with the expectation that, particularly in dilute solution, the collapse is governed by the probability of the functionalities meeting in solution. Differences between the phenyl or hexyl spacer were more subtle, with the flexible hexyl unit resulting in a slightly smaller particle size. Especially for furan incorporations at or below 30%, the external cross-linker with the phenyl spacer was less successful in the DA reaction. This is highlighted in Figure 50. This can be attributed to the inductive effect of the phenyl group on the maleimide unit.

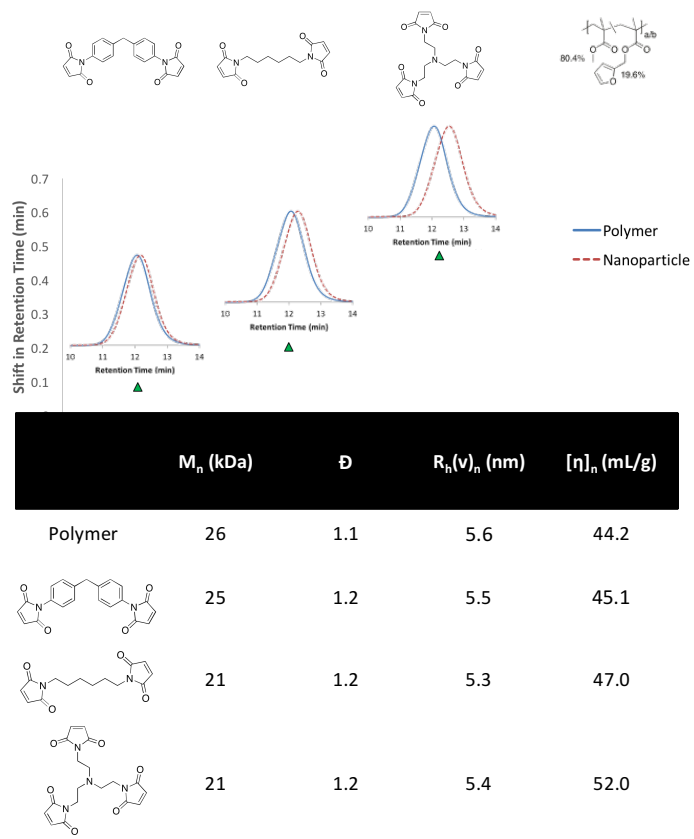


Figure 50. A focused comparison of the effects of varying cross-linker for polymer B.

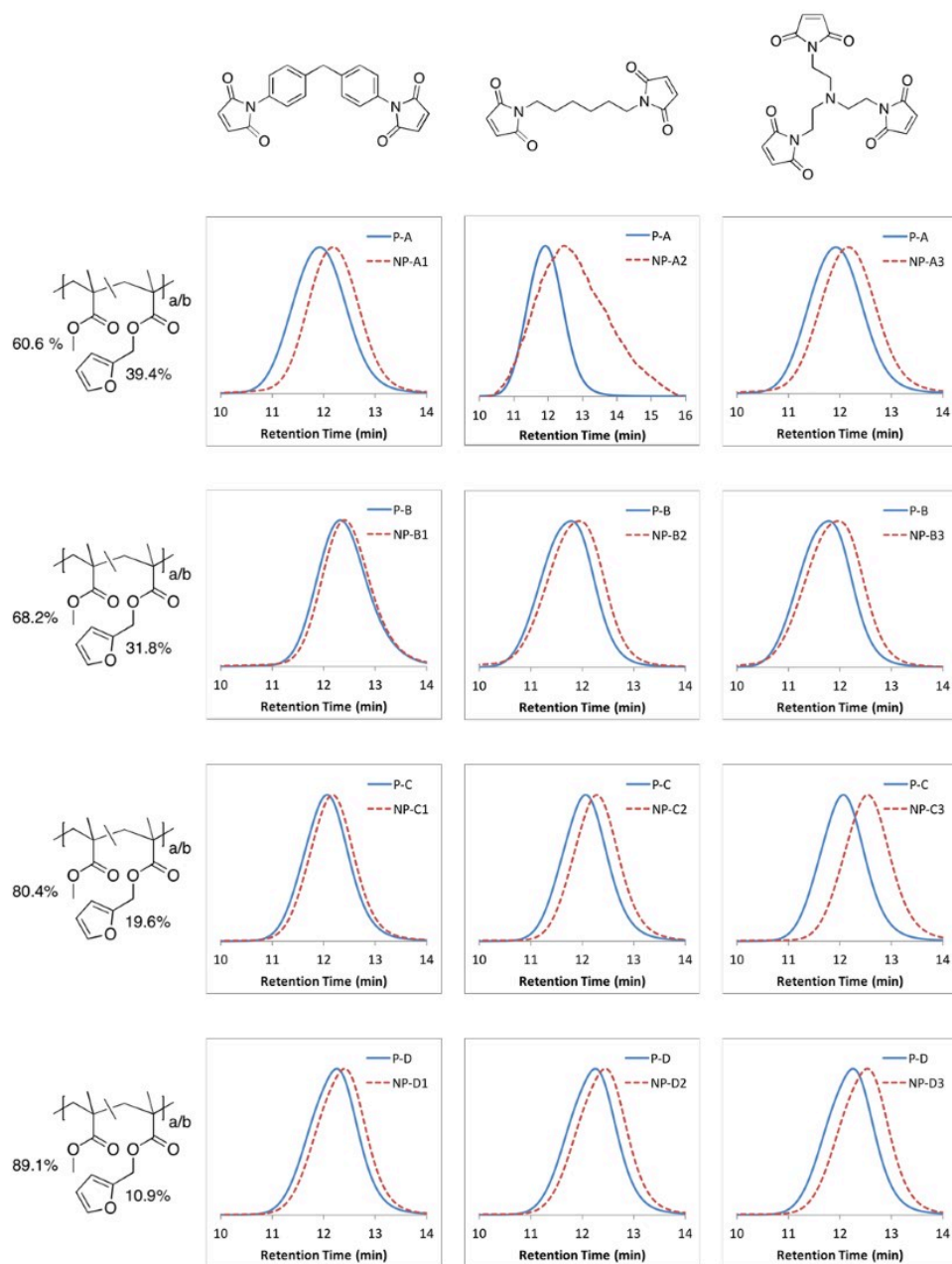


Figure 51. Array of GPC-MALS traces showing the collapse to form SCNP using rigid or flexible di- or tri- functional cross-linkers with 10–40 mol% furfuryl methacrylic parents.

Although all levels of FMA incorporation showed DA activity, the greatest degree of collapse was achieved using parents with a functional incorporation of approximately 20 mol%. Furthermore, some complications were observed at higher percent incorporations. These were interpreted as reactions among the furan units along the polymer backbone, detected by tailing

and broadening of the size distribution in the MALS trace (see NP-A2 in Figure 51). In particular, parent polymer samples around 40% incorporation developed solubility challenges even absent cross-linker. Because both the success of a 20% incorporation and challenges near 40%, 10-30% incorporations are presented as the ideal operating range for this system; these findings are consistent with other SCNP systems, including the analogous internal Diels-Alder cross-linked system.

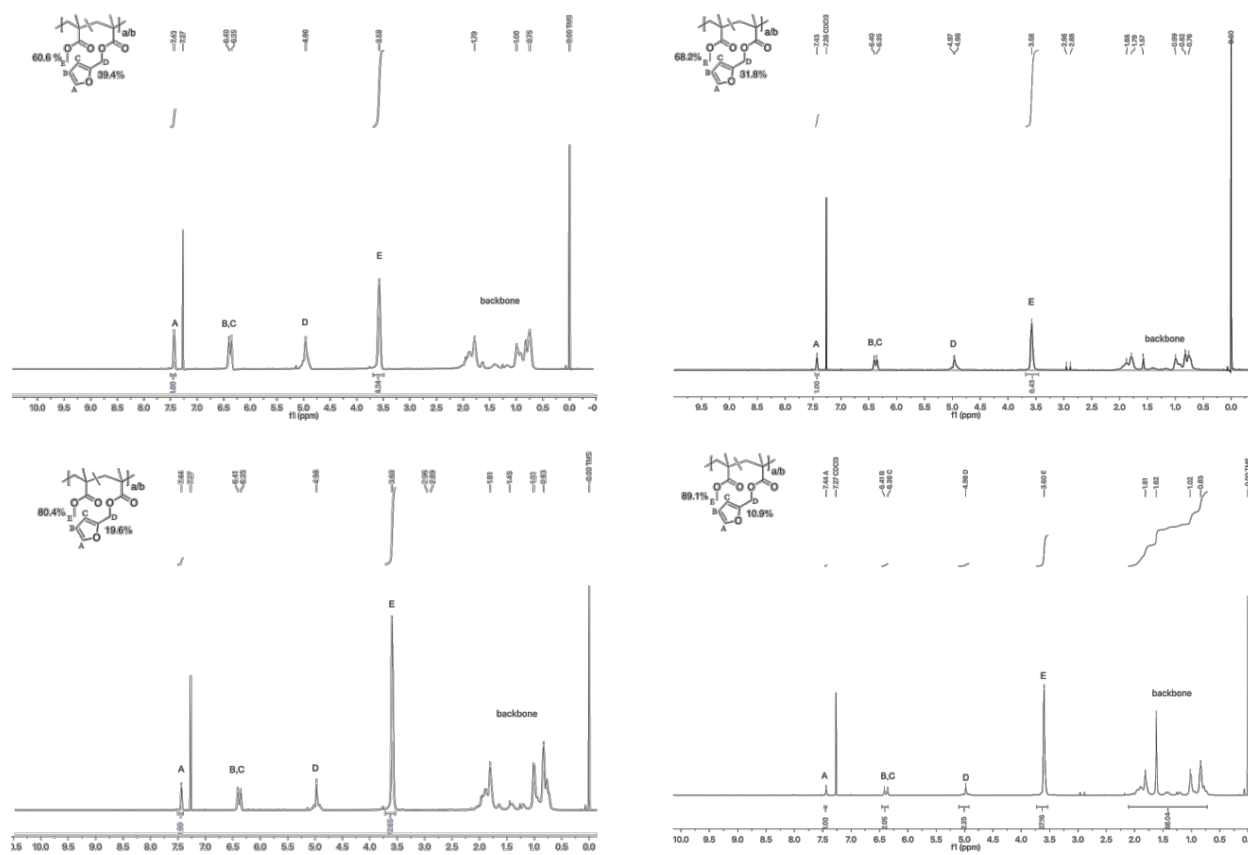


Figure 52. ¹H NMR of furan-functionalized methacrylate parent polymers. Clockwise from top left: P-A, P-B, P-C, and P-D.

Although these optimizations result in an improved collapse efficiency, the ultra-dilute conditions remain prohibitive for many applications. To address this concern, we adapted a continuous addition methodology pioneered by Harth for the purpose of conducting intramolecular collapses at concentrations two to ten times greater than is customary (a typical concentration for SCNP formation is 0.5-1 mg/mL).⁸³ In this method, a concentrated polymer solution is slowly

added to a solution of the external cross-linker (Figure 53). Each aliquot of polymer, then, is effectively cross-linked under ultradilute conditions. This method was effective in increasing the total reaction concentration while preventing undesired intermolecular cross-linking. Furthermore, the degree of collapse increased with concentration; this result is in stark contrast to the control experiment employing the standard procedure. When the entire polymer solution is added at once, intermolecular cross-linking occurs at higher polymer concentrations, and multi-chain aggregates are observed in the broadened and left-shifted MALS trace of the products (Figure 54).

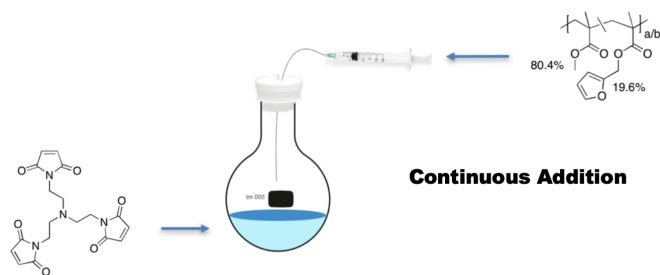


Figure 53. A syringe pump is used to slowly add concentrated polymer solution.

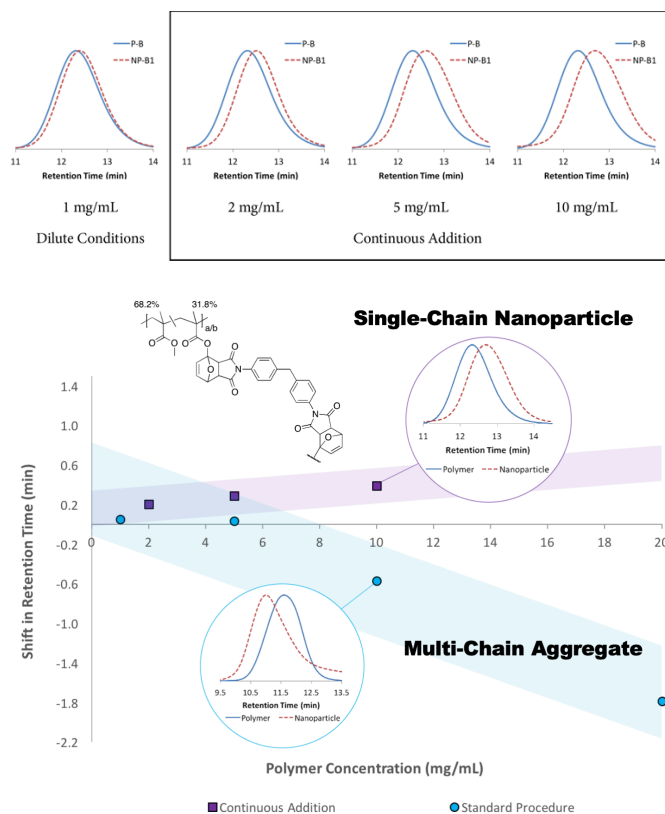


Figure 54. Polymer concentrations can be increased ten-fold using the continuous addition procedure, with higher degree of collapse being observed at higher concentrations without the appearance of multi-chain aggregates.

Conclusions

SCNP were prepared using a facile thermal Diels-Alder reaction between furan-functionalized methacrylic copolymers and di- or trifunctional maleimide cross-linkers. At identical functional equivalencies, examples prepared with tri-functional cross-linkers demonstrated higher degrees of collapse than observed in difunctional cross-linked systems. In addition, parent polymers with a functional incorporation of 20 to 30 mol% resulted in the most globular and well-controlled morphologies. A continuous addition methodology was used to reduce the solvent requirement and thereby improve the scalability of the design. The method also promoted intra-chain cross-linking as evidenced by longer retention times than those observed for samples prepared using standard methods. Overall, the results of this study speak to the potential of physical characteristics and process development to address some of the most

pressing challenges in SCNP chemistry, including scalability, modified stoichiometry, and the entropic penalty of folding.